

**Bulk and Molecular-Level Characterization of Laboratory-Aged Biomass Burning Organic Aerosol from  
Oak Leaf and Heartwood Fuels**

Claire F. Fortenberry<sup>1</sup>, Michael J. Walker<sup>1</sup>, Yaping Zhang<sup>1</sup>, Dhruv Mitroo<sup>1,a</sup>, William H. Brune<sup>2</sup>, Brent J. Williams<sup>1</sup>

<sup>1</sup> Department of Energy, Environmental, and Chemical Engineering, Washington University in Saint Louis, Saint

5 Louis, MO 63130, USA

<sup>2</sup> Department of Meteorology and Atmospheric Science, Pennsylvania State University, State College, PA 16801,  
USA

<sup>a</sup> Now at the Department of Atmospheric Sciences, Rosenstiel School of Marine and Atmospheric Sciences,  
University of Miami, Miami, FL 33149, USA

10 *Correspondence to:* Brent J. Williams (brentw@wustl.edu)

**Authors' Response**

*12/19/2017 – This document was updated to include responses to co-editor comments (p.2-3).*

We thank the reviewers for their helpful comments and insight. In this document, we provide author responses to  
reviewer 1 (p. 4-7), reviewer 2 (p. 8-14), and reviewer 3 (p. 15-24), as well as the edited marked-up manuscript (p.

15 25-88).

20

## RESPONSES TO EDITOR COMMENTS

Editor comments are italicized; author responses are in normal font.

25 *L136: There is an issue with the section heading*

The section heading has been modified.

*L154, L186, L257, L699: missing space after the period*

Necessary spaces have been added in the indicated lines.

30 *L314: Figures S13 and S14 are mentioned before earlier SI figures. Along the same lines, Table S9 is mentioned before tables S4, S5, S6, S7 on page 10. I am not sure whether it is easy to fix the order of appearance with the current organization of the SI section. I encourage you to think how you can reorganize the SI section to avoid (or at least minimize) jumping up and down through it while reading the manuscript.*

We have re-ordered the figures in the supplemental information so the reader has an easier time following along while reading the manuscript.

35 *L320: missing period and space after the subsection title*

The subsection title has been modified to match the rest of the subsection titles.

*L337: It is not clear to me how this can even be done: "the compound structure was inferred by retention time and manually evaluating possible fragmentation patterns". A more specific description would help. Have you tried running the molecules you came up with as standards?*

40 This method of compound identification was particularly relevant for long-chain aliphatic compounds, including alkenes and even-carbon aldehydes. For these compounds, the parent ion was first determined, then major ions were identified (e.g., in tetracosanal,  $m/z$  334 corresponds to  $C_{24}H_{46}^+$  following loss of  $H_2O$ ). The feasibility of the identified structure was confirmed based on predicted vapor pressures and retention times from even alkane standards.

45 The description of this identification method has been incorporated into the text (lines 339-343):

“Identification method (D) was particularly relevant for long-chain aliphatic compounds, including alkenes and even-carbon aldehydes. For these compounds, the parent ion was first determined, then major ions were identified (e.g., in tetracosanal,  $m/z$  334 corresponds to  $C_{24}H_{46}^+$  following loss of  $H_2O$ ). The feasibility of the identified structure was confirmed based on predicted vapor pressures and retention times from even alkane standards.”

50 *Figure 3: the text in the legend is too small.*

We have made the legend text larger to improve readability.

*Figures 4, 5, 9, 10: some of the text label are too small and will be hard to see in the final version*

*Most of the figures: the image quality appears to be too low in the PDF file. I would increase the dpi in the final images produced for the final paper.*

55 We have submitted all manuscript figures with 300 dpi resolution.

*Points raised by the reviewer 3: I tend to agree with the comment by reviewer 3 that matrix effects could affect the interpretation of the results, and that using internal standards added to the sample would help avoid such matrix effects. While it is not going to be possible to address this in this paper, I think it would be good if you make it happen for your future papers of this sort.*

60 Thank you for your input. We agree that matrix effects could be significant in certain circumstances, and we aim to address this issue in future studies.

*Supporting Information (SI) section:*

*Figures S6/S7 and Tables S4/S5:*

- Structure 19 is unlikely, allenes are quite uncommon in the atmosphere. Perhaps it is an alkyne?

65 Thank you for the suggestion. After re-examining this compound, we identified it using the mass spectral library as 4-(1,2-propadienyl)-guaiacol with a match quality of 64%. However, there appear to be multiple matches that return a moderate match quality (50-75%), so we have changed the certainty of ID designation from B to C. Without adequate standards, it is challenging to identify the structure with certainty. We were not aware that allenes are uncommon in the atmosphere, so while we retain this identification, we will continue to examine the feasibility of this structure, as with all compounds identified with tentative certainty.

70 - Structure 23 is also unlikely, its saturation vapor pressure is way too low for this compound or its decomposition products to be detectable by GC or TAG without derivatization. This could be a library mismatch.

75 After re-examining this compound, we have identified it as methyl- $\beta$ -D-glucopyranoside with a library match quality of 38%. This compound was particularly difficult to identify due to multiple co-eluting molecules. Based on estimated vapor pressures, we think this identification makes more sense than our previous identification of guanosine.

76 - Does it make sense to split one figure (images of your molecules) in two S6 and S7? Same question for the table? I understand that they stretch over 2 pages; you can say "Figure S6 continued" in the caption

80 In reordering supplemental figures, we have merged these figures into one (Figure S9, with the figure continued over two pages). Similarly, the tables are now a single table (Table S5).

Figure S9: the step with the four-membered ring is probably incorrect. The classical RO<sub>2</sub> -> RO -> CC bond fission reaction sequence is much more likely.

85 We are grateful for this insight. In figure S9, we retain the four-ring formation step described by Wong et al. (now R2). However, we have also added another proposed mechanism for aldehyde formation (R3) that involves the C-C bond fission after the peroxide O-O cleavage (Ziemann and Atkinson, 2012). We have also added the following sentence to the figure caption:

“A third reaction sequence (R3) could also proceed after R1 following loss of an oxygen from the peroxy radical through reaction with either HO<sub>2</sub> or another peroxy radical (RO<sub>2</sub>; Ziemann and Atkinson, 2012).”

90 Figure S14: was there an issue with H/C analysis? How is it possible to end up with unphysical H/C around 0 or above 3? I would add a clarification on the atomic ratio measurements.

After re-examining the figures, the points with unphysical H/C ratios (above 3 or around 0) occur at points where AMS signal was very low, either shortly after the chamber had cleared or during regular blanks. These points have been removed from the plots. The figure caption has been modified to address this point:

95 “To minimize noise, AMS data is plotted only for points where sufficient total organic concentrations were achieved.”

Figure S15: calling sulfate (SO<sub>4</sub><sup>2-</sup>) is going to be misleading. Even though SO<sub>4</sub><sup>2-</sup> may be the ion measured by AMS (I do not actually know how AMS does it), the calibrated axis actually refers to SO<sub>4</sub>(2-). I would fix it.

The AMS calculates total sulfate mass concentrations from a variety of ions. The figure has been updated to simplify the terminology used and remain consistent with previous literature (e.g., Xu et al., J. Geophys. Res., 121:18, 2016).

100 Table S2: too many significant figures in the reported results. The general rule is that the error bar should have 1 or at most 2 significant digits. Therefore, 314.20 +/- 78.59 should be 314 +/- 79, etc.

For Table S2, we have reduced the number of significant figures in the error to 1-2.

Tables S10, S11 – the same issue with significant digits.

For Tables S10-S11, we have reduced the number of significant figures in the error to 1-2.

105

## RESPONSES TO REVIEWER 1

Reviewer comments are italicized; author responses are in normal font.

Fortenberry *et al.* present a study that examines links between chemically speciated fresh and aged BBOA data to more bulk measurements of the AMS. They use PMF technique to pull out mass spectral trends in the speciated data and looked mass spectra from compounds that eluted during the thermal decomposition window of the TAG. Their results show 60 m/z, a traditionally used ion for the AMS to track biomass burning, depends on fuel type and aging of the aerosol particles. They also suggest that 44 m/z ion could be used as an estimate for aerosol particle's aging state. This manuscript is written clearly and contributes to the understanding of both the complexity of BBOA and interpreting results from the AMS. I recommend this paper be published in ACP with some minor revisions.

110 115 We thank the reviewer for his/her comments and insight. We address comments individually below. Where appropriate, approximate line numbers corresponding to the edited (with markup) manuscript provided, along with line numbers relative to the section/paragraph number.

### Minor Comments:

Line 38: *parallel structure, change to “and impacts” or something along those lines*

120 125 In line 36 (Section 1, Paragraph 1, Line 2), “...and can impact the global energy balance...” was changed to “... and impacts the global energy balance...”

Line 39: *awkward sentence starting with “Organic aerosol. . .” In addition, aerosol refers to both the particle and gas phase. When the authors mean particle phase, please change aerosol to aerosol particle.*

We reworded this sentence to improve clarity (lines 37-39; Section 1, Paragraph 1, Lines 7-9):

130 135 “Organic aerosol (OA) particles compose 20-90% of submicron PM (PM<sub>1</sub>) and may consist of thousands of distinct organic compounds (Goldstein and Galbally, 2007; Ng *et al.*, 2010; Zhang *et al.*, 2007).”

In addition, we minimized our use of the word “aerosol” throughout the text, instead using “particles,” “gases,” and “emissions” where necessary.

Line 164: *Traditionally, the radical dot of OH is left off, though the authors are technically correct. The dot just looks a bit strange when used, for example, in line 580.*

To remain consistent with previous literature, we removed the radical dot from each reference to the hydroxyl radical.

Line 166: *How well-mixed in the PAM reactor? Could large concentration gradients in aerosol particles affect the observed results?*

140 145 150 Recent work demonstrates that the PAM reactor used in this study is approximately well mixed if sufficient time is given prior to sample collection to establish a well-mixed and near steady-state concentration throughout the combustion chamber and PAM chamber (Mitroo, 2017). We therefore do not expect concentration gradients within the PAM reactor to significantly impact observed results.

This question has been addressed in-text with the addition of the following sentence in lines 219-223 (Section 2.3, Paragraph 7):

“Flow field simulations and chemical tracer tests have demonstrated that the PAM reactor used in this study is approximately well mixed if sufficient time (at least 15 minutes) is given prior to sample collection to establish a well-mixed and near steady-state concentration throughout the combustion chamber and PAM chamber (Mitroo, 2017). The TAG therefore consistently collected 30 minutes after the biomass heat pulse to minimize particle concentration gradients within the reactor.”

Line 180: *add fuels after leaf*

In line 188 (Section 2.3, Paragraph 2, Line 9), “For both heartwood and leaf, ...” was changed to “For both heartwood and leaf fuels, ...”

150 *Line 210: What is the rate at which the cells are heated to 310°C? There is some discussion that heating rate will affect which compounds desorb vs. thermal decompose. The authors do illustrate the ramping time in Figure 1, but it would be helpful to have it written down in the text.*

In line 258 (Section 2.4.1, Paragraph 1, Line 2), a typical collection and thermal desorption heating rate of 50°C min<sup>-1</sup> has been added to the text per the reviewer's suggestion.

*Line 222: combustion chamber were clean*

155 Here (now line 278; Section 2.4.1, Paragraph 3, Line 4), we clarified the language by replacing "... to ensure that the emissions and combustion chamber was clean prior to ..." with "... to ensure that both the emissions chamber and the PAM reactor were clean prior to ..."

*Line 469: have specific standards been observed to decompose at these ions in this thermal decomposition window?*

160 We thank the reviewer for this question. We have not observed these ions in any recent standard work, though this is an area of active research.

Developing satisfactory analytical standards for the TAG decomposition window has been particularly challenging. While we can tentatively identify the fragments eluting in the decomposition window using available mass spectral identification tools, we often cannot infer the source of the fragments, since they are products of compound thermal decomposition rather than volatilization. With that, many of the compounds undergoing decomposition during sample desorption are potentially too involatile for typical GC-MS analysis.

165 We have expanded our conclusion to include a discussion of the challenges of interpreting thermal decomposition window data (now lines 766-774; Section 4, Paragraph 6):

170 "The utility of the thermal decomposition window is limited by a lack of adequate analytical standards, particularly for organic components. Although ammonium sulfate and ammonium nitrate standards have been used to quantify sulfate and nitrate particles in previous work (Williams et al., 2016), the development of satisfactory standards for decomposing organics remains difficult for several reasons. While fragments eluting in the decomposition window may be tentatively identified using available mass spectral identification tools, we often cannot infer the source of the fragments, since they are products of compound thermal decomposition rather than volatilization. Many of the compounds undergoing decomposition during sample desorption are therefore too thermally labile for typical GC-MS analysis, and the original molecular structure remains undetermined. Despite these challenges, analytical standards composed of complex organic mixtures are currently under development to aid interpretation of decomposition window results based on molecular functionality."

175 *Line 534 (though may happen earlier): No comma after Kessler. This comma is not needed as Kessler and others (in English) requires no comma even when used in line. Please remove comma in previous+subsequent usages.*

180 We thank the reviewer for pointing out this mistake. The unnecessary commas have been eliminated from in-line references throughout the text.

*Figure 2 (a): The three types of green are very difficult to distinguish. I understand the authors were aiming for green=leaf and warm colors for heartwood, but greens all look the same. Maybe cool colors for leaf and warm colors for heartwood?*

185 The colors in Figure 2(a) have been changed to teal, purple, and pink to improve figure readability. Subsequent leaf BBOA plots have been changed to match this color scheme.

*Figure 3 (b): Why are syringol, syringaldehyde, and vanillin dotted lines? Is it because they are observed to increase with aging time? If so, please mention that in the caption.*

190 These compounds were indicated with the dotted lines to visually distinguish that unlike the rest of the compounds, they do not directly decrease abundance with equivalent aging. The following sentence has been added at the end of the figure caption:

"Compounds that decrease in abundance are indicated with solid lines, while compounds that deviate from this trend are displayed with dotted lines."

Figure 8 (a): The greens are hard to distinguish.

195 As with figure 2(a), the colors were changed to teal, purple, and pink to improve figure readability.

Figure 10 (a): The green color gradient is not great and implies there was a near continuous gradient of samples collected for that range of aging time. There were only three sampled times, so a gradient seems a bit misleading. Also, the colored right-hand and top axes are a bit confusing because the reader is trying to match the green points to the green axis instead of TAG to green. Also, the caption says the dotted lines are guidelines for where the points tend to be concentrated. This doesn't seem to be the case for the green AMS points. The blue dotted line for these points would look more like a rectangle covering the bottom half of the graph then a downward pointing cone. Is there greater meaning behind this cone?

200 We agree with the reviewer that the continuous color gradient may be misleading. In both figure 10(a) and 10(b), we have changed the legend to reflect the three distinct aging times for each fuel type. We have also changed the color scheme in figure 10(a) to match the colors used in figure 2(a).

205 The triangle formed by the dotted lines provides a visual guideline for the evolution of OA chemical composition in  $f_{43}/f_{44}$  space. The apex of the triangle formed by the lines indicates the direction of increasing photochemical oxidation. These triangles have been used as visual aids in previous presentations of AMS  $f_{43}$  and  $f_{44}$  data (Ng et al., 2010) and are provided by default by the AMS Squirrel analysis software. We agree that in the case of our leaf BBOA AMS data, the points do not fit well within the confines of the dotted lines, so we have modified the position of the triangle to better fit our AMS data points. In addition, we have clarified the functionality of the triangle in the figure caption (what is now Figure 8) by modifying the last sentence:

210 “The triangles formed by the blue dotted lines provide visual guidelines for the evolution of OA chemical composition across  $f_{44}$  vs  $f_{43}$  space; the apex of the triangle indicates the direction of photochemical oxidation for AMS measurements (Ng et al., 2010)”

Figure 15 (A): same comment about the green.

As with figure 2(a), the colors were changed to teal, purple, and pink to improve figure readability.

Even more minor comments for the SI:

215 Figure S4: the TAG collection 1 blue shaded region does not look to start at 30 minutes after start of heat pulse as the caption indicates.

Now Figure S5, the location of the shaded region has been fixed to start at 30 minutes after the heat pulse.

Table S5-6: The raw SIC integration numbers have too many significant digits (and is difficult to read). Maybe consider limiting it to 2-3 with scientific notation.

220 The raw SIC integrations have been fixed as suggested: the values now have 3 significant digits and are presented in scientific notation.

#### Literature Cited:

Goldstein, A. H. and Galbally, I. E.: Known and Unexplored Organic Constituents in the Earth's Atmosphere, Environ. Sci. Technol., 41(5), 1514–1521, doi:10.1021/es072476p, 2007.

225 Mitroo, D.: Applications and Flow Visualization of a Potential Aerosol Mass Reactor, PhD Thesis, Washington University in St. Louis, St. Louis, MO., 2017.

Ng, N. L., Canagaratna, M. R., Zhang, Q., Jimenez, J. L., Tian, J., Ulbrich, I. M., Kroll, J. H., Docherty, K. S., Chhabra, P. S., Bahreini, R., Murphy, S. M., Seinfeld, J. H., Hildebrandt, L., Donahue, N. M., DeCarlo, P. F., Lanz, V. A., Prévôt, A. S. H., Dinar, E., Rudich, Y. and Worsnop, D. R.: Organic aerosol components observed in

235 Northern Hemispheric datasets from Aerosol Mass Spectrometry, *Atmos Chem Phys*, 10(10), 4625–4641,  
doi:10.5194/acp-10-4625-2010, 2010.

Williams, B. J., Zhang, Y., Zuo, X., Martinez, R. E., Walker, M. J., Kreisberg, N. M., Goldstein, A. H., Docherty, K. S. and Jimenez, J. L.: Organic and inorganic decomposition products from the thermal desorption of atmospheric particles, *Atmos Meas Tech*, 9(4), 1569–1586, doi:10.5194/amt-9-1569-2016, 2016.

240 Zhang, Q., Jimenez, J. L., Canagaratna, M. R., Allan, J. D., Coe, H., Ulbrich, I., Alfarra, M. R., Takami, A., Middlebrook, A. M., Sun, Y. L., Dzepina, K., Dunlea, E., Docherty, K., DeCarlo, P. F., Salcedo, D., Onasch, T., Jayne, J. T., Miyoshi, T., Shimono, A., Hatakeyama, S., Takegawa, N., Kondo, Y., Schneider, J., Drewnick, F., Borrmann, S., Weimer, S., Demerjian, K., Williams, P., Bower, K., Bahreini, R., Cottrell, L., Griffin, R. J., Rautiainen, J., Sun, J. Y., Zhang, Y. M. and Worsnop, D. R.: Ubiquity and dominance of oxygenated species in organic aerosols in anthropogenically-influenced Northern Hemisphere midlatitudes, *Geophys. Res. Lett.*, 34(13), L13801, doi:10.1029/2007GL029979, 2007.

250

255

260

265

## RESPONSES TO REVIEWER 2

Reviewer comments are italicized; author responses are in normal font.

*This paper describes experiments and analysis examining the composition of fresh and aged aerosol emissions from volatilization/combustion of oak wood and leaf matter using powerful and novel analytical methods. The paper describes repeated experiments heating the biomass in a combustion chamber and sampling it via a Potential Aerosol Mass (PAM) reactor into a Thermal desorption Aerosol Gas Chromatograph – Mass Spectrometer (TAG), High-Res AMS and a SMPS. Emissions were sampled unaged and under two different PAM aging conditions. TAG data were analyzed in a number of ways, including for specific eluted compounds, positive matrix factorization of chromatograms, and analysis of chemical fragments from thermal decomposition of particles. These analyses are compared to more 'standard' analyses of bulk aerosol composition from the AMS.*

*The suite of different approaches taken to analyze these data leads to a number of interesting and potentially important conclusions that will be of interest to the broad community interested in emissions from biomass burning and how they evolve in the atmosphere. For example, the emission of aliphatic aldehydes from leaf coating volatilization is nicely supported. The emission and evolution of components contributing mass at m/z 60 in both TAG and AMS spectra receives special attention and evidence for contribution from components formed during oxidation to mass at m/z 60 is given. It does an especially nice job of spanning levels of chemical detail from compound-specific determination using the TAG, to PMF of tag chromatograms to point to compound classes, to the AMS measurements of bulk fragments.*

*Overall, this is a very nicely written and clear paper that makes an important contribution to understanding of a complex and important source of atmospheric aerosol. Therefore, I find it to be suitable for publication in ACP once my concerns are addressed. I have identified a number of points that, when addressed, will help the paper better fit into the existing literature on the topic.*

We thank the reviewer for his/her insight. We address each comment individually below (the reviewer's major and minor points have been numbered for ease of reference). Where appropriate, approximate line numbers corresponding to the edited (with markup) manuscript provided, along with line numbers relative to the section/paragraph number.

### Major points:

**[1]** *While the analytical methods applied here are unique and provide strong insights, I have a concern about how these results can be compared to other 'forms' of biomass combustion, and so I think that more effort should be made to qualify/compare the types of emissions that were sampled. The emphasis in emission generation was clearly on repeatability and consistency, rather than on representativeness, which makes sense for these experiments. However, it would be helpful to put the OA studied here a bit more clearly in the context of 'biomass burning OA (BBOA)', which typically refers to ambient observations of biomass burning emissions emitted from a range of different fuels/types/combustion conditions. In this case, the nature of the 'combustion' that was the source of the sampled aerosols is someone unclear to me. Very small portions of biomass (0.2-0.5 g) were 'combusted' in the chamber, but it is not clear to me if flame was involved, or strictly smoldering, and so how the results might be compared to what might come from a fire. For example, flame typically produces black carbon, was any generated here? The experiments are called 'devolatilization and combustion', but is there any way to classify this combustion more broadly or put it in the context of biomass burning more generally? If not, can anything be said about the representativeness of the emissions from this setup relative to other studies?*

**305** The authors agree this point is important to clarify for future comparisons of lab and field observations. To provide better context for the type of emissions sampled here, we expanded the description of the devolatilization and combustion process in the Materials and Methods section. Specifically, while we had previously specified that smoldering combustion was observed only in the final minute of the heat ramp, we now also clarify that no flaming combustion occurred during any of the experiments (lines 153-154; Section 2.2, Paragraph 2, Lines 5-6)

**310** We also provide a more thorough discussion of the influence of combustion conditions on the relevance of our measurements to real world systems. We provide more detailed discussion in the Conclusion section of the main text (lines 737-748; Section 4, Paragraph 3):

"Based on previous studies, combustion conditions are expected to significantly impact the chemical composition of both primary and secondary BBOA (Ortega et al., 2013; Reece et al., 2017; Weimer et al., 2008; see "AMS Chemical

315 Characterization" in Supplemental Information). The resistive heating technique applied in these experiments allows for the isolation of devolatilization (pre-combustion) and low-temperature ( $\leq 300^{\circ}\text{C}$ ) smoldering conditions, which is difficult to achieve in combustion chambers that require ignition of a flame. For example, Tian et al. designed a chamber that allows the user to control the relative contributions of smoldering and flaming combustion, though smoldering combustion is only achieved in this chamber following the introduction of a flame to the biomass fuel (Tian et al., 2015). The devolatilization and combustion procedure presented here is thus advantageous for investigating aerosol from small masses of biomass fuel under tightly controlled conditions. However, these results alone are likely not representative of many real-world fire systems, where smoldering combustion often occurs alongside flaming combustion. Our results may therefore serve to complement field measurements, where either smoldering or flaming combustion may dominate, as well as laboratory studies where combustion conditions are controlled."

320  
325 In addition, we have added a new section in Supplemental Information ("AMS Chemical Characterization"; see response to Major Comment #2) in which we compare AMS chemical composition to relevant data reported in literature.

330 [2] *The relative change in f60 for the study of Ortega et al. is shown in Fig. 16, but the chemical character of the OA is not compared to that measured in that or other studies, even of the same type of fuel. Several studies have shown that combustion phase/type can have a substantial effect on OA emission properties (Weimer et al. 2008; Reece et al. 2017) and as you noted, observations of SOA production in lab and field studies have been found to be highly variable and distinct. Therefore, to the extent that you can include information about your combustion and the basic characteristics of your emissions, it will enable comparison with existing measurements and analysis.*

335 In addition to expanding the description of the devolatilization/combustion characteristics (see major comment #1), we have reviewed the recommended sources and now discuss them in our expanded analysis. To more thoroughly compare the chemical character of the OA produced here to previous measurements, we have added a section to the Supplemental Information titled "AMS Chemical Characterization." This section includes the following figures:

340

- An average AMS mass spectrum for each fuel at each level of oxidation, as well as difference mass spectra (Figure S13)
- A van Krevelen plot for both heartwood and leaf BBOA (Figure S14)
- Total organics, potassium, and sulfate concentrations (Figure S15)

345 In this section, we discuss the impact of combustion techniques and conditions on the chemical composition of both aged and unaged oak BBOA, contextualizing our results with information from previous studies. We refer to this section in the manuscript in lines 336-339 (Section 3.1, Paragraph 2):

"According to AMS mass spectra, the BBOA measured in these experiments is chemically consistent with BBOA from similar oak fuel sources, though with key differences related to combustion conditions (Cubison et al., 2011; Ortega et al., 2013; Reece et al., 2017; Weimer et al., 2008). Detailed analysis and contextualization of the AMS chemical composition data is provided in Supplemental Information (Section: AMS Chemical Characterization)."

350 [3] *In a similar vein, one of the motivations discussed for the use of the PAM was to understand SOA production, but this is never discussed in the paper, though some evidence is presented in Table S2 that there is SOA production for the wood experiments but not for leaf experiments. These outcomes are of interest in the context of the variability in SOA production discussed above, but also because they may influence interpretation of the 'relative to unaged' presentation of data that is used in a number of figures (e.g. Fig. 3, 16). For example, are changes in fragments/compounds due to 'dilution' of primary OA by SOA, or strictly due to gas-phase or heterogeneous oxidation? This is mentioned in the paper's final paragraph, but it seems at least some further evidence/data could be presented.*

360 Decoupling effects of SOA formation from other processes occurring in the PAM reactor remains challenging and is the subject of ongoing study. However, we have added discussion of the potential relative contributions of other mechanisms (e.g. gas-particle partitioning and heterogeneous vs homogeneous reactions) for certain key species. We address each of these changes below:

- In lines 390-401 (Section 3.2.1, Paragraph 3), we use gas-phase reaction rate constants from literature (Kwok and Atkinson, 1995) to justify the assumption that gas-phase reactions contribute little to overall trends in oak leaf tracer compounds.

365        - Similarly, in lines 407-411 (Section 3.2.1, Paragraph 4, Lines 6-10), we use the literature-reported sinapaldehyde/OH gas phase reaction rate constant (Lauraguais et al., 2015) to justify the assumption that sinapaldehyde decay occurs primarily in the particle phase.

370        - We calculated approximate particle-phase partitioning fractions (Table S12) for levoglucosan in both heartwood and leaf BBOA and include an expanded discussion of levoglucosan phase partitioning in lines 680-694 (Section 3.4, Paragraph 8).

375        - We evaluated phase partitioning for syringol, syringaldehyde, and vanillin, species in the heartwood BBOA that increase in abundance with photochemical aging (e.g. those that may be formed through secondary processes). These calculations are discussed in lines 415-431 (Section 3.2.1, Paragraphs 5-6).

375        **[4]** *The authors rightly point out that the operation of the PAM during experiments was not fully constrained by the SO<sub>2</sub> calibration of integrated OH exposure, but then in the paper use quite tightly constrained values (3.4 and 9.8 days) of equivalent oxidation to describe the aging under the two operation conditions. The fact that there are repeated experiments and repeatable results is great (and difficult to do for biomass burning) and suggests that aging within an experiment type should be consistent. However, your 'sensitivity' analysis (Table S1) shows that actual OH exposure estimates for your experiments may vary by a factor of 5 to 10 given the assumed range of external OH reactivities. Therefore, it seems strange to specify your aging conditions to such a precise degree. I would feel more comfortable if a range of days were reported or if you can find a way to estimate OH reactivity during your experiments (e.g. using published VOC profiles and a tracer ratio?) to better constrain this. At the very least, uncertainty in this value should be clearly stated when it is discussed (e.g. in the context of Table 1), so that the values given are not over-interpreted.*

380        385        This is an excellent comment, and the authors have considered thoroughly the best way to handle this point. To better constrain the equivalent aging times characteristic of our system, we conducted additional experiments to estimate total gas-phase OHR<sub>ext</sub>. A full description of these experiments is provided in Supplemental Information (“Methods: PAM Calibrations and Equivalent Aging Estimations, “Estimation of External OH Reactivity (OHR<sub>ext</sub>)”). In the main text, we discuss these experiments briefly in lines 191-218 (Section 2.3, Paragraphs 3-6).

390        395        400        In these experiments the burn procedure was repeated for both leaf and heartwood fuels, and CO was measured using a trace-level CO monitor. Aerosol was sampled alternately through the PAM reactor and through a bypass line to obtain CO measurements for aged and unaged emissions. During these experiments, the PAM light settings corresponded to approximately 3 equivalent days of aging according to the most recent offline calibration.

405        410        With this method, we found that in both types of BBOA, aged and unaged CO concentrations exhibited little variation, giving OHR<sub>ext</sub> values of 0.56 and 0.52 s<sup>-1</sup>, respectively. To estimate total OHR<sub>ext</sub>, we took the reviewer’s suggestion and estimated typical emissions by scaling published VOC profiles from laboratory studies of oak forest emissions (Burling et al., 2010) to our measured CO concentrations. Using rate constants from the NIST Chemical Kinetics Database, we obtained OHR<sub>ext</sub> for each relevant species, and, taking the sum of all calculated species-specific OHR<sub>ext</sub>, obtain a total OHR<sub>ext</sub> of 2.21 s<sup>-1</sup> and 2.17 s<sup>-1</sup>. We therefore use 2.2 s<sup>-1</sup> in subsequent estimations of OH<sub>exp</sub> and equivalent aging time ranges.

420        425        In addition, to better inform our use of the Oxidation Flow Reactor Exposure Estimator tool, we measured reactor-produced O<sub>3</sub> with no external O<sub>3</sub> addition and report the measurements in the supplemental information (Table S1). Based on these data, and assuming an OHR<sub>ext</sub> of 2.2 s<sup>-1</sup>, we obtain a lower limit for equivalent aging times at each level of oxidation, which we provide in Table 1. We retain the OH<sub>exp</sub> values calculated from the offline SO<sub>2</sub> calibration as the upper limits for each oxidation condition, but we reduce the significant figures in the corresponding equivalent aging times from two to one.

#### Specific points

430        **[5]** *Page 4; Line 138 - Initially it was unclear to me whether this heading referred to separate experiments or one type. As noted above, more of an effort should be made to describe/qualify the approach taken and how the resultant emissions compare to what might come from a fire. In addition, it would make sense to be clear and consistent when using ‘BBOA’ in the context of your experiments.*

To better qualify our experimental setup and approach, we have added expanded discussion of the combustion characteristics of our procedure, contextualizing our results with data from previous studies (see Major Comment #1)

*Page 5; Line 165 - Was level of external O<sub>3</sub> injection always the same?*

415 Yes, the level of external O<sub>3</sub> injection was consistent. In all experiments, we passed 0.4 L min<sup>-1</sup> of oxygen through the lamps, which were held at a constant intensity (lines 171; Section 2.3, Paragraph 1, Line 7).

*Page 6; Line 194-195 - As noted above, this uncertainty should be reflected in estimated atmospheric ages used throughout paper.*

420 We thank the reviewer for this suggestion and believe we have addressed his/her concerns above (see Major Comment #4.)

*Page 7; Line 234-235 - Also related to combustion emission properties. Why are SMPS volumes used and not AMS OA concentrations? For example, if there is a contribution from BC, this will both effect the determination of OA mass by adding to volume, and also potentially affecting DMA sizing. This may not be an issue, but could at least compare AMS OA to SMPS volume?*

425 We used SMPS volumes rather than AMS total OA concentrations because we did not obtain satisfactory AMS data during the first set of TAG experiments (lines 509-521; Section 3.3, Paragraph 2). We do agree that normalizing to AMS total organic concentrations would otherwise be more appropriate, and we plan to do so where possible in all future experiments.

430 We have provided a table in supplemental information (Table S3) with total organic concentrations alongside co-measured SMPS volume concentrations.

*Page 9; Line 298 - Need to be clear that this is referring to relative abundance - important if SOA production is 'diluting' primary species.*

As suggested, we have modified the sentence to specify that this is a relative abundance (lines 376-377; Section 3.2.1, Paragraph 2, Lines 4-5):

435 "Nearly all compounds identified after 35 minutes decrease in relative abundance with photochemical aging."

*Page 9; Line 296 - I noted this included in Supplemental tables, but it might be helpful to translate to effective saturation concentration.*

440 As requested, we have added this information into the main text (now lines 368-371; Section 3.2.1, Paragraph 1, Lines 9-10):

"Based on even-numbered alkane standard injections, compounds eluting after minute 35 exhibit approximate saturation vapor pressures not exceeding that of docosane (approximately  $2.73 \times 10^{-5}$  torr at 25°C), which corresponds approximately to  $\log_{10}(C^*) = 2.76$ "

445 We also include saturation concentration values in our discussion of oak heartwood compound volatilities (lines 403-405; Section 3.2.1, Paragraph 4, Lines 2-4):

"Based on even alkane standard injections, compounds eluting within this time window exhibit approximate vapor pressures within  $4.52 \times 10^{-3}$ - $2.73 \times 10^{-5}$  torr at 25°C ( $\log_{10}(C^*) \approx 4.85$ - $2.76$ ; Table S4 in Supplemental Information; ACD/Labs, 2017)."

450 *Page 9; Line 299 - Where possible (e.g. Fig 3), would be best to include error bars to show inter-test variability. You have done this in some places, but would be good to see it here.*

We thank the reviewer for the suggestion. We initially tried including error bars in this figure, but found that it made the figure difficult to read. For this reason, we included raw chromatographic abundances and errors in the supplemental information (Tables S6 and S7). We now refer the reader to these tables in the caption of figure 3.

455 *Page 10; Line 323-324 - These don't seem to be fully depleted -seems to be 50-100% of relative abundance at the start?*

We have changed "fully depleted" to "depleted" in this sentence (line 417; Section 3.2.1, Paragraph 5, Line 3).

*Page 12; Line 412-413 - A useful comparison to quantify inter-test variability might be to do this calculation on repeated experiments at same loading. E.g., what are dot products between repeated tests at same conditions that are averaged together for other analyses?*

460 We thank the reviewer for the suggestion. We have repeated the procedure and provide the results in supplemental information (Table S9).

*Page 13; Line 425 - Isn't really clear if this is indicating an increase in the presence of material containing m/z 44 that can thermally decompose or an increase in thermal decomposition?*

465 While this is an interesting question, the temperature cycle is consistent from run to run and any change in this signal would be due to a combination of the type of material present and the associated thermal decomposition potential of that material. It has been shown in past work that this signal correlates best with oxygenated OA concentrations (Williams et al. 2016). With the lack of adequate standards, we do not know the relative decomposition potential of all types of OA, and include this point in our discussion of the need for standard calibrations in the Conclusions section of the manuscript (lines 766-774; Section 4, Paragraph 6).

470 The text has been updated to reflect this point (lines 534-538; Section 3.3.1, Paragraph 1, Lines 12-16):

"For both types of BBOA, the decomposition  $m/z$  44 integrated signal increases overall from 0 days to 6-10 days of equivalent aging, indicating an increase in OA material that can thermally decompose with increased PAM oxidation. This trend is consistent with relative increased decomposition of highly oxidized aerosol within the PAM reactor, as was also indicated in previous ambient aerosol observations (Williams et al., 2016)."

475 *Page 13; Line 431 - As noted above, to be most useful, this should be placed in the context of other BBOA measured by AMS. How do these numbers compare to those measured in other studies - e.g. Ortega et al, 2013, Reece et al, 2017*

We thank the reviewer for this suggestion and believe that we have addressed his/her concerns (see Major Comment #3).

480 *Page 13; Line 433-436 - Significant figures not justified (or, really, linear regression advised) for 3 data points unless there is a very strong argument for there being a linear relationship*

In general, we agree with the reviewer, and we reduce the number of significant figures in our regressions to 1. We retain the linear regression because we feel that it serves as a useful comparison between trends in leaf and heartwood BBOA  $m/z$  44 signals.

485 *Page 13; Line 439 - It seems as or more plausible that fragmentation leads to more volatile species that aren't captured by the TAG?*

Implicit in this explanation is that the TAG does not capture the highly volatile products of fragmentation. We have modified the sentence to clarify this point (lines 547-551; Section 3.3.1, Paragraph 2, Lines 6-10):

490 "The non-linear trend in TAG decomposition  $m/z$  44 for leaf BBOA may indicate a shift in the dominant oxidation mechanisms between moderate and high levels of OH within the PAM chamber; at the highest  $\text{OH}_{\text{exp}}$ , primary gas and/or particle-phase components may undergo increased fragmentation, leading to a net decrease in production of the aged OA that thermally decomposes during TAG analysis, along with an increase in highly volatile fragmentation products that are not captured by the TAG."

495 *Page 15; Line 504-505 - This is a good point, but here the distinction may be as much type of emission/combustion as type of biomass, as it appears that at least some OA is from volatilized leaf coating so is not 'burned' (for leaf e.g. Fig. S7)*

We have modified this point to acknowledge the role that combustion characteristics play in measured  $m/z$  60 (lines 621-623; Section 3.4, Paragraph 2, Lines 10-12):

500 "Additionally, the presence of  $m/z$  60 is likely dependent on the combustion characteristics, as combustion processes can influence the emission and phase of different compounds."

Page 15; Line 511-513 - If possible, it would be helpful to quantify (even approximately) the relative amount of material contributing  $m/z$  60 in the compound window vs decomposition window. I take it there is more in the former? The AMS will presumably see a weighted average of the two?

505 We thank the reviewer for this suggestion. We have quantified relative  $m/z$  60 abundances as percentages for both compound and decomposition window signals and provide them in a separate supplemental table (Table S11). Based on these calculations, the AMS likely does measure an approximately weighted average of the two signals, which is displayed in figure 12 (was figure 16 previously).

Minor points

Page 7; Line 219 - data were, not data was

510 "Data was" has been changed to "data were" in this sentence (line 275; Section 2.4.1, Paragraph 3, Line 1) and in subsequent occurrences.

Page 14; Line 461 - I think I know what 'triplicate averages' is meant to say, but can be said more clearly.

We have modified this sentence for clarity (Lines 524-526; Section 3.3.1, Paragraph 1, Lines 2-4):

515 "At each oxidation condition, SICs from the triplicate chromatograms were blank subtracted, normalized to maximum volume concentrations, and averaged to obtain the displayed trace."

Page 15; Line 508 - I think 'distinct' would work better than 'unique'.

As suggested, "unique" has been replaced with "distinct" in this sentence (line 627; Section 3.4, Paragraph 3, Line 4).

Page 15; Line 506-507 - Would be good to point to Fig. 16 here.

520 We now reference figures 11 and 12 (figure 12 was figure 16 previously) in line 626 (Section 3.4, Paragraph 3, Line 3).

Page 17; Line 578-579 - Not sure if a species can be called a 'tracer' (for a primary source) if it is increasing w/ atmospheric processing. At the very least, it's not a tracer of a unique source.

We have replaced "tracers" with "components present in freshly-emitted BBOA" in this sentence (line 723; Section 4, Paragraph 1, Line 6).

525

#### Literature Cited:

Burling, I. R., Yokelson, R. J., Griffith, D. W. T., Johnson, T. J., Veres, P., Roberts, J. M., Warneke, C., Urbanski, S. P., Reardon, J., Weise, D. R., Hao, W. M. and de Gouw, J.: Laboratory measurements of trace gas emissions from biomass burning of fuel types from the southeastern and southwestern United States, *Atmos Chem Phys*, 10(22), 530 11115–11130, doi:10.5194/acp-10-11115-2010, 2010.

Cubison, M. J., Ortega, A. M., Hayes, P. L., Farmer, D. K., Day, D., Lechner, M. J., Brune, W. H., Apel, E., Diskin, G. S., Fisher, J. A., Fuelberg, H. E., Hecobian, A., Knapp, D. J., Mikoviny, T., Riemer, D., Sachse, G. W., Sessions, W., Weber, R. J., Weinheimer, A. J., Wisthaler, A. and Jimenez, J. L.: Effects of aging on organic aerosol from open biomass burning smoke in aircraft and laboratory studies, *Atmos Chem Phys*, 11(23), 12049–12064, 535 doi:10.5194/acp-11-12049-2011, 2011.

Kwok, E. S. C. and Atkinson, R.: Estimation of hydroxyl radical reaction rate constants for gas-phase organic compounds using a structure-reactivity relationship: An update, *Atmos. Environ.*, 29(14), 1685–1695, doi:10.1016/1352-2310(95)00069-B, 1995.

540 Lauraguais, A., Bejan, I., Barnes, I., Wiesen, P. and Coeur, C.: Rate Coefficients for the Gas-Phase Reactions of Hydroxyl Radicals with a Series of Methoxylated Aromatic Compounds, *J. Phys. Chem. A*, 119(24), 6179–6187, doi:10.1021/acs.jpca.5b03232, 2015.

Ortega, A. M., Day, D. A., Cubison, M. J., Brune, W. H., Bon, D., de Gouw, J. A. and Jimenez, J. L.: Secondary organic aerosol formation and primary organic aerosol oxidation from biomass-burning smoke in a flow reactor during FLAME-3, *Atmos Chem Phys*, 13(22), 11551–11571, doi:10.5194/acp-13-11551-2013, 2013.

545 Reece, S. M., Sinha, A. and Grieshop, A. P.: Primary and Photochemically Aged Aerosol Emissions from Biomass Cookstoves: Chemical and Physical Characterization, *Environ. Sci. Technol.*, 51(16), 9379–9390, doi:10.1021/acs.est.7b01881, 2017.

550 Tian, J., Chow, J., Cao, J., Han, Y., Ni, H., Chen, L.-W. A., Wang, X., Huang, R., Moosmüller, H. and Watson, J.: A Biomass Combustion Chamber: Design, Evaluation, and a Case Study of Wheat Straw Combustion Emission Tests, *Aerosol Air Qual. Res.*, 15(5), 2104–2114, 2015.

Weimer, S., Alfarra, M. R., Schreiber, D., Mohr, M., Prévôt, A. S. H. and Baltensperger, U.: Organic aerosol mass spectral signatures from wood-burning emissions: Influence of burning conditions and wood type, *J. Geophys. Res. Atmospheres*, 113(D10), D10304, doi:10.1029/2007JD009309, 2008.

555

560

565

570

### RESPONSES TO REVIEWER 3

Reviewer comments are italicized; author responses follow in normal font.

575 *Fortenberry et al. present chemical composition measurements of photochemically aged laboratory biomass burning organic aerosols (BBOA). BBOA was generated from the combustion of oak leaves and oak wood samples in a burn chamber, then exposed to OH radicals in a Potential Aerosol Mass oxidation flow reactor. Ensemble aerosol mass spectra were obtained with an AMS, and GC-MS samples were obtained with a TAG. The authors used factor analysis to identify characteristic groups of GC effluent signals that behaved differently as a function of OH exposure. In my opinion, the manuscript presents an interesting experiment and application of the measurement techniques that were used to mimic aging of BBOA surrogates. Publication in ACP may be appropriate after consideration of my comments below.*

580 We thank the reviewer for his/her insight and address each comment individually below. Where appropriate, approximate line numbers corresponding to the edited (with markup) manuscript provided, along with line numbers relative to the section/paragraph number.

#### 585 General/Major Comments

1. *Given the goal of using TAG measurements to interpret ensemble/bulk techniques such as the AMS, and given the large number of oxygenated/polar compounds present in BBOA (and oxidized BBOA), it wasn't clear to me why the authors chose not to incorporate the online derivatization technique used in previous TAG measurements (Isaacman et al., 2014), which reports "complete derivatization of [...] alkanoic acids, polyols, diacids, sugars, and multifunctional compounds." In principle, derivatization should offer the following advantages:*
  - a. *improved recovery of methoxyphenols, levoglucosan, and other sugars and primary species that are measured in this work, along with potentially less significant matrix effects (see Comment #2).*
  - b. *recovery of oxidation products formed following OH exposure in the PAM reactor (e.g. dicarboxylic acids) that were not resolved here.*
  - c. *evaluation/supplementation of the thermal decomposition window because the TAG recovery and resolution of highly polar compounds is still low, as implied by discussion in L441-L454 (see Comment #16) and L493-L494. The authors should explain in the manuscript why they chose not to incorporate/adapt the TAG derivatization technique published by Isaacman et al.*

600 Although online derivatization would provide several advantages for measuring both primary and secondary BBOA components, the derivatization technique used in Isaacman et al., 2014 was not used in these experiments for multiple reasons. First, this derivatization technique was developed for a metal filter collection cell and has not been successfully adapted for the impaction CTD cell featured on our system. In fact, the thermal decomposition window is not available when derivatizing since the derivatization agent needs to be purged from the cell and derivatized molecules are refocused on a secondary trap. Through this process, any decomposing material is also purged. Additionally, derivatization may complicate the identification of unknown compounds by altering mass spectral fragmentation patterns. Finally, not all compounds derivatize with 100% efficiency, further complicating quantification efforts. Further study may incorporate evaluation of the metal filter cell and online derivatized measurements to complement decomposition window analysis.

610 As requested, we briefly address the lack of derivatization in the manuscript in lines 267-274 (Section 2.4.1, Paragraph 2):

615 "The TAG system developed by Isaacman et al. features an online derivatization technique designed to improve analysis of oxidized species, including methoxyphenols, levoglucosan, and other compounds unique to BBOA (Isaacman et al., 2014). Although this technique presents multiple analytical advantages, it was developed for a metal filter collection cell and is not suitable for the impactor-style CTD cell used in these experiments. We chose to use the impactor-style CTD cell to allow analysis of the thermal decomposition window, since other collection cells purge this material when transferring to a secondary trap. Additionally, we were interested to identify new molecular marker compounds that could be associated with these source

types. We therefore performed all experiments without sample derivatization prior to chromatographic analysis.”

625 2. *The TAG recovery of the selected tracers is potentially influenced by BBOA matrix effects, which could be either positive or negative in magnitude. Using a different TD-GC/MS system, Lavrich and Hays et al. (2007) showed that the thermal extraction of large PAHs from a soot matrix was hindered. Using a TAG system, Lambe et al. (2010) showed that the recovery of a C<sub>30</sub>D<sub>62</sub> alkane internal standard in a lubricating oil matrix increased by a factor of 2-3 as a function of matrix loading. Matrix effects may be even more significant for the polar analytes measured in BBOA (e.g. methoxyphenols and sugars). Without application of representative internal standards for at least a subset of experiments, in my opinion the authors cannot unambiguously rule out the contribution of matrix effects. For example, in Fig. 3b, the authors show an increase in the abundance of vanillin, syringol, and syringaldehyde when the OH exposure in the PAM reactor is increased to 2-3.4 days. In the manuscript, a plausible formation mechanism for vanillin was provided (Figure S8). The increase in vanillin, other methoxyphenols, and other tracers (including the integrated m/z = 44 SIC) that display similar behavior could also be due to higher concentrations of desorbed primary or secondary organic aerosols that adsorbed onto active sites in the TAG sample transfer path, e.g. the effect observed in Lambe et al. (2010). At the least, the discussion should be revised to acknowledge that the above scenarios can plausibly explain the observed trends regarding increase and decrease in abundance as a function of OH exposure. A more convincing response – which may prove the above hypotheses incorrect – would be to repeat one or two of the combustion experiments, while manually spiking each collected TAG sample with an appropriate set of isotopically labeled standards. For example, there are sugars that are readily available with a range of levels of deuterium-substitution, and I also found suppliers of vanillin-5-d1 and isovanillin-2,5,6-d3.*

630

635

640

645 We thank the reviewer for this insight. While we acknowledge that the impacts of matrix effects cannot be unambiguously ruled out for our experiments, we do not think that the effects observed by Lambe et al. cited by the reviewer can adequately explain our findings.

650 Lambe et al. observed a two-fold increase in C<sub>30</sub>D<sub>62</sub> TAG responses with motor oil co-injected over a range of 0-60 µg, possibly due to greater competition for active sites in the TAG sampling system with greater masses of organic matter (i.e. the motor oil). They also found that uncertainties in TAG responses were large throughout these experiments, and that the effect varied depending on the tracer compound (e.g. the size of the tracer molecule) tested. From SMPS estimated maximum mass concentrations (assuming a typical BBOA density of 1.2 g m<sup>-3</sup>; e.g. Li et al., 2015), we estimate that for each experiment, the TAG collected total particle masses ranging from 6-16 µg for leaf BBOA and 22-36 µg for wood BBOA.

655 Based on the high replicability of our TAG measurements between triplicate experiments within a fuel type and the small ranges of collected masses (relative to 0-60 µg motor oil), we do not expect the effect reported in Lambe et al. to explain the trends observed in our TAG data, especially the eight-fold increase in vanillin abundance. Additionally, based on the results from the previous work cited by the reviewer, we expect matrix effects to be more significant for components with very high molecular masses, e.g. large PAHs and long-chain alkanes, and less so for smaller compounds like syringol, syringaldehyde, and vanillin.

660

665 However, we do agree that the influence of matrix effects should be investigated further to rule out bias in future experiments. Unfortunately, due to time and resource constraints, we were not able to conduct the suggested tracer tests, but these will be incorporated into future combustion experiments. We have therefore added a brief discussion of potential matrix effects to the manuscript (lines 749-759; Section 4, Paragraph 4):

670 “Future work will focus on characterizing sources of bias to improve quantification of material in both the TAG compound and decomposition window. For example, particle matrix effects, whereby certain compounds exhibit enhanced or diminished recovery due to the presence of a particle matrix, have been reported to influence compound responses in previous work with the TAG and other thermal desorption GC systems, particularly for large molecular weight compounds (Lambe et al., 2009; Lavrich and Hays, 2007). Lambe et al. quantified this effect for the TAG by co-injecting a constant C<sub>30</sub> deuterated alkane standard with 0-60 µg motor oil and found that the presence of the motor oil matrix enhanced recovery of the standard by

675 a factor of 2-3 (Lambe et al., 2009). In these experiments, the TAG collected estimated ranges of 6-16  $\mu\text{g}$  particles for leaf BBOA and 22-36  $\mu\text{g}$  particles for heartwood BBOA. Based on these mass ranges, we do not expect these matrix effects to contribute significantly to our results, especially for the lower molecular weight compounds. However, future work will incorporate an evaluation of matrix effects to minimize bias in TAG measurements.”

680 3. *Aerosol loadings corresponding to primary BBOA, oxidized BBOA, and/or SOA formed from oxidation of VOCs/IVOCs in the PAM reactor are not presented. In my opinion this data should be added to provide information about (1) the magnitude of SOA formation and corresponding SOA-to-BBOA ratio (2) phase partitioning of the selected biomass burning tracers. For example:*

685 *a. C23, C25, C29 alkane signals decrease ~60%, ~70%, and ~75% following 9.8 days aging time (Fig. 3a). At an OH exposure of  $\sim 1.1\text{E}12 \text{ molec/cm}^3/\text{sec}$  (8.5 days), Smith et al. (2009) observed ~70% decay of squalane particles subjected to heterogeneous oxidation by OH. Thus, the observed C23, C25, & C29 decay rates are broadly consistent with heterogeneous oxidation in the condensed phase. On the other hand, if the same compounds were oxidized in the gas phase, the observed decay rates should be much faster because the reaction is no longer rate-limited by diffusion of OH to the particle surface. Applying estimated gasphase OH rate constants of  $2.9\text{E-}11$ ,  $3.2\text{E-}11$ , and  $3.8\text{E-}11 \text{ cm}^3/\text{molec/sec}$ , for C23, C25, C29 alkanes (Kwok and Atkinson, 1995) suggests that ~100% of the alkanes should be reacted at only 3.4 days' OH exposure if the reaction occurs in the gas phase. Information about the experimental partitioning of this tracers would provide context for interpreting the observed decay rates.*

690 We are grateful to the reviewer for providing this insight. We agree with the reviewer's analysis of C23, C25, and C29 partitioning, though using the information provided in Kwok and Atkinson, 1995, we obtained slightly different gas-phase OH reaction constants. Still, we found the overall conclusion to be the same: if these compounds were reacting in the gas phase only, they would be entirely depleted at 3 days of equivalent aging. Using parameters from Kwok and Atkinson's work, we also performed a similar analysis to evaluate the gas-phase kinetics of the long-chain aldehydes identified in the leaf BBOA. These findings have been summarized in the manuscript in lines 390-401 (Section 3.2.1, Paragraph 3):

695 “Literature information available for hydrocarbon particle- and gas-phase OH kinetics indicates that the trends observed in leaf BBOA alkanes and aldehydes with  $\text{OH}_{\text{exp}}$  are consistent with heterogeneous OH oxidation. For example, Smith et al. report approximately 70% decay of squalane (a C<sub>30</sub> branched alkane) particles when exposed to an  $\text{OH}_{\text{exp}}$  of  $1.1 \times 10^{12} \text{ molec cm}^{-3} \text{ s}^{-1}$  (8.5 days of equivalent aging; Smith et al., 2009), a figure approximately consistent with the observed C<sub>29</sub> alkane decay of 75% at 6-10 days of equivalent aging. Additionally, based on parameters provided by Kwok and Atkinson, gas-phase OH reaction rate constants at 298K are estimated to be  $2.5 \times 10^{-11}$ ,  $2.7 \times 10^{-11}$ , and  $3.1 \times 10^{-11} \text{ cm}^3 \text{ molec}^{-1} \text{ s}^{-1}$  for C<sub>23</sub>, C<sub>25</sub>, and C<sub>29</sub> alkanes, respectively (Kwok and Atkinson, 1995). Taking these rate constants into account, if purely gas-phase chemistry is assumed, all three alkanes would react nearly 100% before 1-3 days of equivalent aging. A similar analysis on relevant aldehydes gave estimated gas-rate constants of  $2.5 \times 10^{-11}$ ,  $2.8 \times 10^{-11}$ , and  $3.0 \times 10^{-11} \text{ cm}^3 \text{ molec}^{-1} \text{ s}^{-1}$  for C<sub>24</sub>, C<sub>26</sub>, and C<sub>28</sub> aldehydes, respectively (Kwok and Atkinson, 1995), which in all cases would lead to complete depletion by 3.4 days of equivalent aging if gas-phase chemistry is assumed.”

700 *b. Levoglucosan signal decreases ~80% following 9.8 days aging time (Fig. 16). The authors reference literature rate constants of  $3.09\text{E-}13 \text{ cm}^3/\text{molec/sec}$  and  $1.1\text{E-}11 \text{ cm}^3/\text{molec/sec}$ . The levoglucosan decay rate reported in this paper is somewhere in between the referenced literature values. Is it possible that some of the discrepancy is related to phase partitioning? This is alluded to near the end of the paper (L558-L571), but it wasn't clear to me why the authors didn't explore this further by calculating the levoglucosan phase partitioning in the oak leaf and 3 oak wood experiments and comparing to phase partitioning in the literature studies.*

725

730 We thank the reviewer for this insight. Per the reviewer's suggestion, particle-phase fractions for levoglucosan were calculated based on AMS total organic concentrations ( $C_{OA}$ ,  $\mu\text{g m}^{-3}$ ) and levoglucosan effective saturation concentrations ( $C_{LG}$ ,  $\mu\text{g m}^{-3}$ ) based on previous work (Donahue et al., 2006). The equation used to calculate partitioning is now included as equation 1 in the main text. We discuss these calculations and the relative contribution of phase partitioning to our results in lines 680-694:

735 "While levoglucosan decays rapidly in the leaf BBOA with increasing  $\text{OH}_{\text{exp}}$ , levoglucosan in the wood BBOA is depleted more slowly. Levoglucosan is classified as semivolatile (at 25°C,  $p_L^\circ \sim 1.81 \times 10^7$  torr; ACD/Labs, 2017) and is therefore expected to partition between the gas and particle phases. To approximate phase partitioning, particle-phase fractions for levoglucosan ( $\xi_{LG}$ ) were calculated based on AMS total organic concentrations and effective saturation concentrations ( $C_{LG}^*$ ,  $\mu\text{g m}^{-3}$ ) using equation 1. The resulting values and relevant parameters are reported in Table S12. For each fuel, little variance is expected in levoglucosan particle-phase fraction between oxidation conditions, so we conclude that phase partitioning is unlikely to be driving trends in levoglucosan abundances observed in these experiments. Based on the partitioning approximations, the leaf BBOA is expected to contain a higher percentage of levoglucosan in the particle phase than the heartwood BBOA ( $91.1 \pm 1.65\%$  vs  $77.8\% \pm 2.26\%$ ), though in both cases, gas-phase levoglucosan concentrations are likely to remain low. The prevalence of levoglucosan in the particle phase during photochemical aging is consistent with previous laboratory measurements of aged levoglucosan particles (Kessler et al., 2010). Considering that heartwood BBOA exhibited lower total organic concentrations than the leaf BBOA, the slower depletion of levoglucosan in the heartwood samples is perhaps consistent with OH suppression effects, wherein OH experiences increased reactivity with gas-phase species at the particle surface."

740  
745  
750  
755  
760  
765  
770  
775

c. *Increased condensed-phase partitioning of vanillin and other methoxyphenols following potentially significant SOA formation after ~3.4 days aging time (~4.4e11 molec/cm3\*sec) might explain their increase in concentration from 0 to 3.4 days' oxidation. At this approximate OH exposure, the "peak" SOA yield from oxidation of a specific precursor has been observed in previous studies, e.g. Lambe et al. (2012), Ortega et al. (2016). Although vanillin is relatively volatile, without knowing the aerosol loadings and ensuing partitioning, one can hypothesize plausible scenarios to explain some or all of the effect observed in Figure 3b. I encourage the authors to expand their discussion to analyze the observed tracer decay rates in the context of the expected phase partitioning. They already report calculated  $C^*$ 's, which, together with the aerosol loadings provided by AMS, facilitate this discussion. While I don't view it as the authors' responsibility to resolve the discrepancy in reported levoglucosan decay rates, it would certainly increase the impact of the paper if a plausible explanation is possible (L533-L549).*

In addition to expanding discussion on levoglucosan phase partitioning (see above comment), we evaluated phase partitioning of relevant methoxyphenols (syringol, syringaldehyde, and vanillin) using AMS total organic concentrations and effective saturation concentrations. In doing so, we determined that under standard conditions, all three methoxyphenols are expected to exist almost exclusively in the gas phase (Table S12). We therefore agree with the reviewer's suggestion that increased SOA formation with oxidation may be driving these compounds into the particle phase.

The following discussion has been added to the main text (lines 420-431; Section 3.2.1, Paragraphs 6-7):

"To examine the potential impacts of phase partitioning for these compounds, particle-phase fractions for syringol, syringaldehyde, and vanillin ( $\xi$ ) were calculated based on AMS total organic concentrations ( $C_{OA}$ ,  $\mu\text{g m}^{-3}$ ) and effective saturation concentrations ( $C_i^*$ ,  $\mu\text{g m}^{-3}$ ) using the basic partitioning equation (Donahue et al., 2006):

$$\xi_i = \left(1 + \frac{C_i^*}{C_{OA}}\right)^{-1} \quad (1)$$

Resulting particle-phase fractions are tabulated in supplemental information (Table S12). Based on these approximations, syringol, syringaldehyde, and vanillin are expected to partition primarily to the gas phase. For these compounds, the increase in abundances at low-mid levels of oxidation could therefore result from increased SOA formation driving these compounds into the particle phase. This observation is consistent with previous measurements where maximum SOA concentrations were observed at similar levels of  $\text{OH}_{\text{exp}}$  for aerosol generated from oxidation of a single precursor (Lambe et al., 2012; Ortega et al., 2016)."

780

785 4. *Photobleaching of biomass burning particles has reported in previous literatures studies, e.g. Zhao et al., ACP, 2015; Wong et al., ES&T, 2017. The authors should discuss the potential role of 254 nm photolysis in these experiments, especially in regard to degradation of condensed-phase aromatic species that strongly absorb 254 nm radiation and react relatively slowly with OH due to diffusion limitations. Were control experiments conducted with 254 nm radiation (no 185 nm radiation) and no ozone addition to investigate whether photolysis induces changes in BBOA composition?*

790

We did not perform control experiments with only 254 nm radiation, but will do so in future experiments. We agree with the reviewer that more attention should be given to the potential contribution of 254 photolysis and diffusional effects. We therefore provide further discussion to contextualize our results (lines 224-230; Section 2.3, Paragraph 8):

795

800 "Photobleaching of BBOA, particularly at 254 nm, has been reported in previous literature (e.g. Sumlin et al., 2017; Wong et al., 2017; Zhao et al., 2015) and therefore should be considered when estimating oxidative aging. With the spreadsheet provided by Peng et al., we estimate 254 and 185 nm exposure ratios (ratio of photon flux, photons  $\text{cm}^{-2}$ , to  $\text{OH}_{\text{exp}}$ ; Peng et al., 2016) to be  $1.2 \times 10^5 \text{ cm s}^{-1}$  and  $8.1 \times 10^2 \text{ cm s}^{-1}$ , respectively, as a measured internally-generated  $\text{O}_3$  concentration of 1.7 ppm (at the highest PAM UV lamp intensity), a water mixing ratio of 1% (RH = 30%), and assuming a maximum  $\text{OHR}_{\text{ex}}$  value of 1 (Peng et al., 2016). Using Figures 1 and 2 of Peng et al., 2016 to interpret these values, we find that photolysis at both 185 nm and 254 nm is likely less than 10% in both cases."

805 5. *To the extent possible, I recommend that the authors make additional effort to simplify, consolidate, and streamline the results that are presented, so that the reader is not overwhelmed – especially with the PMF results (see Comment #21).*

810 We thank the reviewer for the suggestions for improvement. To improve the readability of our results, we made many of the changes suggested by the reviewer in the technical/minor comments, which we address individually.

#### Technical/Minor Comments

815 6. *L139: Out of curiosity, what factor(s) led to the use of oak leaves and oak wood as opposed to, for example, a soft wood fuel that might have generated a much different range of tracers? Please briefly explain why the chosen systems were studied.*

We chose oak leaves and wood because these fuels are of interest to us in Missouri, which is characterized by oak deciduous forests, and the different fuel fractions represent different types of wildfire or controlled combustion. Ongoing experiments seek to characterize BBOA from various other relevant fuels.

We address our chosen system in lines 139-142 (Section 2.2, Paragraph 1, Lines 1-4):

820 "White oak (*Q. alba*) heartwood and leaves were chosen for these studies due to their high abundance in Missouri and the southeastern U.S. While comparing different tree species is also of interest, two different plant fractions of the same species are studied here to investigate different types of wildfire or controlled combustion processes, some of which may only impact leaf litter-fall and others would have wood available as a fuel."

825 7. *L163: Clarify that the chromate coating increases the electrical conductivity of the chamber, which decreases charge buildup, and consequently loss of charged particles to the walls of the reactor.*

We have modified the description of the chromate coating to provide the appropriate clarification (lines 166-168; Section 2.2, Paragraph 1, Lines 2-4):

830 "The reactor consists of a 13 L cylindrical aluminum chamber coated internally with Iridite 14-2 (MacDermid, Inc., Waterbury, CT), a chromate conversion film designed to decrease charge buildup and thereby inhibit losses of charged particles to the walls of the reactor."

835 8. *L164-L166: State here the range of ozone mixing ratios that were added to the reactor via the ozone chamber, and the range of ozone mixing ratios that were generated inside the reactor via 185 nm irradiance of O<sub>2</sub>.*

840 As requested, we have included the externally added ozone mixing ratio (4 ppm, line 172; Section 2.3, Paragraph 1, Line 8) and the internally produced ozone mixing ratios (0.3-1.7 ppm, line 212; Section 2.3, Paragraph 6, Line 1). Internally produced ozone is also tabulated in supplemental information (Table S1).

845 9. L172: Here, and elsewhere, please be more precise with statements such as "The role of RH in OH-formation...". Changing [H<sub>2</sub>O] does change the rate of OH formation, and from the text, it appears that the authors did manipulate [H<sub>2</sub>O]. Changing RH by itself, however – for example, changing the temperature inside the reactor – does not change the rate of OH production.

850 We altered the wording as suggested to provide clarity (lines 177-179; Section 2.3, Paragraph 1, Lines 13-15):

855 "The reactor water concentration, and therefore RH, was altered by controlling N<sub>2</sub> flow through a Nafion membrane humidifier (Perma Pure LLC, Lakewood, NJ). The role of water concentration in OH formation is discussed in detail in Supplemental Information (Method: PAM Calibrations and Figure S3)."

860 10. *L183-L195: It wasn't clear why the authors didn't simply add SO<sub>2</sub> during a "representative" combustion experiment to conduct an online OH exposure calibration in the presence of (I)VOCs that might have suppressed OH. I would certainly encourage this, if practical, as this approach should introduce less uncertainty than attempting to apply the OH exposure estimator when the OH reactivity of the biomass smoke emissions is not known.*

865 We did not add SO<sub>2</sub> during a representative experiment for several reasons. First, we had concerns about the impacts of SO<sub>2</sub> on the chemical pathways occurring during atmospheric aging. Previous work demonstrates that addition of SO<sub>2</sub> can accelerate heterogeneous reactions of OH with organic aerosol by reacting with peroxy radicals to produce alkoxy radicals, propagating a chain reaction (Richards-Henderson et al., 2016). Additionally, long-chain aliphatics, particularly alkenes and fatty acids, have been observed to react with SO<sub>2</sub> to create long-chain organosulfate molecules (Passananti et al., 2016). Second, the sulfuric acid created in the PAM reactor tends to damage inert coatings on the equipment used in these experiments (Williams et al., 2016).

870 With additional CO measurements (described in Supplemental Information: Methods: PAM Calibrations and Equivalent Aging Estimations, "Estimation of External OH Reactivity (OHR<sub>ext</sub>)"), we have attempted to better constrain the calibration. However, in future experiments, we hope to directly measure both total VOCs and concentrations of specific VOCs to obtain a more quantitative calibration.

875 11. *L282: I suggest replacing "determined" with "inferred" or similar.*

880 As suggested, "determined" has been replaced with "inferred" in this sentence (now line 356; Section 3.2, Paragraph 2, Line 8).

885 12. *L309: This wording is confusing. Were oak leaves placed in a solvent to extract compounds on the surface of the leaves, and was this extract then injected into the TAG CTD? If so, please rewrite the sentence to clarify. What solvent(s) were used?*

The wording here was altered for clarity (lines 385-389; Section 3.2.1, Paragraph 2, Lines 13-17):

885

"To confirm the presence of aldehydes in the leaf waxes, solvent extractions were performed on oak leaves and were manually injected onto the TAG CTD cell (Method: Oak Leaf Solvent Extractions and Figure S8 in Supplemental Information). Analysis of these extractions confirm that the aldehydes are present in the leaf wax prior to devolatilization and combustion."

890

All details regarding oak leaf solvent extractions are provided in Supplemental Information in the section titled "Method: Oak leaf solvent extractions."

895

13. *L316-L318: It's true that sinapaldehyde signal decays more quickly than other tracers (e.g. alkanes), but ~70% decay over 3.4 days' aging is still slow in the context of gas phase oxidation rates – this corresponds to an effective rate constant of ~2.7E-12 cm<sup>3</sup> /molec/sec, whereas, for example, the gas-phase OH rate constant of syringol is 8.5E- 11 cm<sup>3</sup> /molec/sec (Lauraguais et al., 2015).*

900

We have modified the manuscript to include relative information on the reaction rate constants of sinapaldehyde (lines 407-411; Section 3.2.1, Paragraph 4, Lines 6-10):

905

"Of the compounds examined, sinapaldehyde decays most rapidly in the PAM reactor, with the normalized average integrated peak area decreasing by approximately 70% from 0 days to 2-3 days of equivalent aging (Figure 3b). Based on a rapid gas-phase OH reaction rate constant of  $2.7 \times 10^{-12}$  cm<sup>3</sup> molec<sup>-1</sup> s<sup>-1</sup> (Lauraguais et al., 2015), the observed sinapaldehyde decay is likely occurring in the particle phase."

910

14. *L387-L395: This paragraph seems out of place here, I would consider paraphrasing and moving to Conclusions.*

As suggested, this paragraph has been moved to the Conclusions section (now lines 728-736; Section 4, Paragraph 2).

915

15. *L417: What is the signal-to-noise ratio for the m/z = 44 decomposition SICs? I understand that the SIC's presented are background corrected – how large are gas-phase CO<sub>2</sub> + backgrounds compared to the background + sample m/z = 44 SIC's? This might be useful information to add to the Supplement.*

920

We thank the reviewer for this suggestion. We have incorporated raw m/z 44 background signals and example decomposition m/z 44 SICs for each fuel type into a new supplemental figure (Figure S16).

925

16. *L441-L454 and Figure 10: Implicit in this discussion is the observation that TAG recovery of highly oxidized/oxygenated species is low (even with inclusion of the thermal decomposition window). One or two sentences should be added that states this explicitly. Another point that should be made is that this attempt at a direct f43 and f44 comparison assumes AMS flash vaporization at T = 600 deg C and TAG thermal decomposition at T < 310 deg C produce the same m/z = 43 and m/z = 44 ion signals. It's not clear to me that this assumption is justified, but at the least, this assumption should also be stated explicitly.*

The purpose of this figure is to suggest that inclusion of the thermal decomposition window facilitates more thorough TAG analysis of oxidized OA. We provide AMS f43 and f44 for comparison because this is a well-established technique for interpreting OA oxidative evolution.

930

Implicit in the interpretation of this figure is that the m/z 43 and m/z 44 detected by the TAG and the AMS are similar enough to merit some form of comparison, at least in how the signals trend with oxidative aging. However, we wish to clarify that this comparison does not entail that f43 and f44 measurements are the same between the two instruments (hence the distinct axes for both TAG and AMS f43 and f44).

The reviewer's comments have been considered, and lines 564-570 (Section 3.3.1, Paragraph 3, Lines 11-17) now read:

935 "In general, the TAG fractions tend to fall to the left of AMS  $f_{44}$  vs  $f_{43}$  data points, indicating that the TAG excels at throughput of less-oxygenated hydrocarbon OA and struggles with throughput of oxidized species in the compound window. However, the increase in TAG  $f_{44}$  with inclusion of decomposition window material shows a clearer oxidation trend that is in greater agreement with the AMS oxidation trend. This interpretation implies that the  $m/z$  43 and  $m/z$  44 signals obtained in the TAG decomposition window from sample thermal desorption at 310°C is similar in nature to material flash-vaporized at 600°C in the AMS."

940 17. *L483-L489: Consider also moving this to Conclusions.*

This paragraph has been removed in favor of a more thorough discussion of thermal decomposition window analysis in the conclusion section (lines 766-774; Section 4, Paragraph 6).

945 18. *L539-L549: In my opinion, Lai et al.'s explanation for discrepancy in levoglucosan oxidation kinetics requires two unlikely scenarios: 5 a. using  $m/z$ 144 rather than  $m/z$ 162 would bias  $kLG$  ~ 30x too low -- Fortenberry et al.'s measurements are not subject to mass spectra interference either, and their levoglucosan decay rate is much closer to Kessler et al. than than Hennigan/Lai et al. (L564). A calculated levoglucosan + OH rate constant of 2.21E-13 cm<sup>3</sup>/molec/sec (Bai et al., 2013), which is based on a theoretical study, may help put the different results in context. OR b. oxidation kinetics of OH + levoglucosan (or other model organics) are not firstorder with respect to OH. Previous studies suggest otherwise (e.g. Renbaum and Smith, 2011). I don't think it benefits the discussion in this paper to cite someone else's (in my opinion) incomplete explanation. I would consider removing it.*

950 955 We thank the reviewer for this insight. In the heartwood BBOA, the kinetics do agree best with those presented by Kessler et al., but in the leaf BBOA, the kinetics are most similar to those of Hennigan et al./Lai et al. Because we do not believe we have an adequate explanation for this discrepancy, the goal of this discussion was to investigate all potential explanations currently available in the literature. Therefore, we retain the explanation provided in Lai et al. because we believe it provides additional context for discrepancies in literature-reported levoglucosan kinetics, though we clarify that our chromatographic methods are not subject to the same mass spectral interferences (lines 673-674; Section , Paragraph 7, Lines 960 14-15):

965 "However, our chromatographic methods are not subject to this mass spectral interference, and in the case of the heartwood BBOA, the TAG-measured levoglucosan decay matches the decay predicted by Kessler et al."

970 19. *Figure 2 and related text: It is hard to distinguish the multiple shades of green in Fig. 2a, and for some compounds it is hard to distinguish changes in relative abundance between chromatograms representing "3.4 days" and "9.8 days". Please consider changing the colors in Fig. 2a. Additionally, consider removing the "3.4 days" TIC from Figs. 2a and 2b – this figure seems to be a general, "big picture" type of plot, so this would simplify the chromatogram without changing the take-home points.*

975 980 The color scheme has been changed to teal, purple, and pink in all leaf BBOA figures. Because we want to demonstrate visually that a select few compounds may increase in abundance with photochemical aging, we retain the trace for low-mid level of oxidation in the figure. However, we believe the change in color scheme greatly improves figure readability for the leaf BBOA data.

20. *Figure 3 and related text: Please add a subpanel plotting the concentrations of organics and any relevant inorganic species (e.g. K<sup>+</sup>) measured by AMS following OH exposure in the PAM reactor.*

985 Since the focus of this figure was intended to be solely on trends in TAG species, and because AMS total organics are presented in later figures (e.g. Figure 12), we did not include these species in Figure 3a and 3b. However, we have incorporated total organics, potassium (K<sup>+</sup>), and sulfate (SO<sub>4</sub><sup>2-</sup>) concentrations, which were the most abundant species in our samples, in a supplemental plot (Figure S15).

21. *Figures 4-5, Figures 6-7, Figures 11-12, Figures 13-14: I find these figures to be complex and overwhelming. I found it difficult to quickly "match up" 37 sets of chromatograms and mass spectra (15 + 18 + 4) for each*

990 PMF factor across separate figures as is currently presented. In my opinion, reorganizing these figures to put the mass spectra next to their corresponding chromatograms would improve their clarity and usefulness.

995 Here is one idea for consideration:

995 Figs. 4, 6, 11, 13: Put each factor "TIC" for 0, 3.4 days, 9.8 days on the same x-axis, (as was done in Fig. 2). Choose a three colors, one each for 0, 3.4, 9.8 days, that are shared across all factors. Then place the corresponding mass spectra shown in Figs. 5, 7, 12, 14 to the right of the TICs. This modification would: (i) reduce the number of "PMF figures" from 8 to 4 (ii) remove the number of subpanels in Figs. 4, 6, 11, 13 by 3x (iii) allow enough room to put the mass spectra from Figs. 5, 7, 12, 14 to the right of their chromatograms 1000 6 (iv) make it unnecessary to use unique colors for each factor in attempt to match up the chromatograms and mass spectra across figures. If this is not agreeable, the authors might consider just labeling the factors in Figs. 4, 6, 11, 13 and moving the mass spectral figures (5, 7, 12, 14) to the Supplement. This would save space/publication costs in the main part of the manuscript without making it any more difficult to "match up" the chromatograms and spectra.

1005 To improve readability, we modified all PMF figures according to the reviewers first suggestion: time series and mass spectra for each factor are now presented side-by-side. This change has allowed for consolidation of PMF mass spectra and time series figures into one figure (Figures 4, 5, 9, and 10).

1010 22. Figure S13: The caption states 15 micrograms of levoglucosan and 5 micrograms of quinic acid were injected. That seems like a very large analyte mass for a single compound injection – is there any chance this is a typo, and that the injected quantities were actually 15 and 5 nanograms?

1015 This mass was not a typo. We experienced difficult single-component throughput of the injected levoglucosan and quinic acid standards, necessitating much larger injected masses. The mass injected here is much larger than found in the samples of interest, and the signal is larger than would be necessary as seen with peak "frunting" that appears in these chromatograms, a sign that excess mass was injected. While significantly lower concentrations can be observed, poor transfer of highly oxidized standard compounds from the CTD cell to the column has been reported as a persistent problem in previous TAG literature (Williams et al., 2006), spurring the development of *in situ* derivatization methods (Isaacman et al., 2014), as discussed previously. We expect that, as reported for previous TAG measurements, a particle matrix improves throughput of these oxidized compounds compared to liquid standard injections (Lambe et al., 2009). Thus, 1020 while the standards presented here are sufficient for identification of compound retention time, they are not adequate for mass calibration of levoglucosan or quinic acid. Ongoing work focuses on better characterizing particle matrix effects for BBOA compounds of interest and improving TAG mass calibration methods.

#### Literature Cited:

1025 1. Donahue, N. M., Robinson, A. L., Stanier, C. O. and Pandis, S. N.: Coupled Partitioning, Dilution, and Chemical Aging of Semivolatile Organics, *Environ. Sci. Technol.*, 40(8), 2635–2643, doi:10.1021/es052297c, 2006.

1030 2. Isaacman, G., Kreisberg, N. M., Yee, L. D., Worton, D. R., Chan, A. W. H., Moss, J. A., Hering, S. V. and Goldstein, A. H.: Online derivatization for hourly measurements of gas- and particle-phase semi-volatile oxygenated organic compounds by thermal desorption aerosol gas chromatography (SV-TAG), *Atmos Meas Tech*, 7(12), 4417–4429, doi:10.5194/amt-7-4417-2014, 2014.

Kessler, S. H., Smith, J. D., Che, D. L., Worsnop, D. R., Wilson, K. R. and Kroll, J. H.: Chemical Sinks of Organic Aerosol: Kinetics and Products of the Heterogeneous Oxidation of Erythritol and Levoglucosan, *Environ. Sci. Technol.*, 44(18), 7005–7010, doi:10.1021/es101465m, 2010.

1035 Kwok, E. S. C. and Atkinson, R.: Estimation of hydroxyl radical reaction rate constants for gas-phase organic compounds using a structure-reactivity relationship: An update, *Atmos. Environ.*, 29(14), 1685–1695, doi:10.1016/1352-2310(95)00069-B, 1995.

1040 Lambe, A. T., Logue, J. M., Kreisberg, N. M., Hering, S. V., Worton, D. R., Goldstein, A. H., Donahue, N. M. and Robinson, A. L.: Apportioning black carbon to sources using highly time-resolved ambient measurements of organic molecular markers in Pittsburgh, *Atmos. Environ.*, 43(25), 3941–3950, doi:10.1016/j.atmosenv.2009.04.057, 2009.

1045 Lavrich, R. J. and Hays, M. D.: Validation studies of thermal extraction-GC/MS applied to source emissions aerosols. 1. Semivolatile analyte-nonvolatile matrix interactions, *Anal. Chem.*, 79(10), 3635–3645, doi:10.1021/ac0623282, 2007.

1050 Li, C., Ma, Z., Chen, J., Wang, X., Ye, X., Wang, L., Yang, X., Kan, H., Donaldson, D. J. and Mellouki, A.: Evolution of biomass burning smoke particles in the dark, *Atmos. Environ.*, 120(Supplement C), 244–252, doi:10.1016/j.atmosenv.2015.09.003, 2015.

Passananti, M., Kong, L., Shang, J., Dupart, Y., Perrier, S., Chen, J., Donaldson, D. J. and George, C.: Organosulfate Formation through the Heterogeneous Reaction of Sulfur Dioxide with Unsaturated Fatty Acids and Long-Chain Alkenes, *Angew. Chem. Int. Ed.*, 55(35), 10336–10339, doi:10.1002/anie.201605266, 2016.

1055 Peng, Z., Day, D. A., Ortega, A. M., Palm, B. B., Hu, W., Stark, H., Li, R., Tsigaridis, K., Brune, W. H. and Jimenez, J. L.: Non-OH chemistry in oxidation flow reactors for the study of atmospheric chemistry systematically examined by modeling, *Atmos. Chem. Phys.*, 16(7), 4283–4305, doi:10.5194/acp-16-4283-2016, 2016.

Richards-Henderson, N. K., Goldstein, A. H. and Wilson, K. R.: Sulfur Dioxide Accelerates the Heterogeneous Oxidation Rate of Organic Aerosol by Hydroxyl Radicals, *Environ. Sci. Technol.*, 50(7), 3554–3561, doi:10.1021/acs.est.5b05369, 2016.

1060 Smith, J. D., Kroll, J. H., Cappa, C. D., Che, D. L., Liu, C. L., Ahmed, M., Leone, S. R., Worsnop, D. R. and Wilson, K. R.: The heterogeneous reaction of hydroxyl radicals with sub-micron squalane particles: a model system for understanding the oxidative aging of ambient aerosols, *Atmos. Chem. Phys.*, 9(9), 3209–3222, doi:10.5194/acp-9-3209-2009, 2009.

Sumlin, B. J., Pandey, A., Walker, M. J., Pattison, R. S., Williams, B. J. and Chakrabarty, R. K.: Atmospheric Photooxidation Diminishes Light Absorption by Primary Brown Carbon Aerosol from Biomass Burning, *Environ. Sci. Technol. Lett.*, doi:10.1021/acs.estlett.7b00393, 2017.

1065 Williams, B. J., Goldstein, A. H., Kreisberg, N. M. and Hering, S. V.: An In-Situ Instrument for Speciated Organic Composition of Atmospheric Aerosols: Thermal Desorption Aerosol GC/MS-FID (TAG), *Aerosol Sci. Technol.*, 40(8), 627–638, doi:10.1080/02786820600754631, 2006.

Williams, B. J., Zhang, Y., Zuo, X., Martinez, R. E., Walker, M. J., Kreisberg, N. M., Goldstein, A. H., Docherty, K. S. and Jimenez, J. L.: Organic and inorganic decomposition products from the thermal desorption of atmospheric particles, *Atmos. Meas. Tech.*, 9(4), 1569–1586, doi:10.5194/amt-9-1569-2016, 2016.

1070 Wong, J. P. S., Nenes, A. and Weber, R. J.: Changes in Light Absorptivity of Molecular Weight Separated Brown Carbon Due to Photolytic Aging, *Environ. Sci. Technol.*, 51(15), 8414–8421, doi:10.1021/acs.est.7b01739, 2017.

Zhao, R., Lee, A. K. Y., Huang, L., Li, X., Yang, F. and Abbatt, J. P. D.: Photochemical processing of aqueous atmospheric brown carbon, *Atmos. Chem. Phys.*, 15(11), 6087–6100, doi:10.5194/acp-15-6087-2015, 2015.

**Bulk and Molecular-Level Characterization of Laboratory-Aged Biomass Burning Organic Aerosol from Oak Leaf and Heartwood Fuels**

1075 Claire F. Fortenberry<sup>1</sup>, Michael J. Walker<sup>1</sup>, Yaping Zhang<sup>1</sup>, Dhruv Mitroo<sup>1,a</sup>, William H. Brune<sup>2</sup>, Brent J. Williams<sup>1</sup>

<sup>1</sup> Department of Energy, Environmental, and Chemical Engineering, Washington University in Saint Louis, Saint Louis, MO 63130, USA

<sup>2</sup> Department of Meteorology and Atmospheric Science, Pennsylvania State University, State College, PA 16801, USA

1080 <sup>a</sup>Now at the Department of Atmospheric Sciences, Rosenstiel School of Marine and Atmospheric Sciences, University of Miami, Miami, FL 33149, USA

*Correspondence to:* Brent J. Williams (brentw@wustl.edu)

**Abstract.**

1085 The chemical complexity of biomass burning organic aerosol (BBOA) greatly increases with photochemical aging in the atmosphere, necessitating controlled laboratory studies to inform field observations. In these experiments, BBOA from American white oak (*Quercus alba*) leaf and heartwood samples was generated in a custom-built emissions and combustion chamber and photochemically aged in a Potential Aerosol Mass (PAM) flow reactor. A Thermal desorption Aerosol Gas chromatograph (TAG) was used in parallel with a high-resolution time-of-flight Aerosol Mass Spectrometer (AMS) to analyze BBOA chemical composition at different levels of photochemical aging. Individual 1090 compounds were identified and integrated to obtain relative decay rates for key molecular components. A recently-developed chromatogram binning positive matrix factorization (PMF) technique was used to obtain mass spectral profiles for factors in TAG BBOA chromatograms, improving analysis efficiency and providing a more complete determination of unresolved complex mixture (UCM) components. Additionally, the recently characterized TAG decomposition window was used to track molecular fragments created by the thermal decomposition of thermally 1095 labile BBOA during sample desorption. We demonstrate that while most components of primary BBOA decrease with photochemical aging, certain components eluting within the TAG thermal decomposition window instead increase. Specifically, the increasing trend in decomposition  $m/z$  44 ( $\text{CO}_2^+$ ) signals formation of secondary organic aerosol (SOA) in the PAM reactor. Sources of  $m/z$  60 ( $\text{C}_2\text{H}_4\text{O}_2^+$ ), typically attributed to freshly-emitted BBOA in AMS field 1100 measurements, were also investigated. From the TAG chemical speciation and decomposition window data, we observed a decrease in  $m/z$  60 with photochemical aging due to the decay of anhydrosugars (including levoglucosan) and other compounds, as well as an increase in  $m/z$  60 due to the formation of thermally labile organic acids within the PAM reactor, which decompose during TAG sample desorption. When aging both types of BBOA (leaf and wood), the AMS data exhibit a combination of these two contributing effects, causing limited change to the overall  $m/z$  60 signal. Our observations demonstrate the importance of chemically-specified data in fully understanding bulk aerosol 1105 measurements provided by the AMS in both laboratory and field studies.

**1 Introduction**

Atmospheric particulate matter (PM) negatively affects human health (e.g. Kampa and Castanas, 2008), impedes visibility (e.g. Appel et al., 1985), and ~~can impact~~impacts the global energy balance through direct radiative forcing or by acting as cloud condensation nuclei (e.g. Kanakidou et al., 2005). Organic aerosol (OA) ~~particles~~ composes 20-90% of submicron PM (PM<sub>1</sub>) ~~and may consist and is composed~~ of thousands of distinct organic compounds (Goldstein and Galbally, 2007; Ng et al., 2010; Zhang et al., 2007). Given the multitude of organic compounds in the atmosphere and the numerous chemical reactions they can experience during atmospheric processing (e.g. Goldstein and Galbally, 2007; Kroll et al., 2009), laboratory studies are needed to obtain a complete understanding of the chemical composition and oxidative evolution of source-specific primary OA (POA, aerosol emitted directly into the atmosphere) and secondary OA (SOA, formed from gas-phase material that partition into the particle phase following photooxidation) components.

Biomass burning organic aerosol (BBOA) may contribute up to 90% of global combustion OA and 75% of combustion POA (Bond et al., 2004; May et al., 2013). Previous molecular-level BBOA studies over the past several decades have focused on the chemical composition of primary emissions (e.g. Fine et al., 2002; Oros and Simoneit, 1999; Rogge et al., 1998; Simoneit et al., 2000). In recent years, improved understanding of SOA formation in BBOA plumes has motivated the use of oxidation chambers in laboratory BBOA experiments (e.g. Cubison et al., 2011; Grieshop et al., 2009; Ortega et al., 2013). Some of these BBOA photooxidation studies have demonstrated that OA production can exceed decay under certain conditions due to oxidation and phase partitioning of gas-phase semivolatile and intermediately volatile compounds (SVOCs and IVOCs, respectively) (Grieshop et al., 2009). Other field measurements indicate minimal OA enhancement with aging of primary biomass plumes (Capes et al., 2008). During the third Fire Lab at Missoula Experiment (FLAME-3) campaign (2013), OA enhancements following photooxidation were shown to vary widely depending on the biomass source; while BBOA from some sources doubled in mass after photochemical aging, other types of BBOA were depleted (Ortega et al., 2013). The variation in OA enhancement observed by Ortega ~~et al.~~ et al. in the FLAME-3 study suggests that the amount of SOA from biomass emissions depends on the fuel type, illustrating the need for source-specific oxidation studies to investigate reactions and products leading to SOA formation.

Many previous BBOA oxidation studies (e.g. Grieshop et al., 2009; Ortega et al., 2013) have utilized a High-Resolution Time-Of-Flight Aerosol Mass Spectrometer (HR-ToF-AMS, Aerodyne, Inc., Billerica, MA). The Aerosol Mass Spectrometer (AMS) was developed to obtain chemical information on bulk aerosol including total mass concentrations and high-resolution ion signals, allowing for determination of bulk aerosol chemical composition (Canagaratna et al., 2007; DeCarlo et al., 2006). Hydrogen-to-carbon ratios (H:C) and oxygen-to-carbon ratios (O:C) can also be calculated using high-resolution AMS data, which are incorporated into estimations of an average carbon oxidation state ( $\overline{OS}_C \approx 2 \times H:C - O:C$ ; Kroll et al., 2011). Although the AMS provides real-time measurements of ensemble-averaged properties for submicron non-refractory aerosol, it does not achieve molecular speciation and thus cannot be used to identify individual compounds present in OA. Typical AMS BBOA studies use  $m/z$  60 ( $C_2H_4O_2^+$ ) and  $m/z$  44 ( $CO_2^+$ ) signals to quantify primary and aged emissions, respectively (e.g. Cubison et al., 2011; Ng et al., 2010, 2011). Levoglucosan, a cellulose decomposition product often used as a molecular tracer for freshly-emitted

1145 BBOA (e.g. Simoneit et al., 1999, 2004), is frequently considered to be a primary contributor to  $m/z$  60 in AMS laboratory and field studies (e.g. Lee et al., 2010; Ng et al., 2011b). However, while levoglucosan has traditionally been understood to remain stable over relevant timescales (Fraser and Lakshmanan, 2000; Locker, 1988; Simoneit et al., 1999), multiple laboratory studies suggest that hydroxyl radical ( $\text{OH-OH}$ )-driven levoglucosan decay occurs at a timescale similar to transport and deposition timescales (Hennigan et al., 2010; Hoffmann et al., 2010; Lai et al., 2014). Additionally, recent measurements demonstrate that  $m/z$  60 abundances may remain above background levels with sufficient atmospheric processing, suggesting that not all  $m/z$  60 originates from BBOA (Cubison et al., 2011; 1150 Ortega et al., 2013). These two considerations highlight the need for *in situ* molecular speciation measurements to complement bulk aerosol chemical data supplied by the AMS.

1155 The Thermal desorption Aerosol Gas chromatograph (TAG) pairs automated aerosol collection and thermal desorption with gas chromatography-mass spectrometry (GC-MS), providing molecular level speciation with *in situ* analysis and hourly time resolution (Williams et al., 2006). The TAG has been used in field studies to identify molecular tracers in ambient air and to link different chemical profiles to unique sources (e.g. Kreisberg et al., 2009; Lambe et al., 2009; Williams et al., 2007, 2010, 2014; Worton et al., 2011; Zhang et al., 2014, 2016). The TAG is capable of providing spiculated compound measurements for approximately 20% of total organic aerosol mass on average, depending on the type of aerosol collected (Williams et al., 2006). While the TAG reliably detects a high fraction (up to 100%) of hydrocarbon OA mass, which is typical of POA, the analyzed fraction of oxidized OA mass is often much lower 1160 (Williams et al., 2010, 2016; Zhang et al., 2014). This discrepancy is attributed to low mass throughput of oxidized species through the 30 m non-polar GC capillary column (Williams et al., 2006, 2016) and presents a disadvantage for TAG analysis of oxidized components typical of SOA.

1165 Recent advances have expanded the TAG's analytical capability. Traditional gas chromatography utilizes a solvent delay to prevent detector damage from large solvent or water signals. In the TAG, much of the solvent can be purged prior to sample injection, and the solvent delay is no longer applied. The lack of a solvent delay allows volatile components and aerosol thermal decomposition products to reach the detector during thermal sample desorption (5-15 minutes of TAG GC program) from the TAG collection cell to the GC column. The mass-spectral signal within this period, called the thermal decomposition window, typically features an air signal (e.g.,  $m/z$  32 for  $\text{O}_2^+$ ,  $m/z$  40 for  $\text{Ar}^+$ ,  $m/z$  44 for  $\text{CO}_2^+$ ), but can also contain ions characteristic of decomposing nitrates ( $m/z$  30 for  $\text{NO}^+$ ,  $m/z$  46 for  $\text{NO}_2^+$ ), sulfates ( $m/z$  48 for  $\text{SO}^+$ ,  $m/z$  64 for  $\text{SO}_2^+$ ), and organics ( $m/z$  44 for  $\text{CO}_2^+$ ). These ion signals were shown to correlate with corresponding AMS ions for ambient data collected during the Saint Louis Air Quality Regional Study in 2013 (Williams et al., 2016). However, because the TAG thermal decomposition window has only recently been used to analyze ambient data, more laboratory studies are needed to explore the thermal decomposition products of OA from unique sources.

1175 In this work, we present results from laboratory studies aimed at characterizing BBOA chemical composition using both the TAG compound window (minutes 20-55 of the chromatogram; Figure 1) and the TAG thermal decomposition window (minutes 6-16 of the chromatogram; Figure 1) in parallel with an AMS. A custom-built emissions and combustion chamber was used to generate BBOA, and a Potential Aerosol Mass (PAM) oxidative flow reactor (OFR),

which can mimic up to 16 days of atmospheric aging with residence times on the order of 100 seconds (Kang et al., 1180 2007; Lambe et al., 2011), was used to oxidize laboratory-generated BBOA plumes at different levels of accelerated photochemistry. Our experiments addressed three primary objectives. First, the chemical composition of laboratory-generated BBOA was explored to identify molecular tracers from the leaf and heartwood of the American white oak (*Quercus alba*). Recently developed chromatogram-binning Positive Matrix Factorization (PMF) techniques (Zhang et al., 2014, 1185 2016) were applied to the TAG compound window to determine the prevalence of different compound classes and functionalities unique to BBOA from each fuel type. Trends in compounds and compound classes of interest with oxidation were evaluated using both individual compound integrations and chromatogram binning PMF results. Second, the TAG thermal decomposition window was used to investigate how the chemical composition of thermally decomposing BBOA varies with PAM aging. Concurrent AMS measurements were taken to complement TAG decomposition window data, providing  $\overline{OS}_C$  estimations and high-resolution ion signals for bulk BBOA samples. 1190 These AMS parameters were used to inform interpretation of TAG decomposition ion signals, particularly the variation of TAG decomposition  $m/z$  44 and  $m/z$  60 signals with extent of oxidation in the PAM chamber. Additionally, chromatogram-binning PMF techniques (Zhang et al., 2014, 2016) were applied to the decomposition window to 1195 investigate the presence and covariance of key ion signals. Finally, trends in TAG and AMS  $m/z$  60 signals with PAM aging were explored to evaluate the utility of  $m/z$  60 as a tracer for freshly-emitted BBOA. We present evidence that, depending on biomass source and atmospheric conditions, a significant fraction of AMS  $m/z$  60, which is typically used to track primary BBOA in the atmosphere, may be attributed to aged OA mass.

## 2 Materials and Methods

### 2.1 Emissions and Combustion Chamber

1200 A flow diagram of the experimental setup and a diagram of the custom-built emissions and combustion chamber are given in Supplemental Information (Figures S1 and S2, respectively). [A complete description of the emissions and combustion chamber is available elsewhere \(Mellott, 2012\)](#). The chamber is a rectangular 1.48 m<sup>3</sup> chamber made of  $\frac{1}{4}$ " thick tempered glass panels secured by aluminum framing (80/20, Inc., Columbia City, IN). The chamber is divided into two compartments, separated by a sheet of aluminum serving as a baffle with a central hole 3 cm in diameter. In the first compartment, biomass samples are resistively heated in PID-controlled stainless steel cups installed along the chamber floor. The second compartment serves as a mixing chamber from which primary gases and particles are sampled at 10 L min<sup>-1</sup>. Air was treated with a HEPA filter (Pall Corporation, Port Washington, NY) and a hydrocarbon trap (Model BHT-4, Agilent Technologies, Santa Clara, CA), then supplied to the heating compartment of the chamber to promote consistent mixing. Both compartments are extensively vented between experiments to clear the chamber of gases and particles.

**Field Code Changed**

### 2.2 Devolatilization and Combustion Experiments

[White oak \(\*Q. alba\*\) heartwood and leaves were chosen for these studies because of their abundance in the oak-hickory forests of Missouri and the southeastern United States. While comparing different tree species is also of interest, two different plant fractions of the same species are studied here to investigate different types of wildfire or controlled](#)

1215 combustion processes, some of which may only impact leaf litter-fall and others would have wood available as a fuel.

The white oak biomass samples used in this study were collected at the Tyson Research Center in Eureka, MO, located approximately 20 miles outside of St. Louis, MO. An oak trunk segment was taken from the site, and heartwood samples were collected by drilling into the center of the trunk segment. Oak leaves were clipped from a single branch that was taken directly from a live tree. The leaf samples were air-dried for at least one week and milled into fine pieces using a tobacco grinder prior to running the experiment. All biomass was stored at room temperature (20-25°C), and moisture content was not controlled for either fuel type.

1220 Samples of oak wood or leaf were pre-weighed (0.2-0.5 g), placed in the emissions chamber cup, and spread evenly across the bottom rim. The cup was heated for 3.5 minutes, with temperatures in the cup reaching a maximum typical ignition temperatures of 245-300°C. In this work, we use the term “devolatilization” to describe the non-combustive release of emissions from biomass fuels at elevated temperatures. During the heat pulse, the biomass sample was first devolatilized, with smoldering embers observed in the final minute of the heat ramp. No flaming combustion occurred during any of the emissions experiments.

1225 To ensure the TAG and AMS collected particles within a similar size range, primary emissions were passed through a PM<sub>1</sub> cyclone (Thermo Fischer Scientific, Waltham, MA) operated at 16.7 L min<sup>-1</sup> to remove particles too large to be sampled by the AMS (DeCarlo et al., 2006).

1230 Because dilution is known to drive partitioning of SVOCs and IVOCs from the particle phase into the gas phase in BBOA plumes (Grieshop et al., 2009; Ortega et al., 2013), dilution was minimized in the system during devolatilization and combustion experiments. Dilution air, purified using separate zero air generators (Model 737, Aadco Instruments, Cleves, OH), was supplied before the PM<sub>1</sub> cyclone (6.7 L min<sup>-1</sup>) and after the PAM chamber (4 L min<sup>-1</sup>) to provide sufficient flow to the cyclone and to all instruments (Figure S1), giving a net dilution ratio of approximately 5 for all experiments.

### 2.3 PAM Reactor Operation

Particulate and gas-phase emissions were treated together in the PAM flow reactor. A detailed description of the PAM reactor is given elsewhere (Kang et al. 2007, Lambe et al. 2011). The reactor consists of a 13 L cylindrical aluminum chamber coated internally with Iridite 14-2 (MacDermid, Inc., Waterbury, CT), a chromate conversion film designed to decrease charge buildup and thereby inhibit losses of charged particles to the walls of the reactor, applied to inhibit wall losses. Within the PAM chamber, low-pressure mercury lamps emit light at two wavelengths (185 nm and 254 nm) in the UV range, and different OH-OH concentrations are produced by adjusting the intensity of the UV irradiation (Kang et al., 2007). Ozone (O<sub>3</sub>) is produced externally by irradiating 0.4 L min<sup>-1</sup> of pure O<sub>2</sub> with mercury lamps ( $\lambda = 185$  nm; BHK, Inc., Ontario, CA) to produce 4 ppm externally added O<sub>3</sub>. Water vapor is introduced into the PAM reactor with 4.6 L min<sup>-1</sup> of humidified N<sub>2</sub>. A total flow rate of 10 L min<sup>-1</sup> was maintained throughout the experiments, giving an average residence time of 78 seconds within the reactor. To achieve consistent OH-OH formation, the relative humidity (RH) inside of the reactor was kept at 30.0%  $\pm$  3.7% (one standard deviation), measured with a relative humidity and temperature probe with manufacturer-specified accuracy of 1.5% (Vaisala, Inc., Woburn, MA).

1250 The reactor water concentration, and therefore RH, was altered by controlling N<sub>2</sub> flow through a Nafion membrane humidifier (Perma Pure LLC, Lakewood, NJ). The role of RH<sub>water concentration</sub> in OH-OH formation is discussed in detail in Supplemental Information (Method: PAM Calibrations and Figure S3).

1255 OH-OH exposures (OH<sub>exp</sub>) within the PAM reactor were calculated using the offline sulfur dioxide (SO<sub>2</sub>) calibration method described in previous work (Kang et al., 2007). During reactor calibration, SO<sub>2</sub> concentrations (Airgas, Inc., Radnor, PA) were measured with an SO<sub>2</sub> monitor (Model 43i-TLE analyzer, Thermo Fischer Scientific, Waltham, MA) at varied UV lamp intensities; similarly, O<sub>3</sub> was measured downstream of the PAM reactor by UV photometry (Model 49i, Thermo Fischer Scientific, Waltham, MA). Equivalent atmospheric aging times from the SO<sub>2</sub> calibrations(Table 1) were calculated assuming an average atmospheric OH-OH concentration of 1.5 x 10<sup>6</sup> molec cm<sup>-3</sup> (Mao et al., 2009) and are provided as the upper limit on the equivalent aging time ranges obtained for the system (Table 1). PAM reactor calibration details and results are provided in Supplemental Information (Methods: PAM Calibrations and Equivalent Aging Estimations). For both heartwood and leaf fuels, experiments were performed at two level of photochemical aging in addition to a baseline without exposure. Henceforward, the different photochemical aging conditions will be denoted by the corresponding equivalent aging time ranges (Table 1).

1265 Previous PAM reactor studies have demonstrated that high concentrations of volatile organic compounds (VOCs) can suppress OH reactivity (Li et al., 2015; Peng et al., 2015). This suppression occurs because VOCs drive rapid conversion of OH to HO<sub>2</sub>, and recycling of HO<sub>2</sub> back to OH can be slow without addition of sufficient O<sub>3</sub> (Peng et al., 2015, 2016). External OH reactivity (OHR<sub>ext</sub>, s<sup>-1</sup>) is defined as the sum of the products of concentrations of externally reacting species (C<sup>i</sup> for a compound i) and corresponding OH reaction rate constants (k<sub>i</sub>; Peng et al., 2016):

$$OHR_{ext} = \sum k_i C_i \quad (1)$$

1270 This metric is used to describe the potential for interfering gases to react with OH and suppress heterogeneous oxidation. The external production of O<sub>3</sub> featured in our system is expected to reduce OH suppression by introducing additional O<sub>3</sub> to promote recycling of HO<sub>2</sub> back to OH (Peng et al., 2015).

1275 Due to a lack of gas-phase measurements, OHR<sub>ext</sub> values were not calculated during TAG and AMS collections. However, supplementary experiments were conducted to approximate OHR<sub>ext</sub> by repeating the fuel burning procedure and measuring resulting CO emissions with a CO monitor (Peak Laboratories, Mountain View, CA). During these experiments, emissions were sampled alternately through the PAM chamber, set to approximately 3 days of equivalent aging according to the most recent offline SO<sub>2</sub> calibration, and a bypass line. We observed little difference in CO OHR<sub>ext</sub> between PAM-aged emissions (maximum OHR<sub>ext</sub> = 0.558 s<sup>-1</sup>) and bypassed emissions (maximum OHR<sub>ext</sub> = 0.516 s<sup>-1</sup>). Additionally, we estimated total OHR<sub>ext</sub> by scaling trace gas emission factors (EFs) from previous laboratory-generated oak biomass combustion VOC measurements (Burling et al., 2010) to our measured CO concentrations and approximate a total OHR<sub>ext</sub> of 2.2 s<sup>-1</sup>. This OHR<sub>ext</sub> value is assumed for subsequent OH<sub>exp</sub> and equivalent aging estimations. A detailed description of the experimental methods, as well as a discussion of the limitations of this OHR<sub>ext</sub> estimation approach, is provided in supplemental information (Methods: PAM Calibrations and Equivalent Aging Estimations, “Estimation of External OH Reactivity (OHR<sub>ext</sub>)”).

Field Code Changed

1285 Based on an RH of 30%, a typical internally-produced output  $O_3$  range of 0.3-1.7 ppm (measured during reactor calibrations), and an  $OHR_{ext}$  of  $2.2\text{ s}^{-1}$ , we estimated  $OH_{exp}$  ranges for each PAM UV light setting using the Oxidation Flow Reactor Exposure Estimator version 2.3 developed by Peng et al., available for download at <http://sites.google.com/site/pamwiki/hardware/estimation-equations> (Peng et al., 2015, 2016). Results obtained using this spreadsheet are provided in Supplemental Information (Table S1). The “condition type,” which indicates whether VOC suppression is significant under the input conditions, was found to be “safer,” indicating that interferences from VOCs are minimal based on input measurements and assumptions.

1290 Flow field simulations and chemical tracer tests have demonstrated that the PAM reactor used in this study is approximately well mixed if sufficient time (at least 15 minutes) is given prior to sample collection to establish a well-mixed and near steady-state concentration throughout the combustion chamber and PAM chamber (Mitroo, 2017). The TAG therefore consistently collected 30 minutes after the biomass heat pulse to minimize particle concentration gradients within the reactor.

1295 Photobleaching of BBOA, particularly at 254 nm, has been reported in previous literature (e.g. Sumlin et al., 2017; Wong et al., 2017; Zhao et al., 2015) and therefore should be considered when estimating oxidative aging. With the spreadsheet provided by Peng et al., we estimate 254 and 185 nm exposure ratios (ratio of photon flux, photons  $\text{cm}^{-2}$ , to  $OH_{exp}$ ; Peng et al., 2016) to be  $1.2 \times 10^5\text{ cm s}^{-1}$  and  $8.1 \times 10^2\text{ cm s}^{-1}$ , respectively, at a measured internally-generated  $O_3$  concentration of 1.7 ppm (at the highest PAM UV lamp intensity), a water mixing ratio of 1% (RH = 30%), and assuming a maximum  $OHR_{ext}$  value of 1 (Peng et al., 2016). Using Figures 1 and 2 of Peng et al., 2016 to interpret these values, we find that photolysis at both 185 nm and 254 nm is likely less than 10% in both cases.

1300 Previous PAM reactor studies have demonstrated that high concentrations of volatile organic compounds (VOCs) can suppress  $OH$  reactivity (Li et al., 2015; Peng et al., 2015). This suppression occurs because VOCs drive rapid conversion of  $OH$  to  $HO_2$ , and recycling of  $HO_2$  back to  $OH$  can be slow without addition of sufficient  $O_3$  (Peng et al., 2015). The external production of  $O_3$  featured in our system is expected to reduce  $OH$  suppression by introducing additional  $O_3$  to promote recycling of  $HO_2$  back to  $OH$  (Peng et al., 2015). However, because the reactor was calibrated offline without additional injection of VOCs, obtaining  $OH_{exp}$  values characteristic of the experimental setup remains challenging (Ortega et al., 2013). Based on an RH of 30% and a typical output  $O_3$  range of 4.3-8.5 ppm (measured during reactor calibrations), we estimated  $OH_{exp}$  ranges for each PAM UV light setting using the Oxidation Flow Reactor Exposure Estimator version 2.3 developed by Peng, et al., available for download at <http://sites.google.com/site/pamwiki/hardware/estimation-equations> (Peng et al., 2015). Results obtained using this spreadsheet are provided in Supplemental Information (Table S1). The “condition type,” which indicates whether VOC suppression is significant under the input conditions, was found to be largely dependent on the assumed external  $OH$  reactivity ( $OHR_{ext}$ ), which is difficult to assess without direct VOC measurements.

## 2.4 Instrumentation and Data Analysis

Field Code Changed

The TAG and the AMS were used to collect complementary chemical composition data. A Scanning Mobility Particle Sizer (SMPS; Model 3081 DMA, Model 3022A CPC, TSI, Inc., Shoreview, MN) was used to measure aerosol size distributions and volume concentrations.

1320 The devolatilization and combustion experiments were performed in two distinct experimentation periods. In the first period, the procedure was done at each level of PAM oxidation using 0.2 g biomass. Triplicate experiments were done with the TAG and the SMPS during this period to ensure repeatability of the devolatilization and combustion cycle. In the second experimentation period, experiments were performed once more at each level of oxidation to obtain simultaneous TAG, SMPS, and AMS measurements. For these experiments, the devolatilization and combustion procedure was done with more biomass (0.5 g) so the AMS could obtain sufficient signal.

1325

#### 2.4.1 Thermal Desorption Aerosol Gas Chromatograph (TAG)

A full description of the TAG system is provided elsewhere (Williams et al., 2006). Particles are collected via humidification and inertial impaction at a typical flow rate of  $9.3 \text{ L min}^{-1}$ , with a particle cutoff ( $d_{p50}$ ) of approximately 70 nm (Williams et al., 2006). Following sample collection, the collection and thermal desorption (CTD) cell is heated to  $310 \text{ }^{\circ}\text{C}$  ~~at a typical rate of  $50\text{ }^{\circ}\text{C min}^{-1}$~~  to thermally desorb the collected OA. The desorbed sample is flushed through a heated transfer line using helium as an inert carrier gas and transported to a gas chromatography column for separation and mass spectral detection. An Agilent 6890 gas chromatograph (Agilent Technologies, Santa Clara, CA) with a 30m-long 0.25mm i.d. RTX5-MS non-polar fused silica capillary column (Restek Corporation, Bellefonte, PA) was used to achieve chromatographic separation. A 70 eV electron ionization quadrupole mass spectrometer (5973

1330

1335

MSD, Agilent Technologies, Santa Clara, CA), operated to scan between 29-450  $m/z$ , provided mass spectral detection. TAG performance was evaluated regularly (once every 1-3 days) using 5 ng  $\text{C}_{12}\text{-C}_{40}$  even alkane standard mixture (Sigma Aldrich, St. Louis, MO) manually injected onto the CTD cell and thermally desorbed onto the GC column via a helium carrier stream (Kreisberg et al., 2009).

1340 The TAG system developed by Isaacman et al. features an online derivatization technique designed to improve analysis of oxidized species, including methoxyphenols, levoglucosan, and other compounds unique to BBOA (Isaacman et al., 2014). Although this technique presents multiple analytical advantages, it was developed for a metal filter collection cell and is not suitable for the impactor-style CTD cell used in these experiments. We chose to use the impactor-style CTD cell to allow analysis of the thermal decomposition window, since other collection cells purge this material when transferring to a secondary trap. Additionally, we were interested to identify new molecular marker compounds that could be associated with these source types. We therefore performed all experiments without sample derivatization prior to chromatographic analysis.

1345

TAG data ~~was-were~~ collected during the first experimentation period using 0.2 g biomass in the heat pulse. For all the oak leaf and oak wood experiments, particles were collected on the TAG for four minutes, thirty minutes after the heat pulse was performed in the emissions chamber. The TAG collected two additional samples over the course of three hours to ensure that ~~both~~ the emissions ~~and combustion~~ chamber ~~and the PAM was-reactor were~~ clean prior to the subsequent devolatilization cycle.

1350

In this work, the TAG compound and thermal decomposition time windows were analyzed as complementary sets of chemical data (Figure 1). As defined for this study, the thermal decomposition window occurs between minutes 6-16 of GC analysis, which coincides with the thermal desorption of sample from the CTD cell. The compound window 1355 consists of material eluting from minutes 20-55 of analysis following condensation of desorbed sample at the column head. This window contains information on OA components that have been successfully desorbed, transferred, and separated.

Prior to each experiment, a system blank chromatogram was obtained by sampling from the empty emissions chamber through the PAM reactor, with the PAM UV lamps set to the voltage corresponding to the subsequent equivalent aging 1360 time to be tested. A system blank was subtracted from each chromatogram prior to data processing to correct for both TAG system artifacts (e.g. air signal and column bleed) and sampling system (PAM reactor and emissions and combustion chamber) artifacts. Additionally, to isolate changes in aerosol chemical properties from changes in aerosol mass with photochemical aging, each blank-subtracted chromatogram was normalized to volume concentration by 1365 dividing the abundance at each scan by the maximum volume concentration ( $\mu\text{m}^3 \cdot \text{nm}^3 \cdot \text{cm}^3$ ) obtained by the SMPS for each devolatilization cycle (Table S2 and Figure S4 in Supplemental Information). This blank subtraction and normalization process was done for all total ion count (TIC) chromatograms and single-ion chromatograms (SICs) presented in this work.

#### 2.4.2 TAG Positive Matrix Factorization

Positive matrix factorization (PMF) was performed on TAG chromatograms to identify source-specific major 1370 compounds and compound classes present in the oak wood and leaf BBOA. TAG chromatograms were binned by retention time according to the method outlined in previous work (Zhang et al., 2014, 2016). Prior to chromatogram binning, each chromatogram was blank-subtracted to minimize the contribution of background noise in PMF calculations. An instrument error of 10%, chosen based on a typical average TAG instrument error of 10% (Williams et al., 2006), was assumed during PMF calculations.

1375 The GC-resolved mass spectral PMF method for binned TAG data was developed to separate compounds in TAG chromatograms into chemically similar factors, improving analysis efficiency (Zhang et al., 2014). With this method, mass spectral data is supplied to the PMF model, and solutions are obtained using the PMF2 algorithm (Paatero, 1997). Each resulting factor consists of a mass spectrum corresponding to a compound or class of compounds present in the TAG chromatograms (Zhang et al., 2014). This PMF method was performed on the compound and decomposition 1380 analytical windows separately for data obtained from both BBOA sources. PMF output and solutions were evaluated using custom-built pre- and post-processing analysis software in conjunction with the PMF Evaluation Tool (version 3.00A; Ulbrich et al., 2009) in Igor Pro version 6.38Beta01 (WaveMetrics, Inc.). Mass spectral identification of different factors was aided by the NIST MS Search Program version 2.0, available for download at <http://chemdata.nist.gov/mass-spc/ms-search/>.

Field Code Changed

1385 The number of appropriate PMF factors was determined for each solution based on two considerations. First, in a typical PMF analysis, the optimal number of factors in a solution is selected based on the objective function  $Q$ , which

is the sum of weighed squared residuals (Paatero, 1997). The  $Q/Q_{exp}$  value, or the ratio of the actual objective function to the expected objective function assuming normally distributed residuals, should ideally approach 1; too few factors may result in a large  $Q/Q_{exp}$ , indicating that errors have been underestimated in PMF calculations (Ulbrich et al., 2009).

1390 Additionally, if too many factors are specified, the solution may feature split factors, where information from a compound or compound class is distributed across multiple factors. In this work, the number of factors presented for each analysis was selected to minimize split factors while maximizing identifiable factors. Because of the TAG data's high chromatographic resolution, low rotational ambiguity was assumed, and all calculations were performed with  $f_{peak} = 0$ . This assumption is supported by previous work, where TAG data ~~was-were~~ not sensitive to  $f_{peak}$  or starting point (seeds) during PMF analysis (Williams et al., 2010).

#### 2.4.3 AMS

The AMS data presented in this work were obtained using 0.5 g of biomass in the heat pulse instead of 0.2 g to ensure the AMS received sufficient signal. The AMS was operated in V-mode throughout all experiments (DeCarlo et al., 2006). AMS data ~~was-were~~ processed in Igor Pro version 6.38Beta01 using the SQUIRREL version 1.57 toolkit for unit mass resolution analysis and the PIKA version 1.16 toolkit for high resolution analysis. Both AMS data analysis tools are available for download at <http://cires1.colorado.edu/jimenez-group/ToFAMSResources/ToFSoftware/index.html>.

Field Code Changed

### 3 Results and Discussion

#### 3.1 AMS Measurements

1405 Average AMS mass spectra and van Krevelen plots are provided in Supplemental Information (Figures S13 and S14, respectively). In addition, AMS measured concentrations of key species, including total organics, sulfate ( $SO_4$ ), and potassium (K), are provided in Figure S15.

According to AMS mass spectra, the BBOA measured in these experiments is chemically consistent with BBOA from similar oak fuel sources, though with key differences related to combustion conditions (Cubison et al., 2011; Ortega et al., 2013; Reece et al., 2017; Weimer et al., 2008). Detailed analysis and contextualization of the AMS chemical composition data is provided in Supplemental Information (Section: AMS Chemical Characterization).

Field Code Changed

#### 3.1.2 Individual Compound Analysis

1415 The mass spectral dot product method proposed by Stein and Scott was used to determine chemical similarity between each chromatogram and to evaluate inter-test variability. For each blank-subtracted TAG chromatogram, a summed mass spectrum was obtained by summing all ions ( $m/z$  33- $m/z$  450) across all scans (retention times) in the chromatogram and converting the resulting mass spectral vector into a unit vector. To assess the similarity of two mass spectra, the dot product of the mass spectral unit vectors was calculated; a dot product of 1 signifies a perfect mass spectral match, and a dot product of 0 indicates a complete mismatch (Stein and Scott, 1994). Within a fuel type and an oxidation condition, the dot product was assessed for two TAG chromatograms at a time for a total of 3 dot product values. These values are given in Table S9.

Field Code Changed

For both leaf and wood BBOA, key molecules identified within the compound window of the TAG chromatograms are given in Supplemental Information (Tables S3-S4 and S4S5). Corresponding molecular structures for the compounds used in individual compound analysis are also provided (Figures S5-S6 and S6S7). Identification certainty (“Certainty of ID”) was classified for each compound according to the following criteria: A) the compound was positively identified based on external standard injections; B) the compound was identified based on a high match quality ( $MQ > 75\%$ ) using available mass spectral libraries; C) the compound was identified based on a low-to-moderate match quality ( $50\% < MQ < 75\%$ ) using available mass spectral libraries; and D) no adequate mass spectral library match was available for the compound, so the compound structure was determined-inferred by retention time and manually evaluating possible fragmentation patterns. Subcooled liquid vapor pressures at  $25^\circ\text{C}$  were predicted for each compound using the Advanced Chemistry Development (ACD/Labs) Software V11.02 (© 1994-2017 ACD/Labs), available for use on the SciFinder website (ACD/Labs, 2017).

### 3.42.1 Trends in Individual Compounds with Photochemical Aging

Leaf and heartwood BBOA chromatograms at three levels of photochemical aging are overlaid for comparison in Figure 2. Raw peak integration values with standard deviations are provided for each compound at each level of equivalent aging are also provided (Tables S6S and S6-S7 in Supplemental Information). Each plot-chromatogram constitutes an average of triplicate-the triplicate blank-subtracted measurements, with each chromatogram normalized to the maximum total volume concentration measured during the experiment as described previously. For these plots, the averaged, normalized chromatograms at each level of aging were further normalized to the point of highest abundance in the unaged (“0 days”) average chromatogram. In the leaf BBOA chromatograms (Figure 2a), many of the low volatility species eluting after minute 35 of the GC analysis are long-chain alkanes, alcohols, aldehydes, and terpenoids, compounds commonly found in the leaf’s waxy exterior coating (Gulz and Boor, 1992). Based on even-numbered alkane standard injections, compounds eluting after minute 35 exhibit approximate saturation vapor pressures not exceeding that of docosane (approximately  $2.73 \times 10^{-5}$  torr at  $25^\circ\text{C}$ ), which corresponds approximately to  $\log_{10}(C^*) = 2.76$  (Table S3 in Supplemental Information; ACD/Labs, 2017).

Nearly all compounds identified after 35 minutes decrease in abundance with photochemical aging. To illustrate the relative rates of decay that each compound experiences in the PAM reactor, Figure 3a provides integrated abundances, first normalized to appropriate volume concentrations then to corresponding abundances at no oxidation, for nine compounds of interest. Nearly all compounds identified after 35 minutes decrease in relative abundance with photochemical aging. Notably, we have identified an even-carbon aliphatic aldehyde series based on  $[\text{M}-18]^+$  and  $[\text{M}-28]^+$  (where M is the parent mass) peaks present in the mass spectra of each of the compounds (Watson and Sparkman, 2007). As the carbon number ( $n_C$ ) increases, the aldehyde abundance decreases more readily with oxidation. To our knowledge, rate constants for the reaction of long-chain ( $n_C \geq C_{20+}$ ) condensed-phase aliphatic aldehydes with OH-OH have not been reported. However, previous studies on short-chain ( $n_C \leq C_{14}$ ) condensed-phase aliphatic aldehydes demonstrate that OH-OH reaction rate constants increases with increasing carbon chain length (D’Anna et al., 2001; Niki et al., 1978). Although aliphatic aldehydes, particularly  $C_{26}$  and  $C_{28}$  aldehydes, have been characterized as components of oak leaf waxes (Gulz and Boor, 1992), this series of aldehydes has not been previously reported as

components of oak leaf BBOA and may therefore serve as novel tracer species in future field experiments. To confirm the presence of aldehydes in the leaf waxes, Solvent-solvent extractions were performed on oak leaves using and were manually injected onto the TAG CTD cell (Method: Oak Leaf Solvent Extractions and Figure S8 in Supplemental Information). injections Analysis of these extractions confirm that the aldehydes are present in the leaf wax prior to devolatilization and combustion (Method: Oak Leaf Solvent Extractions and Figure S7 in Supplemental Information).

Literature information available for hydrocarbon particle- and gas-phase OH kinetics indicates that the trends observed in leaf BBOA alkane and aldehyde abundances are consistent with heterogeneous OH oxidation. For example, Smith et al. report approximately 70% decay of squalane (a C<sub>30</sub> branched alkane) particles when exposed to an OH<sub>exp</sub> of 1.1 × 10<sup>-12</sup> molec cm<sup>-3</sup> s<sup>-1</sup> (approximately 10 days of equivalent aging; Smith et al., 2009), a figure approximately consistent with the observed C<sub>29</sub> alkane decay of 75% at 6-10 days of equivalent aging. Additionally, based on parameters provided by Kwok and Atkinson, gas-phase OH reaction rate constants at 298K are estimated to be 2.5 × 10<sup>-11</sup>, 2.7 × 10<sup>-11</sup>, and 3.1 × 10<sup>-11</sup> cm<sup>3</sup> molec<sup>-1</sup> s<sup>-1</sup> for C<sub>23</sub>, C<sub>25</sub>, and C<sub>29</sub> alkanes, respectively (Kwok and Atkinson, 1995). Taking these rate constants into account, if purely gas-phase chemistry is assumed, all three alkanes would react nearly 100% before 1-3 days of equivalent aging. A similar analysis on relevant aldehydes gave estimated gas-rate constants of 2.5 × 10<sup>-11</sup>, 2.8 × 10<sup>-11</sup>, and 3.0 × 10<sup>-11</sup> cm<sup>3</sup> molec<sup>-1</sup> s<sup>-1</sup> for C<sub>24</sub>, C<sub>26</sub>, and C<sub>28</sub> aldehydes, respectively (Kwok and Atkinson, 1995), which in all cases would lead to complete depletion by 1-3 days of equivalent aging if gas-phase chemistry is assumed.

Field Code Changed

Compounds characteristic of heartwood primary BBOA are typically more volatile than those found in the leaf primary BBOA, eluting between minutes 28 and 35 of the GC analysis (Figure 2b). Based on even alkane standard injections, compounds eluting within this time window exhibit approximate vapor pressures within 4.52×10<sup>-3</sup>-2.73×10<sup>-5</sup> torr at 25°C ( $\log_{10}(C^*) \approx 4.85-2.76$ ; Table S4 in Supplemental Information; ACD/Labs, 2017). The compound with the highest abundance in unoxidized wood BBOA chromatograms is sinapaldehyde (4-hydroxy-3,5-dimethoxycinnamaldehyde), a phenolic compound derived from lignin. Of the compounds examined, sinapaldehyde decays most rapidly in the PAM reactor, with the normalized average integrated peak area decreasing by approximately 70% from 0 days to 1-3 days of equivalent aging (Figure 3b). Based on a rapid gas-phase OH reaction rate constant of 2.7 × 10<sup>-12</sup> cm<sup>3</sup> molec<sup>-1</sup> s<sup>-1</sup>, the observed sinapaldehyde decay is likely occurring in the particle phase. Sinapaldehyde reacts rapidly in the PAM reactor, with the normalized average integrated peak area decreasing by approximately 70% from 0 days to 3.4 days of equivalent aging (Figure 3b). Other compounds, including guanosine, galactoheptulose, and acetylgalactosamine, also exhibit decreases in abundance; relative rates of decay for these and other wood BBOA tracers are given in Figure 3b.

Syringol (2,6-dimethoxy-phenol), syringaldehyde (4-hydroxy-3,5-dimethoxy-benzaldehyde), and vanillin (4-hydroxy-3-methoxy-benzaldehyde) increase in abundance from 0 days to 3.41-3 days of equivalent aging and are fully depleted with 9.86-10 days of equivalent aging. Since the average volume concentration for runs at 3.41-3 days of aging were larger than those at 0 days of aging by a factor of approximately 1.3 (Table S2 in Supplemental Information), the factor of ~2 increase in syringol and syringaldehyde integrated abundances could occur due to partitioning from the gas phase into the particle phase. To examine the potential impacts of phase partitioning for these

Field Code Changed

1495 compounds, particle-phase fractions for syringol, syringaldehyde, and vanillin ( $\xi_i$ ) were calculated based on AMS total organic concentrations ( $C_{OA}$ ,  $\mu\text{g m}^{-3}$ , Table S3 in Supplemental information) and effective saturation concentrations ( $C_i^*$ ,  $\mu\text{g m}^{-3}$ ; Table S3 in Supplemental information) using a basic partitioning equation (Donahue et al., 2006):

$$\xi_i = \left(1 + \frac{C_i^*}{C_{OA}}\right)^{-1} \quad (2)$$

1500 Resulting particle-phase fractions are tabulated in supplemental information (Table S12). Based on these approximations, syringol, syringaldehyde, and vanillin are expected to partition primarily to the gas phase. For these compounds, the increase in abundances at low-mid levels of oxidation could therefore result from increased SOA formation driving these compounds into the particle phase. This observation is consistent with previous measurements where maximum SOA concentrations were observed at similar levels of  $\text{OH}_{\text{exp}}$  for aerosol generated from oxidation of a single precursor (Lambe et al., 2012; Ortega et al., 2016).

1505 However Although phase partitioning may contribute to the trend in vanillin with photochemical aging, the nearly eight-fold increase in vanillin integrated abundance from 0 days to 3.41-3 days of aging suggests could suggest an alternative formation mechanism driven by reactions occurring in the PAM reactor. One potential mechanism for the formation of aldehydes from larger lignin decomposition products, described in Supplemental Information (Figure S8), involves the cleavage of the  $\text{C}_\alpha\text{-C}_\beta$  unsaturated bond on the benzyl substituent following abstraction of the hydrogen from the phenolic substituent group. A mechanism for vanillin formation from larger lignin decomposition 1510 products has been previously described as part of an alkaline oxygen delignification process and involves the formation and fragmentation of a peroxide radical intermediate (Wong et al., 2010). The presence of  $\text{OH-OH}$  in the PAM reactor may drive a similar process, leading to increases in vanillin abundance at moderate  $\text{OH}_{\text{exp}}$ .

### 3.12.2 Compound Window PMF Analysis

1515 GC-MS PMF results are provided for both leaf and wood BBOA chromatograms using data collected within the TAG compound window (Figures 4, 5, 6, and 57).  $Q/Q_{\text{exp}}$  and residual plots are provided in Supplemental Information (Figures S9 and S10, respectively). The chromatograms (Figures 4 and 6) are displayed as averages of binned data from triplicate measurements at each level of oxidation and are displayed in one trace; different equivalent aging times 1520 are demarcated with vertical lines along the x-axis. Corresponding mass spectra (Figures 5 and 7) are identified and displayed with key ions labeled. High factor solutions ( $\geq 15$ ) were used for compound window data to best deconvolve the large and complex mixture of compounds. However, in some cases, factor splitting resulted in the distribution of ions between two or more factors, made evident by similarities in retention times. Wherever possible, split factors were recombined by summing the binned chromatograms and the mass spectra and are labeled accordingly (e.g. “F10+F12” indicates that factor 10 and factor 12 have been recombined). In general, for the compound window, factor solutions were chosen to maximize the number of identifiable factors while minimizing the number of split factors.

1525 A 15-factor solution was chosen to deconvolve leaf BBOA compound window chromatograms (Figures 4 and 5, Figure 4; additional information provided in Figures S9a and S10a). This solution provided enough factors to resolve the

Field Code Changed

lowest-abundance components (e.g. F1), and increasing the number of factors past 15 led to greater factor splitting without providing additional insight into the chromatograms. Among the factors identifiable with this solution include quinic acid (Factor 2, F2), sugars and anhydrosugars (e.g. mannose; F3), alcohols and alkenes (F6), aldehydes (F10), 1530 terpenoids (e.g. friedelin; F11), and column bleed (F13+F14). Other factors (F1, F5+F7, F9+F12, F15) correspond to different classes of unresolved complex mixture (UCM) and have been tentatively identified by considering the closest matches in the NIST mass spectral database. Factor 4 (F4) is identified as a split factor, exhibiting mass spectral characteristics of multiple factors, including acids ( $m/z$  129) and anhydrosugars ( $m/z$  116). Factors 13 and 14 demonstrate contributions from both terpenoid-like UCM and column bleed and are therefore combined. The presence 1535 of alkylbenzenes (F8), dominated by  $m/z$  91 ( $C_7H_7^+$ ) and  $m/z$  92 ( $C_7H_8^+$ ), is noteworthy, as alkylbenzenes are typical of anthropogenic materials (e.g. detergent precursors produced from petroleum; Forman et al., 2014) and have not been reported as components of biomass. Since the leaves were not cleaned after they were collected, the alkylbenzenes could come from deposition of fuel combustion aerosol onto the leaves' surface prior to biomass sample 1540 collection. The presence of alkylbenzenes on the surface of the leaf was confirmed with TAG analysis of solvent-extracted leaf surface components (Figure S11), supporting the interpretation of deposition of anthropogenic compounds on the leaf's exterior.

1545 An 18-factor solution was applied to deconvolve compounds in the wood BBOA chromatograms (Figure [5s-6-7](#); additional information provided in Figures S9b and S10b). Notable factors correspond to levoglucosan (F1), guaiacol (F4), vanillin and guaiacyl compounds (F7), syringol (F8), syringaldehyde (F10), sinapaldehyde (F11), and column bleed (F18). Based on retention time and mass spectral characteristics (e.g.  $m/z$  77), factor 5 (F5) corresponds to aromatic species and is not matched to a single compound. Factor 6 (F6) is featured in multiple aromatic compounds, but is also present in levoglucosan in very low abundances. Several types of UCM (F2, F3, F9, F12+F13+F14, F15, F16) were deconvolved and tentatively identified using the top matches from the mass spectral database. Factor 16 (F16) is predominated by siloxanes (e.g.  $m/z$  73,  $m/z$  281,  $m/z$  341), though some UCM has been split from other 1550 factors. Finally, factor 17 (F17) exhibits characteristics of multiple classes of compounds and is therefore identified as a split factor.

1555 Nearly all factors obtained in the leaf BBOA compound window analysis decrease with photochemical aging, including quinic acid (F2), sugars and anhydrosugars (F3), alkanes and long-chain aliphatics (F6, F10, F15), alkylbenzenes (F8), terpenoid components (F11), and various classes of UCM (F1, F4, F5+F7, F9+F12). This trend agrees well with the individual compound results and further indicate that primary components undergo increased fragmentation at higher  $OH_{exp}$ . In the wood BBOA, some primary components decrease steadily with photochemical aging, including sinapaldehyde (F11), aromatics (F5), and various classes of UCM (F12+F13+F14, F15, F17). Other factors, including guaiacol (F4), vanillin (F7), syringol (F8), and syringaldehyde, exhibit a strong increase in abundance at [3.41-3](#) days of aging followed by a decrease at [9.86-10](#) days of aging, possibly due to changes in 1560 partitioning as described previously. Levoglucosan (F1) also appears to increase slightly in abundance at [3.41-3](#) days of equivalent aging, though this is likely due to differences in aerosol mass produced between experiments. Results from both types of BBOA show changes in column bleed (F13+14 and F18 for leaf and wood BBOA, respectively)

1565 from unaged chromatograms to 9.86–10 days of aging. While the column bleed decreases with photochemical aging in both cases, this trend is due to differences in blank subtractions from run to run and is not related to changes in photochemical aging.

1570 The PMF deconvolution results support the identification and analysis of individual tracers present in wood and leaf BBOA. Because each chromatogram may contain hundreds of individual compounds, a general knowledge of the compound classes characteristic of each BBOA type can greatly reduce individual compound analysis time and ensure that chromatograms are characterized as completely as possible. The results presented in this study therefore confirm that the chromatogram binning method coupled with PMF, as developed by Zhang, et al. (Zhang et al., 2014, 2016), can aid molecular tracer analysis by elucidating different compound classes of interest present in BBOA. The PMF results obtained in this study for the compound window provide information on characteristic mass spectral signatures within leaf and wood primary BBOA and may be compared to results obtained in future BBOA studies to more fully characterize how different compounds evolve with photochemical aging in the atmosphere.

Field Code Changed

### 1575 3.2.3 TAG Thermal Decomposition Window

1580 The thermal decomposition window has been used in previous work to assess contributions of inorganic (nitrates, sulfates, etc.) and organic species present in atmospheric aerosol (Williams et al., 2016). In this work, we provide evidence that the TAG thermal decomposition window can be used to evaluate the relative level of oxidation of bulk OA samples using the  $m/z$  44 ( $\text{CO}_2^+$ ) ion. In addition, we demonstrate that other fragments within the decomposition window may give insight into the chemical composition of aged, thermally labile BBOA.

1585 Replicable, quantitative TAG data were not obtained during experiments that used 0.5 g biomass, potentially due to a minor system leak. However, the TAG chromatograms that were obtained using 0.5 g biomass were chemically similar to the triplicate TAG chromatograms obtained using 0.2 g biomass, and we therefore compare all AMS data with TAG chromatograms collected using 0.2 g biomass in subsequent analysis. Chemical similarity between chromatograms was confirmed using the dot product mass spectral comparison method outlined by Stein and Scott (Stein and Scott, 1994) described previously. For each blank subtracted TAG chromatogram, a summed mass spectrum was obtained by summing all ions ( $m/z$  33– $m/z$  450) across all scans (retention times) in the chromatogram and converting the resulting mass spectral vector into a unit vector. To assess the similarity of two mass spectra, the dot product of the mass spectral unit vectors was calculated; a dot product of 1 signifies a perfect mass spectral match, and a dot product of 0 indicates a complete mismatch (Stein and Scott, 1994). In this work, the dot product was determined for two chromatograms, one obtained with 0.5 g biomass and one obtained with 0.2 g biomass, at each level of oxidation. The resulting dot products for both leaf and wood oak are all above 0.75 and are provided in Supplemental Information (Figure S172; Table S7S8).

Field Code Changed

#### 3.23.1 $m/z$ 44 as a Tracer for Aged OA

1595 Figures 68a and 68b show  $m/z$  44 TAG decomposition SICs for leaf and wood BBOA, respectively. Raw SICs, along with blanks, are provided in Figure S16. At each oxidation condition, SICs from the triplicate chromatograms were blank subtracted, displayed SICs have each been blank subtracted, normalized to maximum volume

concentrations, and averaged [to obtain the displayed trace across triplicate measurements at each level of oxidation](#). Within each plot, the chromatograms have been further normalized to the point of highest abundance within the unaged ("0 days")  $m/z$  44 signal. The  $m/z$  44 signals were also summed across the entire decomposition window following blank subtraction, normalization to appropriate volume concentrations, and triplicate averaging, and are provided as functions of equivalent aging time ( $\pm$  one standard deviation) in Figure 68c. The upward trend in the  $m/z$  44 signal between minutes 6 and 10 of GC analysis coincides with the CTD temperature ramp from 45°C to 310°C, and is thus consistent with gradual increase in OA thermal decomposition as the temperature rises. The subsequent decrease in  $m/z$  44 signal from minute 10-16 reflects the thermal decomposition of remaining material as the CTD cell is held at 310°C. For both types of BBOA, the decomposition  $m/z$  44 integrated signal increases overall from 0 days to [9.86-10](#) days of equivalent aging, indicating [an increase that in OA thermal decomposition increases OA material that can thermally decompose overall](#) with increased PAM oxidation. This trend is consistent with [relative increased formation decomposition of more highly oxidized aerosol within the PAM reactor, as was also indicated in previous ambient aerosol observations \(Williams et al., 2016\)](#). In the leaf BBOA chromatograms, the increase in integrated  $m/z$  44 signal is most pronounced from 0 to [3.41-3](#) days of equivalent aging, while the wood BBOA data exhibits the most dramatic increase from [3.41-3](#) to [9.86-10](#) days. The variation in the shape of the decomposition  $m/z$  signal between the two types of biomass likely reflects differences in thermal lability between different types of OA.

AMS  $\overline{OS}_C$  values calculated for both types of biomass range from -1.5 to -0.2 (Figure 97). In both types of BBOA, an increase in relative integrated TAG decomposition  $m/z$  44 signal coincides with an increase in  $\overline{OS}_C$  from 0 to [9.86-10](#) days of photochemical aging. [A linear correlation between decomposition  \$m/z\$  44 and AMS  \$\overline{OS}\_C\$  for wood BBOA \( \$r^2 = 10.9986\$ \)](#) indicates that under these experimental conditions, the TAG thermal decomposition window has the potential to provide quantitative measurements of bulk OA oxidation levels. By contrast, leaf BBOA decomposition  $m/z$  44 and AMS  $\overline{OS}_C$  correlate poorly ( $r^2 = 0.87842$  for a linear fit). The non-linear trend in TAG decomposition  $m/z$  44 for leaf BBOA may indicate a shift in the dominant oxidation mechanisms between moderate and high levels of [OH-OH](#) within the PAM chamber; at the highest  $\text{OH}_{\text{exp}}$ , primary gas and/or particle-phase components may undergo increased fragmentation, leading to a net decrease in production of the aged OA that thermally decomposes during TAG analysis, [along with an increase in highly volatile fragmentation products that are not captured by the TAG](#). However, the mechanisms behind this trend remain unclear and merit further investigation.

For each fuel type, AMS  $f_{44}$  vs  $f_{43}$  data have been plotted at each level of equivalent aging (Figure 408). To further explore the TAG's analytical capability in relation to AMS bulk chemical data, TAG integrated ion fractions ( $f_{\text{ion}}$ ) are provided on the plots. These fractions are defined as the blank-subtracted integrated ion signal divided by the blank-subtracted integrated TIC signal. For example, for a chromatogram  $i$ , the TAG  $f_{44}$  signal is defined as:

$$f_{44,i} = \frac{(A_{44})_i - (A_{44})_{\text{blank}}}{(A_{\text{TIC}})_i - (A_{\text{TIC}})_{\text{blank}}}$$

(43)

where  $(A_{44})_i$  is the integrated  $m/z$  44 signal across all (i.e., TAG total chromatogram) or part (i.e., TAG compound window) of  $i$ ,  $(A_{44})_{\text{blank}}$  is the integrated  $m/z$  44 signal across a blank chromatogram,  $(A_{\text{TIC}})_i$  is the integrated TIC across

all or part of  $i$ , and  $(A_{TIC})_{blank}$  is the integrated TIC across the same blank. For wood BBOA, while AMS  $f_{44}$  increases and  $f_{43}$  decreases with photochemical aging, both TAG  $f_{44}$  and  $f_{43}$  increase with increasing oxidation, particularly when the decomposition window is included in analysis (i.e., TAG total chromatogram). However, TAG fractions from the leaf BBOA data are more varied and do not exhibit a clear trend. In general, the TAG fractions tend to fall to the left of AMS  $f_{44}$  vs  $f_{43}$  data points, indicating that the TAG excels at throughput of less-oxygenated hydrocarbon OA and struggles with throughput of oxidized species in the compound window. However, the increase in TAG  $f_{44}$  with inclusion of decomposition window material shows a clearer oxidation trend that is in greater agreement with the AMS oxidation trend. This interpretation implies that the  $m/z$  43 and  $m/z$  44 signals obtained in the TAG decomposition window from sample thermal desorption at 310°C is similar in nature to material flash-vaporized at 600°C in the AMS.

### 3.23.2 Decomposition Window PMF Analysis

To aid identification of key thermal decomposition products, the binning deconvolution PMF method was applied to the TAG chromatogram decomposition window (Figures 41, 42, 43, 149 and 10). Details of the PMF analyses are provided in Supplemental Information (Figures S9 and S10). Tentative identification of different factors was facilitated by the NIST mass spectral database, though standard injections are needed to adequately quantify the decomposition window signal and identify the factors with complete confidence. As with the compound window PMF results, chromatograms are displayed as triplicate averages of binned data at each level of oxidation and are demarcated by vertical lines across the x-axis (Figures 11, 13). Key ions are labeled and tentative identifications are provided above each mass spectrum (Figure 12, 14).

For the leaf BBOA chromatograms, a 4-factor solution gave several distinguishable factors (Figure 9s-11, 12; additional information provided in Figures S9c and S9c), including the  $m/z$  44 ( $\text{CO}_2^+$ ) signal previously identified as originating from thermal decomposition oxidized organics (F1). Factor 3 (F3), dominated by  $m/z$  78 (possibly  $\text{C}_6\text{H}_6^+$ ) with smaller contributions from  $m/z$  39 ( $\text{C}_3\text{H}_3^+$ ) and  $m/z$  51 ( $\text{C}_4\text{H}_3^+$ ), could indicate decomposing aromatics. Factor 2 (F2) matches with nitrogenated compounds in the mass spectral database, and the co-elution of  $m/z$  43 (possibly  $\text{C}_2\text{H}_3\text{O}^+$ ) and  $m/z$  79 (possibly  $\text{C}_4\text{H}_3\text{N}_2\text{O}^+$ ) could signal the presence of nitrogenated oxidized organics. Finally, factor 4 (F4) is dominated by multiple fragments characteristic of less-oxidized or unsaturated organic material, including  $m/z$  55 ( $\text{C}_4\text{H}_7^+$ ),  $m/z$  67 ( $\text{C}_5\text{H}_7^+$ ), and  $m/z$  91 ( $\text{C}_7\text{H}_7^+$ ); this factor may also include contributions from air ( $m/z$  40;  $\text{Ar}^+$ ) and  $m/z$  79 split from factor 3.

A 5-factor solution was chosen for the wood BBOA chromatograms (Figure 10s-13, 14; additional information provided in Figures S9d and S9d). Factor 1 (F1) is dominated by  $m/z$  44, attributed to decomposing oxidized organics ( $\text{CO}_2^+$ ). Acetic acid was identifiable in factor 2 (F2) based on relative abundances of  $m/z$  43 ( $\text{C}_2\text{H}_3\text{O}^+$ ),  $m/z$  45 ( $\text{CHO}_2^+$ ), and  $m/z$  60 ( $\text{C}_2\text{H}_4\text{O}_2^+$ ), suggesting that organic acids comprise part of the thermal decomposition OA. Factor 3 (F3) features  $m/z$  50 and  $m/z$  52 (possibly  $\text{CH}_3^{35}\text{Cl}^+$  and  $\text{CH}_3^{37}\text{Cl}^+$ , respectively) in the 3:1 isotopic ratio characteristic of chlorine, indicating that the wood BBOA may contain chlorinated organics. Based on comparison of retention times, the large contribution of  $m/z$  44 to factor 3 may be due to splitting from factor 1. Factor 4 is dominated by ions characteristic of less-oxygenated or unsaturated organic material, including  $m/z$  55 ( $\text{C}_4\text{H}_7^+$ ),  $m/z$  72 ( $\text{C}_4\text{H}_8\text{O}^+$ ), and  $m/z$

1670 84 ( $C_5H_8O^+$ ). Lastly, factor 5 (F5) has been identified as furfural using the mass spectral database, which has been previously reported in gas-phase mass spectral measurements of biomass burning emissions (Stockwell et al., 2015).

1675 Because of the lack of chemical resolution in the thermal decomposition window, trends in factors with oxidative aging remain difficult to interpret. Notably, the factors featuring  $m/z$  44 (F1 in both Figure 9.44 and 10.3) increase with photochemical aging, consistent with an increase in oxidized OA. In the heartwood BBOA, F2 (acetic acid) and F4 (less-oxidized organics) appear to peak at 3.41-3 days of equivalent aging, though the mechanisms driving this change remain uncertain. The PMF results obtained in this study will be used to develop appropriate standards for the TAG thermal decomposition window, allowing for more quantitative analysis and easier identification of mass spectral fragments in future field and laboratory work.

### 3.3.4 $m/z$ 60 as a Tracer for both Primary and Aged BBOA

1680 The signal eluting between minutes 27 and 32 of GC analysis results from the co-elution of multiple compounds, including levoglucosan. Like levoglucosan, most of these co-eluting species exhibit  $m/z$  60 (dominated by the  $C_2H_4O^+$  ion) as a major fragment in their mass spectra. These compounds are poorly resolved because the non-polar GC column is not designed to resolve such polar compounds. SICs at different levels of oxidation reveal that each compound within this retention time window reacts at a unique rate, allowing for the identification of different co-eluting species.

1685 Heartwood and leaf BBOA  $m/z$  60 single ion chromatograms (SICs) at each level of oxidation are given in Figure 15, and relative abundances of key  $m/z$  60 fragmenting species in the TAG compound window are provided in Supplemental Information (Tables S8-S11 and S12). In the unaged oak wood BBOA chromatograms, approximately 82% of the TAG compound window  $m/z$  60 signal has been identified as levoglucosan (retention time determined from authentic standards; Figure S13 in Supplemental Information), though other sugars and anhydro-sugars exist in lower abundances. While some levoglucosan (between 8.35% and 3.20%) is present in the oak leaf BBOA chromatograms, up to 60% of the TAG compound  $m/z$  60 signal comes from quinic acid, which elutes beginning at minute 29 (retention time determined from authentic standards; Figure S13-S18 in Supplemental Information). The differences in sources of  $m/z$  60 between types of biomass illustrate that the  $m/z$  60 signal in any given BBOA sample may be highly complex and dependent on the type of biomass burned. Additionally, the presence of  $m/z$  60 is likely dependent on the combustion characteristics, as combustion processes can influence the emission and phase of different compounds.

1690 1695 1700 In the leaf and heartwood BBOA, an increase in the  $m/z$  60 signal was observed in the decomposition window from 0 to 9.86-10 days of equivalent aging, in agreement with individual compound and thermal decomposition window integrations (Figures 11, 12). Deconvolution PMF results demonstrate that the  $m/z$  60 decomposition signal co-elutes with  $m/z$  43 and  $m/z$  45 signals, which likely correspond to  $C_2H_3O^+$  and  $CHO_2^+$ , respectively, and is distinct from the mass spectrum of levoglucosan (Figure S14 in Supplemental Information). The co-elution of these three fragments and their relative integrated abundances provides evidence that organic acids constitute a portion of the decomposing OA. Further, the increase in the  $m/z$  60 integrated signal suggests that these acids are formed during

oxidative reactions occurring in the PAM chamber, either through heterogeneous oxidation of primary BBOA or condensation of oxidized SOA material.

1705 Relative rates of decay for integrated  $m/z$  60 fragmenting species are given in Figure 126. For leaf BBOA (Figure 16a-12a), these compounds include levoglucosan, quinic acid, mannose, and octadecanoic acid, and for wood BBOA (Figure 16b-12b), these include levoglucosan, guanosine, galactoheptulose, n-acetyl-d-galactosamine, and 1,6-anhydro- $\alpha$ -d-galactofuranose. The TAG decomposition window  $m/z$  60 signal, total TAG compound window  $m/z$  60 signal, and AMS  $f_{60}$  (the ratio of  $m/z$  60 to the total signal; Ng et al., 2011) are also included in Figure 16a-12a and 16b-12b for comparison. All values have been normalized to the signal obtained at 0 days of equivalent aging. The normalized abundances for TAG species were obtained by integrating each compound's  $m/z$  60 signal at each level of oxidation, then dividing each peak area by the peak area obtained in the unaged chromatograms ("0 days"). As with TAG species, AMS  $f_{60}$  has been normalized at each level of oxidation to the AMS  $f_{60}$  obtained without photochemical aging.

1710 Primary TAG species generally decrease in abundance with photochemical aging, though rates of decay vary depending on the compound. By contrast, in both wood and leaf BBOA, the TAG decomposition  $m/z$  60 summed signal increases overall from zero to 9.86-10 days of equivalent aging, peaking at 3.41-3 days of aging. In the leaf BBOA, the AMS  $m/z$  60 signal decreases by approximately 10% at 9.86-10 days of aging, while the AMS  $f_{60}$  in the wood BBOA is reduced to 50% of its original value at the highest level of oxidation. These trends in AMS  $f_{60}$  may 1715 reflect the combined effects of the oxidative decay of BBOA compounds, including sugars and anhydrosugars, and the formation of organic acids with functionalization reactions in the PAM chamber. Previous BBOA chemical characterization studies have identified organic acids as BBOA tracers (Falkovich et al., 2005; Lin et al., 2016; Mazzoleni et al., 2007), and Ortega et al. report that organic acids formed through OFR-driven oxidation may 1720 contribute to net AMS  $m/z$  60 (Ortega et al., 2013).

1725 Figure 12c displays experimental relative abundances as functions of equivalent aging time for various TAG and AMS markers observed during wood BBOA oxidation, along with levoglucosan decay rates calculated using  $k_{LG}$  values obtained in previous studies (Hennigan et al., 2010; Kessler et al., 2010). In addition, AMS  $f_{60}$  values obtained for PAM-aged turkey oak BBOA (*Q. laevis*) during the FLAME-3 campaign (Ortega et al., 2013) are overlaid for comparison; the values plotted correspond to  $f_{60} = 0.028$  at  $\text{OH}_{\text{exp}} = 0$  molec  $\text{cm}^{-3}$  s and  $f_{60} = 0.016$  at  $\text{OH}_{\text{exp}} = 5.6 \times 10^{11}$  molec  $\text{cm}^{-3}$  s (approximately 4 days of equivalent aging based on their PAM reactor calibration), with each point normalized to  $f_{60} = 0.028$  (Ortega et al., 2013).

Field Code Changed

Field Code Changed

Field Code Changed

1730 The  $\text{OH-OH}$ -driven oxidation kinetics of levoglucosan in BBOA have been investigated in previous chamber oxidation studies. For example, Kessler et al. obtained a second order rate constant of  $k_{LG} = (3.09 \pm 0.18) \times 10^{-13}$  molec $^{-1}$   $\text{cm}^3$  s $^{-1}$  from AMS measurements of OFR-oxidized levoglucosan particles (Kessler et al., 2010), while Hennigan et al. obtained a rate constant of  $k_{LG} = (1.1 \pm 0.5) \times 10^{-11}$  molec $^{-1}$   $\text{cm}^3$  s $^{-1}$  from smog chamber experiments (Hennigan et al., 2010). Lai et al. obtained expressions for  $k_{LG}$  as a function of relative humidity and temperature in their own smog chamber experiments; at 25°C and 30% relative humidity,  $k_{LG} = 1.107 \times 10^{-11}$  cm $^3$

1740 molec<sup>-1</sup> s<sup>-1</sup>, a value in good agreement with Hennigan, et al. et al.'s results (Lai et al., 2014). Lai, et al. et al. attribute the discrepancy between Kessler, et al. et al.'s and Hennigan, et al. et al.'s calculated  $k_{LG}$  to differences in both the levoglucosan detection method and experimental OH-OH concentration ranges. First, while Hennigan, et al. et al. used offline filter collections to determine levoglucosan concentrations, Kessler, et al. et al. took online measurements using an AMS and used  $m/z$  144 as the marker fragment for levoglucosan. Lai, et al. et al. explain suggest that because the parent ion of  $m/z$  162 was not used as the marker fragment in Kessler, et al. et al.'s AMS measurements, any potential effects from reaction products cannot be fully isolated, possibly leading to an underestimate of levoglucosan decay. However, our chromatographic methods are not subject to this mass spectral interference, and in the case of the heartwood BBOA, the TAG-measured levoglucosan decay matches the decay predicted by Kessler et al. Additionally, Lai, et al. et al. suggest that their own results may differ from those obtained by Kessler, et al. et al. because they operated at much lower OH-OH concentrations. During these experiments, During our oxidation experiments, OH-OH concentrations ([OH-OH]) ranged from  $10^9 - 10^{10}$  molec cm<sup>-3</sup>, closer to the operating conditions of Kessler, et al. et al. ([OH-OH] =  $10^9 - 2 \times 10^{11}$  molec cm<sup>-3</sup>; Kessler et al., 2010) than Lai, et al. et al. ([OH-OH] =  $3.50 \times 10^7$  molec cm<sup>-3</sup>; Lai et al., 2014).

1745 While levoglucosan decays rapidly in the leaf BBOA with increasing OH<sub>exp</sub>, levoglucosan in the heartwood BBOA is depleted more slowly. Levoglucosan is classified as semivolatile (at 25°C,  $p_L^{\circ} \sim 1.81 \times 10^{-7}$  torr; ACD/Labs, 2017) and is therefore expected to partition between the gas and particle phases. To approximate phase partitioning, particle-phase fractions for levoglucosan ( $\xi_{LG}$ ) were calculated based on AMS total organic concentrations and effective saturation concentrations ( $C_{LG}^*$ ,  $\mu\text{g m}^{-3}$ ) using equation 2. The resulting values and relevant parameters are reported in Table S12. For each fuel, little variance is expected in levoglucosan particle-phase fraction between oxidation conditions, so we conclude that phase partitioning is unlikely to be driving trends in levoglucosan abundances observed in these experiments. Based on the partitioning approximations, the leaf BBOA is expected to contain a higher percentage of levoglucosan in the particle phase than the heartwood BBOA (91.1 ± 1.65% vs 77.8% ± 2.26%), though in both cases, gas-phase levoglucosan concentrations are likely to remain low. The prevalence of levoglucosan in the particle phase during photochemical aging is consistent with previous laboratory measurements of aged levoglucosan particles (Kessler et al., 2010). Considering that heartwood BBOA exhibited lower total organic concentrations than the leaf BBOA, the slower depletion of levoglucosan in the heartwood samples is perhaps consistent with OH suppression effects, wherein OH experiences increased reactivity with gas-phase species at the particle surface.

1750 Figure 16c displays experimental relative abundances as functions of equivalent aging time for various TAG and AMS markers observed during wood BBOA oxidation, along with levoglucosan decay rates calculated using  $k_{LG}$  values obtained in previous studies (Kessler et al., 2010; Lai et al., 2014). In addition, AMS  $f_{\omega}$  values obtained for PAM-1755 aged turkey oak BBOA (*Q. laevis*) during the FLAME 3 campaign (Ortega et al., 2013) are overlaid for comparison; the values plotted correspond to  $f_{\omega} = 0.028$  at OH<sub>exp</sub> = 0 molec cm<sup>-3</sup> s and  $f_{\omega} = 0.016$  at OH<sub>exp</sub> =  $5.6 \times 10^{14}$  molec cm<sup>-3</sup> s (approximately 4.3 days of equivalent aging based on their PAM reactor calibration), with each point normalized to  $f_{\omega} = 0.028$  (Ortega et al., 2013). While levoglucosan decays rapidly in the leaf BBOA with increasing OH<sub>exp</sub>,

Field Code Changed

Field Code Changed

Field Code Changed

Field Code Changed

1775 levoglucosan in the wood BBOA is depleted more slowly. Levoglucosan is classified as semivolatile (at 25°C,  $p_L^o \sim 1.81 \times 10^{-7}$  torr; ACD/Labs, 2017) and is therefore expected to partition between the gas and particle phases. The discrepancy in levoglucosan decay rates between wood and leaf BBOA could therefore be attributed to increased levoglucosan gas to particle phase partitioning in the wood BBOA, since levoglucosan concentrations are expected to be higher in oak wood BBOA than in oak leaf BBOA due to a higher typical presence of cellulose in oak wood (Jin et al., 2013; Suberkropp et al., 1976). OH suppression, which could result from increased reactivity of OH with other species at the particle surface, may also contribute to a slower rate of levoglucosan decay in wood BBOA than leaf BBOA. The AMS  $m/z$  60 signal agrees well with the levoglucosan decay rate calculated using Kessler, et al., et al.'s  $k_{LG}$ , and decreases with increasing OH<sub>exp</sub>, though displays less overall decay compared to levoglucosan measured by the TAG. Our results demonstrate that although  $m/z$  60 may be an effective tracer for levoglucosan and primary BBOA under certain conditions, the formation of organic acids through photochemical aging may also impact AMS  $m/z$  60 and should be considered when using the AMS to track levoglucosan and primary BBOA in future studies. Furthermore, these results illustrate the utility of TAG data in interpreting AMS bulk OA measurements, as it gives both molecular characterization as well as additional insight on the chemical makeup of the most aged OA through evaluation of thermal decomposition components.

1780 **Field Code Changed**

#### 4 Conclusions and Atmospheric Implications

1790 The experimental methods presented in this work allow repeatable collection, oxidation, and molecular-level analysis of source-specific BBOA. The identification of molecular tracers unique to leaf and wood fuels can aid apportionment of BBOA to different plant fractions. For example, based on our results, a BBOA plume exhibiting high concentrations of aliphatic leaf wax components may be attributed to canopy or leaf litter devolatilization and combustion, while a plume with high concentrations of levoglucosan and lignin decomposition products could be attributed to heartwood combustion. Additionally, our results suggest that certain molecular tracers components present in freshly-emitted BBOA of interest may persist after 3 days of equivalent aging and may even increase in abundance with atmospheric aging due to reaction or gas-to-particle partitioning. The relative rates of OH- $\cdot$  driven decay obtained from TAG measurements may thus inform future field observations where molecular speciation information is obtained for photochemically aged plumes.

1800 The PMF deconvolution results support the identification and analysis of individual compounds present in heartwood and leaf BBOA. Because each chromatogram may contain hundreds of compounds, a general knowledge of the compound classes characteristic of each BBOA type can greatly reduce individual compound analysis time and ensure that chromatograms are characterized as completely as possible. The results presented in this study therefore confirm that the chromatogram binning method coupled with PMF, as developed by Zhang et al. (Zhang et al., 2014, 2016), can aid molecular tracer analysis by elucidating different compound classes of interest present in BBOA. The PMF results obtained in this study for the compound window provide information on characteristic mass spectral signatures within leaf and wood primary BBOA and may be compared to results obtained in future BBOA studies to more fully characterize how different compounds evolve with photochemical aging in the atmosphere.

1810 Based on previous studies, combustion conditions are expected to significantly impact the chemical composition of both primary and secondary BBOA (Ortega et al., 2013; Reece et al., 2017; Weimer et al., 2008; see “AMS Chemical Characterization” in Supplemental Information). The resistive heating technique applied in these experiments allows for the isolation of devolatilization (pre-combustion) and low-temperature ( $\leq 300^{\circ}\text{C}$ ) smoldering conditions, which is difficult to achieve in combustion chambers that require ignition of a flame. For example, Tian et al. designed a chamber that allows the user to control the relative contributions of smoldering and flaming combustion, though smoldering combustion is only achieved in this chamber following the introduction of a flame to the biomass fuel (Tian et al., 2015). The devolatilization and combustion procedure presented here is thus advantageous for investigating aerosol from small masses of biomass fuel under tightly controlled conditions. However, these results alone are likely not representative of a real-world system, where smoldering combustion often occurs alongside flaming combustion. Our results may therefore serve to complement field measurements, where either smoldering or flaming combustion may dominate, as well as laboratory studies where combustion conditions are controlled.

Field Code Changed

1815 Future work will focus on characterizing sources of bias to improve quantification of material in both the TAG compound and decomposition window. For example, particle matrix effects, whereby certain compounds exhibit enhanced or diminished recovery due to the presence of a particle matrix, have been reported to influence compound responses in previous work with the TAG and other thermal desorption GC systems, particularly for large molecular weight compounds (Lambe et al., 2009; Lavrich and Hays, 2007). Lambe et al. quantified this effect for the TAG by co-injecting a constant  $\text{C}_{30}$  deuterated alkane standard with 0.60  $\mu\text{g}$  motor oil and found that the presence of the motor oil matrix enhanced recovery of the standard by a factor of 2-3 (Lambe et al., 2009). In these experiments, the TAG collected estimated ranges of 6-16  $\mu\text{g}$  particles for leaf BBOA and 22-36  $\mu\text{g}$  particles for heartwood BBOA. Based on these mass ranges, we do not expect these matrix effects to contribute significantly to our results, especially for the 1820 lower molecular weight compounds. However, future work will incorporate an evaluation of matrix effects to minimize bias in TAG measurements.

Field Code Changed

1825 Although the TAG’s OA analysis capability has historically been limited by poor mass throughput of highly oxygenated species, we demonstrate here that the TAG decomposition window can be used to gain a better understanding of the molecular composition of oxidized BBOA. While the decomposition window does not provide chemical composition information with molecular resolution, the chromatogram binning PMF results allow identification of different co-eluting factors, many of which correspond to molecular fragments that could be used as source-specific BBOA tracers in future field studies.

1830 The utility of the thermal decomposition window is limited by a lack of adequate analytical standards, particularly for organic components. Although ammonium sulfate and ammonium nitrate standards have been used to quantify sulfate and nitrate particles in previous work (Williams et al., 2016), the development of satisfactory standards for decomposing organics remains difficult for several reasons. While fragments eluting in the decomposition window may be tentatively identified using available mass spectral identification tools, we often cannot infer the source of the fragments, since they are products of compound thermal decomposition rather than volatilization. Many of the compounds undergoing decomposition during sample desorption may therefore be too involatile for typical GC-MS

Field Code Changed

1845 analysis. Despite these challenges, analytical standards are currently under development to aid identification and interpretation of decomposition window results based on molecular functionality.

For both types of BBOA, the  $m/z$  44 signal in the TAG decomposition window increases with photochemical aging, confirming that this signal indicates the presence of thermally labile oxygenated OA and may provide information on the photochemical age of the aerosol sample. The increase in  $m/z$  44 with oxidation in both the TAG decomposition window and the AMS mass spectra is consistent with results from previous studies (Williams et al., 2016). However, our observations suggest that the utility of decomposition  $m/z$  44 as a quantifiable tracer for aged OA varies depending on OA type. For oak wood BBOA, the TAG decomposition  $m/z$  44 signal correlates well with AMS  $\overline{OS}_C$ , suggesting that for this type of BBOA, the decomposition  $m/z$  44 abundance could be used to estimate the aerosol's oxidation state. By contrast, the correlation between TAG decomposition  $m/z$  44 and AMS  $\overline{OS}_C$  is not significant for PAM-aged oak leaf BBOA, perhaps because compounds formed with photochemical aging of leaf BBOA are less thermally labile and more resistant to thermal decomposition than those found in aged wood BBOA. In addition, without mass-based standard calibrations for the decomposition window, distinguishing between an increase in thermally labile mass (i.e. due to SOA formation) and a relative increase in thermally decomposing OA due to changes in chemical composition (i.e. due to heterogeneous oxidation and functionalization) remains challenging.

1860 From the TAG data, we observe two competing effects driving the overall  $m/z$  60 signal measured in the AMS; while many primary BBOA components exhibiting a characteristic  $m/z$  60 fragment, including anhydrosugars like levoglucosan, were depleted with photochemical aging, an enhanced  $m/z$  60 signal in the decomposition window may signal increased formation of organic acids in the PAM reactor. Both processes have been reported in previous literature, though the oxidative depletion of primary BBOA is most typically thought to drive AMS  $m/z$  60 trends in field and laboratory studies. Our data suggest that although AMS measurements provide useful chemical composition information on bulk OA, laboratory studies with molecular-level measurements are needed to complement AMS data and provide a more complete understanding of processes occurring in the atmosphere.

1870 The mechanisms driving compositional changes in BBOA remain difficult to interpret. While many compounds observed in this study are clearly depleted through functionalization reactions, some species may be subjected to phase partitioning effects in addition to PAM-driven oxidation. In particular, the enhancement in TAG thermal decomposition  $m/z$  44 and  $m/z$  60 may occur due to formation of SOA through oxidation and condensation of low-volatility gases, heterogeneous functionalization of compounds in the particle phase, or a combination of these processes. Future studies will focus on investigating the role of phase partitioning in OA chemical composition within BBOA plumes, with emphasis on the thermally labile material eluting in the TAG thermal decomposition window. In addition, different types of biomass will be tested to explore the dependence of phase partitioning and photochemical aging effects on fuel type, broadening the applicability of these techniques to future field measurements.

1875 **Field Code Changed**

#### Data Availability

Data from this study are available upon request by contacting the corresponding author.

#### **Acknowledgements**

1880 The material presented is based on work supported by the National Science Foundation (award no. 1437933). The  
authors would also like to acknowledge support from the International Center for Energy, Environment and  
Sustainability (INCEES) and the McDonnell Academy Global Energy and Environment Partnership (MAGEEP) at  
Washington University in St. Louis. The authors would also like to thank Audrey Dang, Benjamin Sumlin, and  
Junseok Lee for assisting with supplementary CO measurements. Finally, the authors would like to thank Benjamin  
Sumlin for his insight during the editing process.

## 1885 References

ACD/Labs: Advanced Chemistry Development (ACD/Labs) Software V11.02 (© 1994–2012 ACD/Labs), Retrieved  
from <http://www.cas.org/products/scifinder>, 11 May, 2017.

Field Code Changed

1890 Appel, B. R., Tokiwa, Y., Hsu, J., Kothny, E. L. and Hahn, E.: Visibility as related to atmospheric aerosol  
constituents. *Atmospheric Environ.* 1967, 19(9), 1525–1534, doi:10.1016/0004-6981(85)90290-2, 1985.

1895 Bond, T. C., Streets, D. G., Yarber, K. F., Nelson, S. M., Woo, J.-H. and Klimont, Z.: A technology-based global  
inventory of black and organic carbon emissions from combustion. *J. Geophys. Res. Atmospheres*, 109(D14),  
D14203, doi:10.1029/2003JD003697, 2004.

1900 Burling, I. R., Yokelson, R. J., Griffith, D. W. T., Johnson, T. J., Veres, P., Roberts, J. M., Warneke, C., Urbanski,  
S. P., Reardon, J., Weise, D. R., Hao, W. M. and de Gouw, J.: Laboratory measurements of trace gas emissions from  
biomass burning of fuel types from the southeastern and southwestern United States. *Atmos Chem Phys*, 10(22),  
11115–11130, doi:10.5194/acp-10-11115-2010, 2010.

1905 Canagaratna, M. r., Jayne, J. t., Jimenez, J. l., Allan, J. d., Alfarra, M. r., Zhang, Q., Onasch, T. b., Drewnick, F.,  
Coe, H., Middlebrook, A., Delia, A., Williams, L. r., Trimborn, A. m., Northway, M. j., DeCarlo, P. f., Kolb, C. e.,  
Davidovits, P. and Worsnop, D. r.: Chemical and microphysical characterization of ambient aerosols with the  
aerodyne aerosol mass spectrometer. *Mass Spectrom. Rev.*, 26(2), 185–222, doi:10.1002/mas.20115, 2007.

1910 Capes, G., Johnson, B., McFiggans, G., Williams, P. I., Haywood, J. and Coe, H.: Aging of biomass burning  
aerosols over West Africa: Aircraft measurements of chemical composition, microphysical properties, and emission  
ratios. *J. Geophys. Res. Atmospheres*, 113(D23), D00C15, doi:10.1029/2008JD009845, 2008.

1915 Cubison, M. J., Ortega, A. M., Hayes, P. L., Farmer, D. K., Day, D., Lechner, M. J., Brune, W. H., Apel, E., Diskin,  
G. S., Fisher, J. A., Fuelberg, H. E., Hecobian, A., Knapp, D. J., Mikoviny, T., Riemer, D., Sachse, G. W., Sessions,  
W., Weber, R. J., Weinheimer, A. J., Wisthaler, A. and Jimenez, J. L.: Effects of aging on organic aerosol from open  
biomass burning smoke in aircraft and laboratory studies. *Atmos Chem Phys*, 11(23), 12049–12064,  
doi:10.5194/acp-11-12049-2011, 2011.

1920 D'Anna, B., Andresen, Ø., Gefen, Z. and Nielsen, C. J.: Kinetic study of OH and NO<sub>3</sub> radical reactions with 14  
aliphatic aldehydes. *Phys. Chem. Chem. Phys.*, 3(15), 3057–3063, doi:10.1039/B103623H, 2001.

1925 DeCarlo, P. F., Kimmel, J. R., Trimborn, A., Northway, M. J., Jayne, J. T., Aiken, A. C., Gonin, M., Fuhrer, K.,  
Horvath, T., Docherty, K. S., Worsnop, D. R. and Jimenez, J. L.: Field-Deployable, High-Resolution, Time-of-  
Flight Aerosol Mass Spectrometer. *Anal. Chem.*, 78(24), 8281–8289, doi:10.1021/ac061249n, 2006.

1930 Donahue, N. M., Robinson, A. L., Stanier, C. O. and Pandis, S. N.: Coupled Partitioning, Dilution, and Chemical  
Aging of Semivolatile Organics. *Environ. Sci. Technol.*, 40(8), 2635–2643, doi:10.1021/es052297c, 2006.

1935 Falkovich, A. H., Gruber, E. R., Schkolnik, G., Rudich, Y., Maenhaut, W. and Artaxo, P.: Low molecular weight  
organic acids in aerosol particles from Rondônia, Brazil, during the biomass-burning, transition and wet periods.  
*Atmos Chem Phys*, 5(3), 781–797, doi:10.5194/acp-5-781-2005, 2005.

1920 Fine, P. M., Cass, G. R. and Simoneit, B. R. T.: Organic compounds in biomass smoke from residential wood combustion: Emissions characterization at a continental scale, *J. Geophys. Res. Atmospheres*, 107(D21), Art. No 8349, 2002.

Forman, G. S., Hauser, A. B. and Adda, S. M.: Life cycle analysis of gas to liquids (GTL) derived linear alkyl benzene, *J. Clean. Prod.*, 80, 30–37, doi:10.1016/j.jclepro.2014.05.058, 2014.

1925 Fraser, M. P. and Lakshmanan, K.: Using Levoglucosan as a Molecular Marker for the Long-Range Transport of Biomass Combustion Aerosols, *Environ. Sci. Technol.*, 34(21), 4560–4564, doi:10.1021/es991229l, 2000.

Goldstein, A. H. and Galbally, I. E.: Known and Unexplored Organic Constituents in the Earth's Atmosphere, *Environ. Sci. Technol.*, 41(5), 1514–1521, doi:10.1021/es072476p, 2007.

1930 Grieshop, A. P., Logue, J. M., Donahue, N. M. and Robinson, A. L.: Laboratory investigation of photochemical oxidation of organic aerosol from wood fires 1: measurement and simulation of organic aerosol evolution, *Atmos. Chem. Phys.*, 9(4), 1263–1277, doi:10.5194/acp-9-1263-2009, 2009.

Gulz, P. G. and Boor, G.: Seasonal Variations in Epicuticular Wax Ultrastructures of Quercus robur Leaves, *Z. Naturforsch.*, 47c, 807–814, 1992.

1935 Hennigan, C. J., Sullivan, A. P., Collett, J. L. and Robinson, A. L.: Levoglucosan stability in biomass burning particles exposed to hydroxyl radicals, *Geophys. Res. Lett.*, 37(9), doi:10.1029/2010GL043088, 2010.

Hoffmann, D., Tilgner, A., Iinuma, Y. and Herrmann, H.: Atmospheric stability of levoglucosan: a detailed laboratory and modeling study, *Environ. Sci. Technol.*, 44(2), 694–699, doi:10.1021/es902476f, 2010.

1940 Isaacman, G., Kreisberg, N. M., Yee, L. D., Worton, D. R., Chan, A. W. H., Moss, J. A., Hering, S. V. and Goldstein, A. H.: Online derivatization for hourly measurements of gas- and particle-phase semi-volatile oxygenated organic compounds by thermal desorption aerosol gas chromatography (SV-TAG), *Atmos. Meas. Tech.*, 7(12), 4417–4429, doi:10.5194/amt-7-4417-2014, 2014.

Kampa, M. and Castanas, E.: Human health effects of air pollution, *Environ. Pollut.*, 151(2), 362–367, doi:10.1016/j.envpol.2007.06.012, 2008.

1945 Kanakidou, M., Seinfeld, J. H., Pandis, S. N., Barnes, I., Dentener, F. J., Facchini, M. C., Van Dingenen, R., Ervens, B., Nenes, A., Nielsen, C. J., Swietlicki, E., Putaud, J. P., Balkanski, Y., Fuzzi, S., Horth, J., Moortgat, G. K., Winterhalter, R., Myhre, C. E. L., Tsigaridis, K., Vignati, E., Stephanou, E. G. and Wilson, J.: Organic aerosol and global climate modelling: a review, *Atmos. Chem. Phys.*, 5(4), 1053–1123, doi:10.5194/acp-5-1053-2005, 2005.

Kang, E., Root, M. J., Toohey, D. W. and Brune, W. H.: Introducing the concept of Potential Aerosol Mass (PAM), *Atmos. Chem. Phys.*, 7(22), 5727–5744, doi:10.5194/acp-7-5727-2007, 2007.

1950 Kessler, S. H., Smith, J. D., Che, D. L., Worsnop, D. R., Wilson, K. R. and Kroll, J. H.: Chemical Sinks of Organic Aerosol: Kinetics and Products of the Heterogeneous Oxidation of Erythritol and Levoglucosan, *Environ. Sci. Technol.*, 44(18), 7005–7010, doi:10.1021/es101465m, 2010.

Kreisberg, N. M., Hering, S. V., Williams, B. J., Worton, D. R. and Goldstein, A. H.: Quantification of Hourly Speciated Organic Compounds in Atmospheric Aerosols, Measured by an In-Situ Thermal Desorption Aerosol Gas Chromatograph (TAG), *Aerosol Sci. Technol.*, 43(1), 38–52, doi:10.1080/02786820802459583, 2009.

1955 Kroll, J. H., Smith, J. D., Che, D. L., Kessler, S. H., Worsnop, D. R. and Wilson, K. R.: Measurement of fragmentation and functionalization pathways in the heterogeneous oxidation of oxidized organic aerosol, *Phys. Chem. Chem. Phys.*, 11(36), 8005–8014, doi:10.1039/B905289E, 2009.

1960 Kroll, J. H., Donahue, N. M., Jimenez, J. L., Kessler, S. H., Canagaratna, M. R., Wilson, K. R., Altieri, K. E., Mazzoleni, L. R., Wozniak, A. S., Bluhm, H., Mysak, E. R., Smith, J. D., Kolb, C. E. and Worsnop, D. R.: Carbon oxidation state as a metric for describing the chemistry of atmospheric organic aerosol, *Nat. Chem.*, 3(2), 133–139, doi:10.1038/nchem.948, 2011.

1965 Kwok, E. S. C. and Atkinson, R.: Estimation of hydroxyl radical reaction rate constants for gas-phase organic compounds using a structure-reactivity relationship: An update, *Atmos. Environ.*, 29(14), 1685–1695, doi:10.1016/1352-2310(95)00069-B, 1995.

Lai, C., Liu, Y., Ma, J., Ma, Q. and He, H.: Degradation kinetics of levoglucosan initiated by hydroxyl radical under different environmental conditions, *Atmos. Environ.*, 91, 32–39, doi:10.1016/j.atmosenv.2014.03.054, 2014.

1970 Lambe, A. T., Logue, J. M., Kreisberg, N. M., Hering, S. V., Worton, D. R., Goldstein, A. H., Donahue, N. M. and Robinson, A. L.: Apportioning black carbon to sources using highly time-resolved ambient measurements of organic molecular markers in Pittsburgh, *Atmos. Environ.*, 43(25), 3941–3950, doi:10.1016/j.atmosenv.2009.04.057, 2009.

Lambe, A. T., Ahern, A. T., Williams, L. R., Slowik, J. G., Wong, J. P. S., Abbatt, J. P. D., Brune, W. H., Ng, N. L., Wright, J. P., Croasdale, D. R., Worsnop, D. R., Davidovits, P. and Onasch, T. B.: Characterization of aerosol photooxidation flow reactors: heterogeneous oxidation, secondary organic aerosol formation and cloud condensation nuclei activity measurements, *Atmos. Meas. Tech.*, 4(3), 445–461, doi:10.5194/amt-4-445-2011, 2011.

1975 Lavrich, R. J. and Hays, M. D.: Validation studies of thermal extraction-GC/MS applied to source emissions aerosols. 1. Semivolatile analyte-nonvolatile matrix interactions, *Anal. Chem.*, 79(10), 3635–3645, doi:10.1021/ac0623282, 2007.

1980 Lee, T., Sullivan, A. P., Mack, L., Jimenez, J. L., Kreidenweis, S. M., Onasch, T. B., Worsnop, D. R., Malm, W., Wold, C. E., Hao, W. M. and Jr, J. L. C.: Chemical Smoke Marker Emissions During Flaming and Smoldering Phases of Laboratory Open Burning of Wildland Fuels, *Aerosol Sci. Technol.*, 44(9), i–v, doi:10.1080/02786826.2010.499884, 2010.

1985 Li, R., Palm, B. B., Ortega, A. M., Hlywiak, J., Hu, W., Peng, Z., Day, D. A., Knot, C., Brune, W. H., de Gouw, J. A. and Jimenez, J. L.: Modeling the Radical Chemistry in an Oxidation Flow Reactor: Radical Formation and Recycling, Sensitivities, and the OH Exposure Estimation Equation, *J. Phys. Chem. A*, 119(19), 4418–4432, doi:10.1021/jp509534k, 2015.

Lin, P., Aiona, P. K., Li, Y., Shiraiwa, M., Laskin, J., Nizkorodov, S. A. and Laskin, A.: Molecular Characterization of Brown Carbon in Biomass Burning Aerosol Particles, *Environ. Sci. Technol.*, 50(21), 11815–11824, doi:10.1021/acs.est.6b03024, 2016.

1990 Locker, H. B.: The use of levoglucosan to assess the environmental impact of residential wood-burning on air quality, ResearchGate [online] Available from: <https://www.researchgate.net/publication/236428890> The use of levoglucosan to assess the environmental impact of residential wood-burning on air quality (Accessed 16 January 2017), 1988.

1995 Mao, J., Ren, X., Brune, W. H., Olson, J. R., Crawford, J. H., Fried, A., Huey, L. G., Cohen, R. C., Heikes, B., Singh, H. B., Blake, D. R., Sachse, G. W., Diskin, G. S., Hall, S. R. and Shetter, R. E.: Airborne measurement of OH reactivity during INTEX-B, *Atmos. Chem. Phys.*, 9(1), 163–173, doi:10.5194/acp-9-163-2009, 2009.

May, A. A., Levin, E. J. T., Hennigan, C. J., Riipinen, I., Lee, T., Collett, J. L., Jimenez, J. L., Kreidenweis, S. M. and Robinson, A. L.: Gas-particle partitioning of primary organic aerosol emissions: 3. Biomass burning, *J. Geophys. Res. Atmospheres*, 118(19), 2013JD020286, doi:10.1002/jgrd.50828, 2013.

2000 Mazzoleni, L. R., Zielinska, B. and Moosmüller, H.: Emissions of Levoglucosan, Methoxy Phenols, and Organic Acids from Prescribed Burns, Laboratory Combustion of Wildland Fuels, and Residential Wood Combustion, *Environ. Sci. Technol.*, 41(7), 2115–2122, doi:10.1021/es061702c, 2007.

Mellott, P.: Development and Testing of Novel Atmospheric Chemistry Technologies, MS Thesis, Washington University in St. Louis, St. Louis, MO., 2012.

2005 Mitroo, D.: Applications and Flow Visualization of a Potential Aerosol Mass Reactor, PhD Thesis, Washington University in St. Louis, St. Louis, MO., 2017.

2010 Ng, N. L., Canagaratna, M. R., Zhang, Q., Jimenez, J. L., Tian, J., Ulbrich, I. M., Kroll, J. H., Docherty, K. S., Chhabra, P. S., Bahreini, R., Murphy, S. M., Seinfeld, J. H., Hildebrandt, L., Donahue, N. M., DeCarlo, P. F., Lanz, V. A., Prévôt, A. S. H., Dinar, E., Rudich, Y. and Worsnop, D. R.: Organic aerosol components observed in Northern Hemispheric datasets from Aerosol Mass Spectrometry, *Atmos Chem Phys*, 10(10), 4625–4641, doi:10.5194/acp-10-4625-2010, 2010.

2015 Ng, N. L., Canagaratna, M. R., Jimenez, J. L., Chhabra, P. S., Seinfeld, J. H. and Worsnop, D. R.: Changes in organic aerosol composition with aging inferred from aerosol mass spectra, *Atmos Chem Phys*, 11(13), 6465–6474, doi:10.5194/acp-11-6465-2011, 2011a.

Ng, N. L., Canagaratna, M. R., Jimenez, J. L., Zhang, Q., Ulbrich, I. M. and Worsnop, D. R.: Real-Time Methods for Estimating Organic Component Mass Concentrations from Aerosol Mass Spectrometer Data, *Environ. Sci. Technol.*, 45(3), 910–916, doi:10.1021/es102951k, 2011b.

2020 Niki, H., Maker, P. D., Savage, C. M. and Breitenbach, L. P.: Relative rate constants for the reaction of hydroxyl radical with aldehydes, *J. Phys. Chem.*, 82(2), 132–134, doi:10.1021/j100491a002, 1978.

Ortega, A. M., Day, D. A., Cubison, M. J., Brune, W. H., Bon, D., de Gouw, J. A. and Jimenez, J. L.: Secondary organic aerosol formation and primary organic aerosol oxidation from biomass-burning smoke in a flow reactor during FLAME-3, *Atmos Chem Phys*, 13(22), 11551–11571, doi:10.5194/acp-13-11551-2013, 2013.

2025 Paatero, P.: Least squares formulation of robust non-negative factor analysis, *Chemom. Intell. Lab. Syst.*, 37(1), 23–35, doi:10.1016/S0169-7439(96)00044-5, 1997.

Peng, Z., Day, D. A., Stark, H., Li, R., Lee-Taylor, J., Palm, B. B., Brune, W. H. and Jimenez, J. L.: HO<sub>x</sub> radical chemistry in oxidation flow reactors with low-pressure mercury lamps systematically examined by modeling, *Atmos Meas Tech*, 8(11), 4863–4890, doi:10.5194/amt-8-4863-2015, 2015.

2030 Peng, Z., Day, D. A., Ortega, A. M., Palm, B. B., Hu, W., Stark, H., Li, R., Tsigaridis, K., Brune, W. H. and Jimenez, J. L.: Non-OH chemistry in oxidation flow reactors for the study of atmospheric chemistry systematically examined by modeling, *Atmos Chem Phys*, 16(7), 4283–4305, doi:10.5194/acp-16-4283-2016, 2016.

Reece, S. M., Sinha, A. and Grieshop, A. P.: Primary and Photochemically Aged Aerosol Emissions from Biomass Cookstoves: Chemical and Physical Characterization, *Environ. Sci. Technol.*, 51(16), 9379–9390, doi:10.1021/acs.est.7b01881, 2017.

Rogge, W. F., Hildemann, L. M., Mazurek, M. A. and Cass, G. R.: Sources of Fine Organic Aerosol. 9. Pine, Oak, and Synthetic Log Combustion in Residential Fireplaces, *Environ. Sci. Technol.*, 32(1), 13–22, doi:10.1021/es960930b, 1998.

2040 Simoneit, B. R. T., Schauer, J. J., Nolte, C. G., Oros, D. R., Elias, V. O., Fraser, M. P., Rogge, W. F. and Cass, G. R.: Levoglucosan, a tracer for cellulose in biomass burning and atmospheric particles, *Atmos. Environ.*, 33(2), 173–182, doi:10.1016/S1352-2310(98)00145-9, 1999.

Simoneit, B. R. T., Rogge, W. F., Lang, Q. and Jaffé, R.: Molecular characterization of smoke from campfire burning of pine wood (*Pinus elliottii*), *Chemosphere - Glob. Change Sci.*, 2(1), 107–122, doi:10.1016/S1465-9972(99)00048-3, 2000.

2045 Simoneit, B. R. T., Kobayashi, M., Mochida, M., Kawamura, K. and Huebert, B. J.: Aerosol particles collected on aircraft flights over the northwestern Pacific region during the ACE-Asia campaign: Composition and major sources of the organic compounds, *J. Geophys. Res. Atmospheres*, 109(D19), D19S09, doi:10.1029/2004JD004565, 2004.

2050 Smith, J. D., Kroll, J. H., Cappa, C. D., Che, D. L., Liu, C. L., Ahmed, M., Leone, S. R., Worsnop, D. R. and Wilson, K. R.: The heterogeneous reaction of hydroxyl radicals with sub-micron squalane particles: a model system for understanding the oxidative aging of ambient aerosols, *Atmos Chem Phys*, 9(9), 3209–3222, doi:10.5194/acp-9-3209-2009, 2009.

2055 Stein, S. E. and Scott, D. R.: Optimization and testing of mass spectral library search algorithms for compound identification, *J. Am. Soc. Mass Spectrom.*, 5(9), 859–866, doi:10.1016/1044-0305(94)87009-8, 1994.

Stockwell, C. E., Veres, P. R., Williams, J. and Yokelson, R. J.: Characterization of biomass burning emissions from cooking fires, peat, crop residue, and other fuels with high-resolution proton-transfer-reaction time-of-flight mass spectrometry, *Atmos Chem Phys*, 15(2), 845–865, doi:10.5194/acp-15-845-2015, 2015.

2060 Sumlin, B. J., Pandey, A., Walker, M. J., Pattison, R. S., Williams, B. J. and Chakrabarty, R. K.: Atmospheric Photooxidation Diminishes Light Absorption by Primary Brown Carbon Aerosol from Biomass Burning, *Environ. Sci. Technol. Lett.*, doi:10.1021/acs.estlett.7b00393, 2017.

2065 Tian, J., Chow, J., Cao, J., Han, Y., Ni, H., Chen, L.-W. A., Wang, X., Huang, R., Moosmüller, H. and Watson, J.: A Biomass Combustion Chamber: Design, Evaluation, and a Case Study of Wheat Straw Combustion Emission Tests, *Aerosol Air Qual. Res.*, 15(5), 2104–2114, 2015.

Ulbrich, I. M., Canagaratna, M. R., Zhang, Q., Worsnop, D. R. and Jimenez, J. L.: Interpretation of organic components from Positive Matrix Factorization of aerosol mass spectrometric data, *Atmos Chem Phys*, 9(9), 2891–2918, doi:10.5194/acp-9-2891-2009, 2009.

2070 Watson, J. T. and Sparkman, O. D.: *Introduction to Mass Spectrometry: Instrumentation, Applications, and Strategies for Data Interpretation*, 4th ed., John Wiley & Sons Ltd, West Sussex, England., 2007.

Weimer, S., Alfara, M. R., Schreiber, D., Mohr, M., Prévôt, A. S. H. and Baltensperger, U.: Organic aerosol mass spectral signatures from wood-burning emissions: Influence of burning conditions and wood type, *J. Geophys. Res. Atmospheres*, 113(D10), D10304, doi:10.1029/2007JD009309, 2008.

Williams, B. J., Goldstein, A. H., Kreisberg, N. M. and Hering, S. V.: An In-Situ Instrument for Speciated Organic Composition of Atmospheric Aerosols: Thermal Desorption Aerosol GC/MS-FID (TAG), *Aerosol Sci. Technol.*, 40(8), 627–638, doi:10.1080/02786820600754631, 2006.

2075 Williams, B. J., Goldstein, A. H., Millet, D. B., Holzinger, R., Kreisberg, N. M., Hering, S. V., White, A. B., Worsnop, D. R., Allan, J. D. and Jimenez, J. L.: Chemical speciation of organic aerosol during the International Consortium for Atmospheric Research on Transport and Transformation 2004: Results from in situ measurements, *J. Geophys. Res. Atmospheres*, 112(D10), D10S26, doi:10.1029/2006JD007601, 2007.

2080 Williams, B. J., Goldstein, A. H., Kreisberg, N. M., Hering, S. V., Worsnop, D. R., Ulbrich, I. M., Docherty, K. S. and Jimenez, J. L.: Major components of atmospheric organic aerosol in southern California as determined by hourly measurements of source marker compounds, *Atmos Chem Phys*, 10(23), 11577–11603, doi:10.5194/acp-10-11577-2010, 2010.

Williams, B. J., Jayne, J. T., Lambe, A. T., Hohaus, T., Kimmel, J. R., Sueper, D., Brooks, W., Williams, L. R., Trimborn, A. M., Martinez, R. E., Hayes, P. L., Jimenez, J. L., Kreisberg, N. M., Hering, S. V., Worton, D. R.,

2085 Goldstein, A. H. and Worsnop, D. R.: The First Combined Thermal Desorption Aerosol Gas Chromatograph—  
Aerosol Mass Spectrometer (TAG-AMS), *Aerosol Sci. Technol.*, 48(4), 358–370,  
doi:10.1080/02786826.2013.875114, 2014.

Williams, B. J., Zhang, Y., Zuo, X., Martinez, R. E., Walker, M. J., Kreisberg, N. M., Goldstein, A. H., Docherty, K. S. and Jimenez, J. L.: Organic and inorganic decomposition products from the thermal desorption of atmospheric particles, *Atmos Meas Tech*, 9(4), 1569–1586, doi:10.5194/amt-9-1569-2016, 2016.

2090 Wong, J. P. S., Nenes, A. and Weber, R. J.: Changes in Light Absorptivity of Molecular Weight Separated Brown Carbon Due to Photolytic Aging, *Environ. Sci. Technol.*, 51(15), 8414–8421, doi:10.1021/acs.est.7b01739, 2017.

Wong, Z., Chen, K. and Li, J.: Formation of Vanillin and Syringaldehyde in an Oxygen Delignification Process, *BioResources*, 5(3), 1509–1516, doi:10.15376/biores.5.3.1509-1516, 2010.

2095 Worton, D. R., Goldstein, A. H., Farmer, D. K., Docherty, K. S., Jimenez, J. L., Gilman, J. B., Kuster, W. C., de Gouw, J., Williams, B. J., Kreisberg, N. M., Hering, S. V., Bench, G., McKay, M., Kristensen, K., Glasius, M., Surratt, J. D. and Seinfeld, J. H.: Origins and composition of fine atmospheric carbonaceous aerosol in the Sierra Nevada Mountains, California, *Atmos Chem Phys*, 11(19), 10219–10241, doi:10.5194/acp-11-10219-2011, 2011.

Zhang, Q., Jimenez, J. L., Canagaratna, M. R., Allan, J. D., Coe, H., Ulbrich, I., Alfarra, M. R., Takami, A., Middlebrook, A. M., Sun, Y. L., Dzepina, K., Dunlea, E., Docherty, K., DeCarlo, P. F., Salcedo, D., Onasch, T., Jayne, J. T., Miyoshi, T., Shimono, A., Hatakeyama, S., Takegawa, N., Kondo, Y., Schneider, J., Drewnick, F., Borrmann, S., Weimer, S., Demerjian, K., Williams, P., Bower, K., Bahreini, R., Cottrell, L., Griffin, R. J., Rautiainen, J., Sun, J. Y., Zhang, Y. M. and Worsnop, D. R.: Ubiquity and dominance of oxygenated species in organic aerosols in anthropogenically-influenced Northern Hemisphere midlatitudes, *Geophys. Res. Lett.*, 34(13), L13801, doi:10.1029/2007GL029979, 2007.

2105 Zhang, Y., Williams, B. J., Goldstein, A. H., Docherty, K., Ulbrich, I. M. and Jimenez, J. L.: A Technique for Rapid Gas Chromatography Analysis Applied to Ambient Organic Aerosol Measurements from the Thermal Desorption Aerosol Gas Chromatograph (TAG), *Aerosol Sci. Technol.*, 48(11), 1166–1182, doi:10.1080/02786826.2014.967832, 2014.

Zhang, Y., Williams, B. J., Goldstein, A. H., Docherty, K. S. and Jimenez, J. L.: A technique for rapid source apportionment applied to ambient organic aerosol measurements from a thermal desorption aerosol gas chromatograph (TAG), *Atmos Meas Tech*, 9(11), 5637–5653, doi:10.5194/amt-9-5637-2016, 2016.

2110 Zhao, R., Lee, A. K. Y., Huang, L., Li, X., Yang, F. and Abbatt, J. P. D.: Photochemical processing of aqueous atmospheric brown carbon, *Atmos Chem Phys*, 15(11), 6087–6100, doi:10.5194/acp-15-6087-2015, 2015.

ACD/Labs: Advanced Chemistry Development (ACD/Labs) Software V11.02 (© 1994–2012 ACD/Labs), Retrieved from <http://www.eas.org/products/seifinder>, 11 May, 2017.

2115 Appel, B. R., Tokiwa, Y., Hsu, J., Kothny, E. L. and Hahn, E.: Visibility as related to atmospheric aerosol constituents, *Atmospheric Environ.* 1967, 19(9), 1525–1534, doi:10.1016/0004-6981(85)90290-2, 1985.

Bond, T. C., Streets, D. G., Yarber, K. F., Nelson, S. M., Woo, J. H. and Klimont, Z.: A technology-based global inventory of black and organic carbon emissions from combustion, *J. Geophys. Res. Atmospheres*, 109(D14), D14203, doi:10.1029/2003JD003697, 2004.

2120 Canagaratna, M. R., Jayne, J. T., Jimenez, J. L., Allan, J. D., Alfarra, M. R., Zhang, Q., Onasch, T. B., Drewnick, F., Coe, H., Middlebrook, A., Delia, A., Williams, L. R., Trimborn, A. M., Northway, M. J., DeCarlo, P. F., Kolb, C. E., Davidovits, P. and Worsnop, D. R.: Chemical and microphysical characterization of ambient aerosols with the aerodyne aerosol mass spectrometer, *Mass Spectrom. Rev.*, 26(2), 185–222, doi:10.1002/mas.20115, 2007.

2125 Capes, G., Johnson, B., McFiggans, G., Williams, P. I., Haywood, J. and Coe, H.: Aging of biomass burning aerosols over West Africa: Aircraft measurements of chemical composition, microphysical properties, and emission ratios, *J. Geophys. Res. Atmospheres*, 113(D23), D00C15, doi:10.1029/2008JD009845, 2008.

2130 Cubison, M. J., Ortega, A. M., Hayes, P. L., Farmer, D. K., Day, D., Lechner, M. J., Brune, W. H., Apel, E., Diskin, G. S., Fisher, J. A., Fuelberg, H. E., Heebman, A., Knapp, D. J., Mikoviny, T., Riemer, D., Sachse, G. W., Sessions, W., Weber, R. J., Weinheimer, A. J., Wisthaler, A. and Jimenez, J. L.: Effects of aging on organic aerosol from open biomass burning smoke in aircraft and laboratory studies, *Atmos Chem Phys*, 11(23), 12049–12064, doi:10.5194/acp-11-12049-2011, 2011.

D'Anna, B., Andresen, Ø., Gefen, Z. and Nielsen, C. J.: Kinetic study of OH and NO<sub>3</sub> radical reactions with 14 aliphatic aldehydes, *Phys. Chem. Chem. Phys.*, 3(15), 3057–3063, doi:10.1039/B102623H, 2001.

2135 DeCarlo, P. F., Kimmel, J. R., Trimborn, A., Northway, M. J., Jayne, J. T., Aiken, A. C., Gonin, M., Fuhrer, K., Horvath, T., Docherty, K. S., Worsnop, D. R. and Jimenez, J. L.: Field Deployable, High-Resolution, Time-of-Flight Aerosol Mass Spectrometer, *Anal. Chem.*, 78(24), 8281–8289, doi:10.1021/ae061249n, 2006.

2140 Falkovich, A. H., Gruber, E. R., Sehgalnik, G., Rudich, Y., Maenhaut, W. and Artaxo, P.: Low molecular weight organic acids in aerosol particles from Rondônia, Brazil, during the biomass burning, transition and wet periods, *Atmos Chem Phys*, 5(3), 781–797, doi:10.5194/acp-5-781-2005, 2005.

Fine, P. M., Cass, G. R. and Simoneit, B. R. T.: Organic compounds in biomass smoke from residential wood combustion: Emissions characterization at a continental scale, *J. Geophys. Res. Atmospheres*, 107(D21), Art. No 8349, 2002.

2145 Forman, G. S., Hauser, A. B. and Adda, S. M.: Life cycle analysis of gas to liquids (GTL) derived linear alkyl benzene, *J. Clean. Prod.*, 80, 30–37, doi:10.1016/j.jclepro.2014.05.058, 2014.

Fraser, M. P. and Lakshmanan, K.: Using Levoglucosan as a Molecular Marker for the Long-Range Transport of Biomass Combustion Aerosols, *Environ. Sci. Technol.*, 34(21), 4560–4564, doi:10.1021/es991229l, 2000.

Goldstein, A. H. and Galbally, I. E.: Known and Unexplored Organic Constituents in the Earth's Atmosphere, *Environ. Sci. Technol.*, 41(5), 1514–1521, doi:10.1021/es072476p, 2007.

2150 Grieshop, A. P., Logue, J. M., Donahue, N. M. and Robinson, A. L.: Laboratory investigation of photochemical oxidation of organic aerosol from wood fire: I: measurement and simulation of organic aerosol evolution, *Atmos. Chem. Phys.*, 9(4), 1263–1277, doi:10.5194/acp-9-1263-2009, 2009.

Gulz, P. G. and Boor, G.: Seasonal Variations in Epicuticular Wax Ultrastructures of *Quercus robur* Leaves, *Z. Naturforsch.*, 47e, 807–814, 1992.

2155 Hennigan, C. J., Sullivan, A. P., Collett, J. L. and Robinson, A. L.: Levoglucosan stability in biomass burning particles exposed to hydroxyl radicals, *Geophys. Res. Lett.*, 37(9), doi:10.1029/2010GL043088, 2010.

Hoffmann, D., Tilgner, A., Iinuma, Y. and Herrmann, H.: Atmospheric stability of levoglucosan: a detailed laboratory and modeling study, *Environ. Sci. Technol.*, 44(2), 694–699, doi:10.1021/es902476f, 2010.

2160 Jin, W., Singh, K. and Zondlo, J.: Pyrolysis Kinetics of Physical Components of Wood and Wood Polymers Using Isoconversion Method, *Agriculture*, 3(1), 12–32, doi:10.3390/agriculture3010012, 2013.

Kampa, M. and Castanas, E.: Human health effects of air pollution, *Environ. Pollut.*, 151(2), 362–367, doi:10.1016/j.envpol.2007.06.012, 2008.

Kanakidou, M., Seinfeld, J. H., Pandis, S. N., Barnes, I., Dentener, F. J., Facchini, M. C., Van Dingenen, R., Ervens, B., Nenes, A., Nielsen, C. J., Swietlicki, E., Putaud, J. P., Balkanski, Y., Fuzzi, S., Horth, J., Moortgat, G. K.,

2165 Winterhalter, R., Myhre, C. E. L., Tsigaridis, K., Vignati, E., Stephanou, E. G. and Wilson, J.: Organic aerosol and global climate modelling: a review, *Atmos. Chem. Phys.*, 5(4), 1053–1123, doi:10.5194/acp-5-1053-2005, 2005.

Kang, E., Root, M. J., Toohey, D. W. and Brune, W. H.: Introducing the concept of Potential Aerosol Mass (PAM), *Atmos. Chem. Phys.*, 7(22), 5727–5744, doi:10.5194/acp-7-5727-2007, 2007.

2170 Kessler, S. H., Smith, J. D., Che, D. L., Worsnop, D. R., Wilson, K. R. and Kroll, J. H.: Chemical Sinks of Organic Aerosol: Kinetics and Products of the Heterogeneous Oxidation of Erythritol and Levoglucosan, *Environ. Sci. Technol.*, 44(18), 7005–7010, doi:10.1021/es101465m, 2010.

Kreisberg, N. M., Hering, S. V., Williams, B. J., Worton, D. R. and Goldstein, A. H.: Quantification of Hourly Speciated Organic Compounds in Atmospheric Aerosols, Measured by an In-Situ Thermal Desorption Aerosol Gas Chromatograph (TAG), *Aerosol Sci. Technol.*, 43(1), 38–52, doi:10.1080/02786820802459583, 2009.

2175 Kroll, J. H., Smith, J. D., Che, D. L., Kessler, S. H., Worsnop, D. R. and Wilson, K. R.: Measurement of fragmentation and functionalization pathways in the heterogeneous oxidation of oxidized organic aerosol, *Phys. Chem. Chem. Phys.*, 11(36), 8005–8014, doi:10.1039/B905289E, 2009.

2180 Kroll, J. H., Donahue, N. M., Jimenez, J. L., Kessler, S. H., Canagaratna, M. R., Wilson, K. R., Altieri, K. E., Mazzoleni, L. R., Wozniak, A. S., Bluhm, H., Mysak, E. R., Smith, J. D., Kolb, C. E. and Worsnop, D. R.: Carbon oxidation state as a metric for describing the chemistry of atmospheric organic aerosol, *Nat. Chem.*, 3(2), 133–139, doi:10.1038/nchem.948, 2011.

Lai, C., Liu, Y., Ma, J., Ma, Q. and He, H.: Degradation kinetics of levoglucosan initiated by hydroxyl radical under different environmental conditions, *Atmos. Environ.*, 91, 32–39, doi:10.1016/j.atmosenv.2014.03.054, 2014.

2185 Lambe, A. T., Logue, J. M., Kreisberg, N. M., Hering, S. V., Worton, D. R., Goldstein, A. H., Donahue, N. M. and Robinson, A. L.: Apportioning black carbon to sources using highly time resolved ambient measurements of organic molecular markers in Pittsburgh, *Atmos. Environ.*, 43(25), 3941–3950, doi:10.1016/j.atmosenv.2009.04.057, 2009.

Lambe, A. T., Ahern, A. T., Williams, L. R., Slowik, J. G., Wong, J. P. S., Abbatt, J. P. D., Brune, W. H., Ng, N. L., Wright, J. P., Croasdale, D. R., Worsnop, D. R., Davidovits, P. and Onasch, T. B.: Characterization of aerosol photooxidation flow reactors: heterogeneous oxidation, secondary organic aerosol formation and cloud condensation nuclei activity measurements, *Atmos. Meas. Tech.*, 4(3), 445–461, doi:10.5194/amt-4-445-2011, 2011.

2190 Lee, T., Sullivan, A. P., Mack, L., Jimenez, J. L., Kreidenweis, S. M., Onasch, T. B., Worsnop, D. R., Malm, W., Wold, C. E., Hao, W. M. and Jr., J. L. C.: Chemical Smoke Marker Emissions During Flaming and Smoldering Phases of Laboratory Open Burning of Wildland Fuels, *Aerosol Sci. Technol.*, 44(9), i–v, doi:10.1080/02786826.2010.499884, 2010.

2195 Li, R., Palm, B. B., Ortega, A. M., Hlywiak, J., Hu, W., Peng, Z., Day, D. A., Knote, C., Brune, W. H., de Gouw, J. A. and Jimenez, J. L.: Modeling the Radical Chemistry in an Oxidation Flow Reactor: Radical Formation and Recycling, Sensitivities, and the OH Exposure Estimation Equation, *J. Phys. Chem. A*, 119(19), 4418–4432, doi:10.1021/jp509534k, 2015.

2200 Lin, P., Aiona, P. K., Li, Y., Shiraiwa, M., Laskin, J., Nizkorodov, S. A. and Laskin, A.: Molecular Characterization of Brown Carbon in Biomass Burning Aerosol Particles, *Environ. Sci. Technol.*, 50(21), 11815–11824, doi:10.1021/acs.est.6b03024, 2016.

Locke, H. B.: The use of levoglucosan to assess the environmental impact of residential wood-burning on air quality, PhD Thesis, Dartmouth College, Hanover, NH, 137 pp., 1988.

2205 Mao, J., Ren, X., Brune, W. H., Olson, J. R., Crawford, J. H., Fried, A., Huey, L. G., Cohen, R. C., Heikes, B., Singh, H. B., Blake, D. R., Sachse, G. W., Diskin, G. S., Hall, S. R. and Shetter, R. E.: Airborne measurement of OH reactivity during INTEX B, *Atmos. Chem. Phys.*, 9(1), 163–173, doi:10.5194/acp-9-163-2009, 2009.

May, A. A., Levin, E. J. T., Hennigan, C. J., Riipinen, I., Lee, T., Collett, J. L., Jimenez, J. L., Kreidenweis, S. M. and Robinson, A. L.: Gas particle partitioning of primary organic aerosol emissions: 3. Biomass burning, *J. Geophys. Res. Atmospheres*, 118(19), 2013JD020286, doi:10.1002/jgrd.50828, 2013.

2210 Mazzoleni, L. R., Zielinska, B. and Moosmüller, H.: Emissions of Levoglucosan, Methoxy Phenols, and Organic Acids from Prescribed Burns, Laboratory Combustion of Wildland Fuels, and Residential Wood Combustion, *Environ. Sci. Technol.*, 41(7), 2115–2122, doi:10.1021/es061702e, 2007.

2215 Ng, N. L., Canagaratna, M. R., Zhang, Q., Jimenez, J. L., Tian, J., Ulbrich, I. M., Kroll, J. H., Docherty, K. S., Chhabra, P. S., Bahreini, R., Murphy, S. M., Seinfeld, J. H., Hildebrandt, L., Donahue, N. M., DeCarlo, P. F., Lanz, V. A., Prévôt, A. S. H., Dinar, E., Rudich, Y. and Worsnop, D. R.: Organic aerosol components observed in Northern Hemisphere datasets from Aerosol Mass Spectrometry, *Atmos. Chem. Phys.*, 10(10), 4625–4641, doi:10.5194/acp-10-4625-2010, 2010.

2220 Ng, N. L., Canagaratna, M. R., Jimenez, J. L., Chhabra, P. S., Seinfeld, J. H. and Worsnop, D. R.: Changes in organic aerosol composition with aging inferred from aerosol mass spectra, *Atmos. Chem. Phys.*, 11(13), 6465–6474, doi:10.5194/acp-11-6465-2011, 2011a.

2225 Ng, N. L., Canagaratna, M. R., Jimenez, J. L., Zhang, Q., Ulbrich, I. M. and Worsnop, D. R.: Real-Time Methods for Estimating Organic Component Mass Concentrations from Aerosol Mass Spectrometer Data, *Environ. Sci. Technol.*, 45(3), 910–916, doi:10.1021/es102951k, 2011b.

2230 Niki, H., Maker, P. D., Savage, C. M. and Breitenbach, L. P.: Relative rate constants for the reaction of hydroxyl radical with aldehydes, *J. Phys. Chem.*, 82(2), 132–134, doi:10.1021/j100491a002, 1978.

Oros, D. R. and Simoneit, B. R. T.: Identification of Molecular Tracers in Organic Aerosols from Temperate Climate Vegetation Subjected to Biomass Burning, *Aerosol Sci. Technol.*, 31(6), 433–445, doi:10.1080/027868299303986, 1999.

2235 Ortega, A. M., Day, D. A., Cubison, M. J., Brune, W. H., Bon, D., de Gouw, J. A. and Jimenez, J. L.: Secondary organic aerosol formation and primary organic aerosol oxidation from biomass burning smoke in a flow reactor during FLAME 3, *Atmos. Chem. Phys.*, 13(22), 11551–11571, doi:10.5194/acp-13-11551-2013, 2013.

Paatero, P.: Least squares formulation of robust non-negative factor analysis, *Chemom. Intell. Lab. Syst.*, 37(1), 23–35, doi:10.1016/S0169-7439(96)00044-5, 1997.

2240 Peng, Z., Day, D. A., Stark, H., Li, R., Lee Taylor, J., Palm, B. B., Brune, W. H. and Jimenez, J. L.: HO<sub>x</sub> radical chemistry in oxidation flow reactors with low pressure mercury lamps systematically examined by modeling, *Atmos. Meas. Tech.*, 8(11), 4863–4890, doi:10.5194/amt-8-4863-2015, 2015.

Rogge, W. F., Hildemann, L. M., Mazurek, M. A. and Cass, G. R.: Sources of Fine Organic Aerosol. 9. Pine, Oak, and Synthetic Log Combustion in Residential Fireplaces, *Environ. Sci. Technol.*, 32(1), 13–22, doi:10.1021/es960930b, 1998.

2245 Simoneit, B. R. T., Schauer, J. J., Nolte, C. G., Oros, D. R., Elias, V. O., Fraser, M. P., Rogge, W. F. and Cass, G. R.: Levoglucosan, a tracer for cellulose in biomass burning and atmospheric particles, *Atmos. Environ.*, 33(2), 173–182, doi:10.1016/S1352-2310(98)00145-9, 1999.

Simoneit, B. R. T., Rogge, W. F., Lang, Q. and Jaffé, R.: Molecular characterization of smoke from campfire burning of pine wood (*Pinus elliottii*), *Chemosphere – Glob. Change Sci.*, 2(1), 107–122, doi:10.1016/S1465-9972(99)00048-3, 2000.

2250 Simoneit, B. R. T., Kobayashi, M., Mochida, M., Kawamura, K. and Huebert, B. J.: Aerosol particles collected on aircraft flights over the northwestern Pacific region during the ACE Asia campaign: Composition and major sources of the organic compounds, *J. Geophys. Res. Atmospheres*, 109(D19), D19S09, doi:10.1029/2004JD004565, 2004.

2250 Stein, S. E. and Scott, D. R.: Optimization and testing of mass spectral library search algorithms for compound identification, *J. Am. Soc. Mass Spectrom.*, 5(9), 859–866, doi:10.1016/1044-0305(94)87009-8, 1994.

Stockwell, C. E., Veres, P. R., Williams, J. and Yokelson, R. J.: Characterization of biomass burning emissions from cooking fires, peat, crop residue, and other fuels with high-resolution proton transfer reaction time-of-flight mass spectrometry, *Atmos. Chem. Phys.*, 15(2), 845–865, doi:10.5194/acp-15-845-2015, 2015.

2255 Suberkropp, K., Godshalk, G. L. and Klug, M. J.: Changes in the Chemical Composition of Leaves During Processing in a Woodland Stream, *Ecology*, 57(4), 720–727, doi:10.2307/1936185, 1976.

Ulbrich, I. M., Canagaratna, M. R., Zhang, Q., Worsnop, D. R. and Jimenez, J. L.: Interpretation of organic components from Positive Matrix Factorization of aerosol mass spectrometric data, *Atmos. Chem. Phys.*, 9(9), 2891–2918, doi:10.5194/acp-9-2891-2009, 2009.

2260 Watson, J. T. and Sparkman, O. D.: *Introduction to Mass Spectrometry: Instrumentation, Applications, and Strategies for Data Interpretation*, 4th ed., John Wiley & Sons Ltd, West Sussex, England., 2007.

Williams, B. J., Goldstein, A. H., Kreisberg, N. M. and Hering, S. V.: An In-Situ Instrument for Speciated Organic Composition of Atmospheric Aerosols: Thermal Desorption Aerosol GC/MS-FID (TAG), *Aerosol Sci. Technol.*, 40(8), 627–638, doi:10.1080/02786820600754631, 2006.

2265 Williams, B. J., Goldstein, A. H., Millet, D. B., Holzinger, R., Kreisberg, N. M., Hering, S. V., White, A. B., Worsnop, D. R., Allan, J. D. and Jimenez, J. L.: Chemical speciation of organic aerosol during the International Consortium for Atmospheric Research on Transport and Transformation 2004: Results from in situ measurements, *J. Geophys. Res. Atmospheres*, 112(D10), D10S26, doi:10.1029/2006JD007601, 2007.

2270 Williams, B. J., Goldstein, A. H., Kreisberg, N. M., Hering, S. V., Worsnop, D. R., Ulbrich, I. M., Docherty, K. S. and Jimenez, J. L.: Major components of atmospheric organic aerosol in southern California as determined by hourly measurements of source marker compounds, *Atmos. Chem. Phys.*, 10(23), 11577–11603, doi:10.5194/acp-10-11577-2010, 2010.

Williams, B. J., Jayne, J. T., Lambe, A. T., Hohaus, T., Kimmel, J. R., Sueper, D., Brooks, W., Williams, L. R., Trimborn, A. M., Martinez, R. E., Hayes, P. L., Jimenez, J. L., Kreisberg, N. M., Hering, S. V., Worton, D. R., Goldstein, A. H. and Worsnop, D. R.: The First Combined Thermal Desorption Aerosol Gas Chromatograph—Aerosol Mass Spectrometer (TAG-AMS), *Aerosol Sci. Technol.*, 48(4), 358–370, doi:10.1080/02786826.2013.875114, 2014.

2275 Williams, B. J., Zhang, Y., Zuo, X., Martinez, R. E., Walker, M. J., Kreisberg, N. M., Goldstein, A. H., Docherty, K. S. and Jimenez, J. L.: Organic and inorganic decomposition products from the thermal desorption of atmospheric particles, *Atmos. Meas. Tech.*, 9(4), 1569–1586, doi:10.5194/amt-9-1569-2016, 2016.

2280 Wong, Z., Chen, K. and Li, J.: Formation of Vanillin and Syringaldehyde in an Oxygen Delignification Process, *BioResources*, 5(3), 1509–1516, doi:10.15376/biores.5.3.1509-1516, 2010.

Worton, D. R., Goldstein, A. H., Farmer, D. K., Docherty, K. S., Jimenez, J. L., Gilman, J. B., Kuster, W. C., de Gouw, J., Williams, B. J., Kreisberg, N. M., Hering, S. V., Benet, G., McKay, M., Kristensen, K., Glasius, M., Surratt, J. D. and Seinfeld, J. H.: Origins and composition of fine atmospheric carbonaceous aerosol in the Sierra Nevada Mountains, California, *Atmos. Chem. Phys.*, 11(19), 10219–10241, doi:10.5194/acp-11-10219-2011, 2011.

2285 Zhang, Q., Jimenez, J. L., Canagaratna, M. R., Allan, J. D., Cao, H., Ulbrich, I., Alfarra, M. R., Takami, A., Middlebrook, A. M., Sun, Y. L., Dzepina, K., Dunlea, E., Docherty, K., DeCarlo, P. F., Salcedo, D., Onasch, T., Jayne, J. T., Miyoshi, T., Shimono, A., Hatakeyama, S., Takegawa, N., Kondo, Y., Schneider, J., Drewnick, F., Borrmann, S., Weimer, S., Demerjian, K., Williams, P., Bower, K., Bahreini, R., Cottrell, L., Griffin, R. J., Rautiainen, J., Sun, J. Y., Zhang, Y. M. and Worsnop, D. R.: Ubiquity and dominance of oxygenated species in

organic aerosols in anthropogenically influenced Northern Hemisphere midlatitudes, *Geophys. Res. Lett.*, 34(13), L13801, doi:10.1029/2007GL029979, 2007.

2295 Zhang, Y., Williams, B. J., Goldstein, A. H., Docherty, K., Ulbrich, I. M. and Jimenez, J. L.: A Technique for Rapid Gas Chromatography Analysis Applied to Ambient Organic Aerosol Measurements from the Thermal Desorption Aerosol Gas Chromatograph (TAG), *Aerosol Sci. Technol.*, 48(11), 1166–1182, doi:10.1080/02786826.2014.967832, 2014.

Zhang, Y., Williams, B. J., Goldstein, A. H., Docherty, K. S. and Jimenez, J. L.: A technique for rapid source apportionment applied to ambient organic aerosol measurements from a thermal desorption aerosol gas chromatograph (TAG), *Atmos. Meas. Tech.*, 9(11), 5637–5653, doi:10.5194/amt-9-5637-2016, 2016.

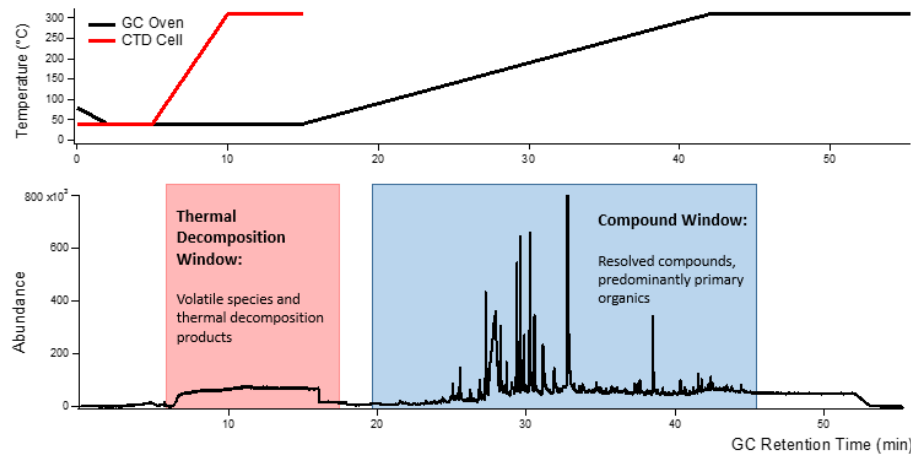
2300

2305

2310

2315

2320



2325 **Figure 1:** An example TAG chromatogram with GC oven and TAG collection and thermal desorption (CTD) cell temperature ramp programs.

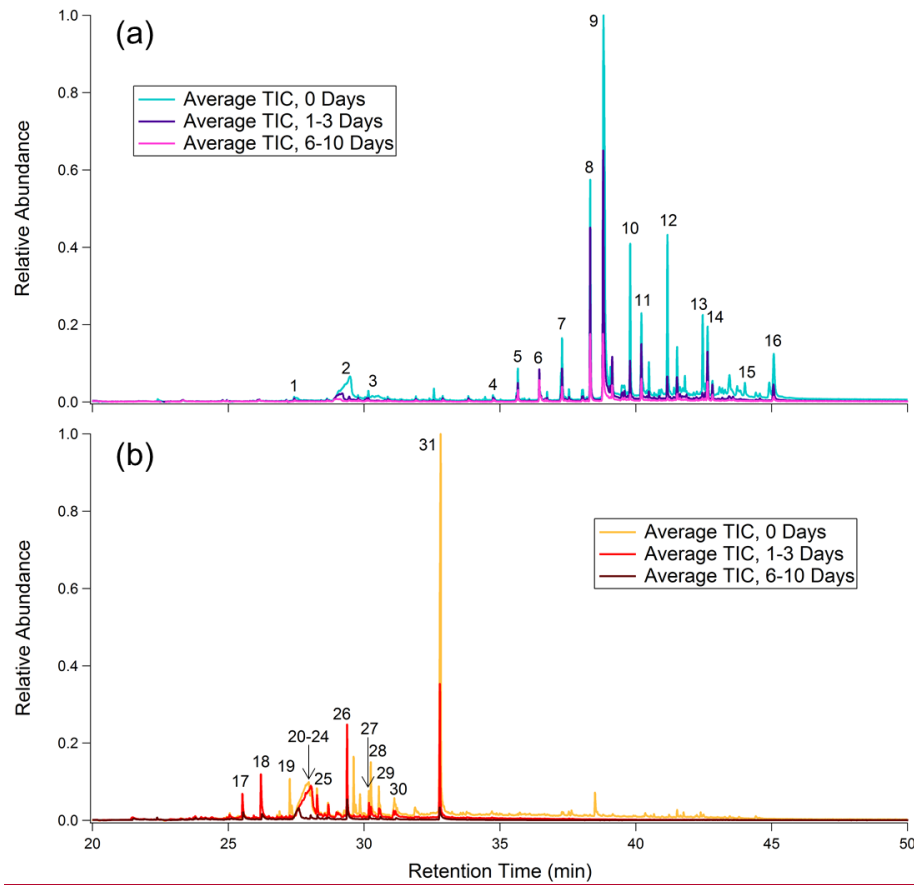
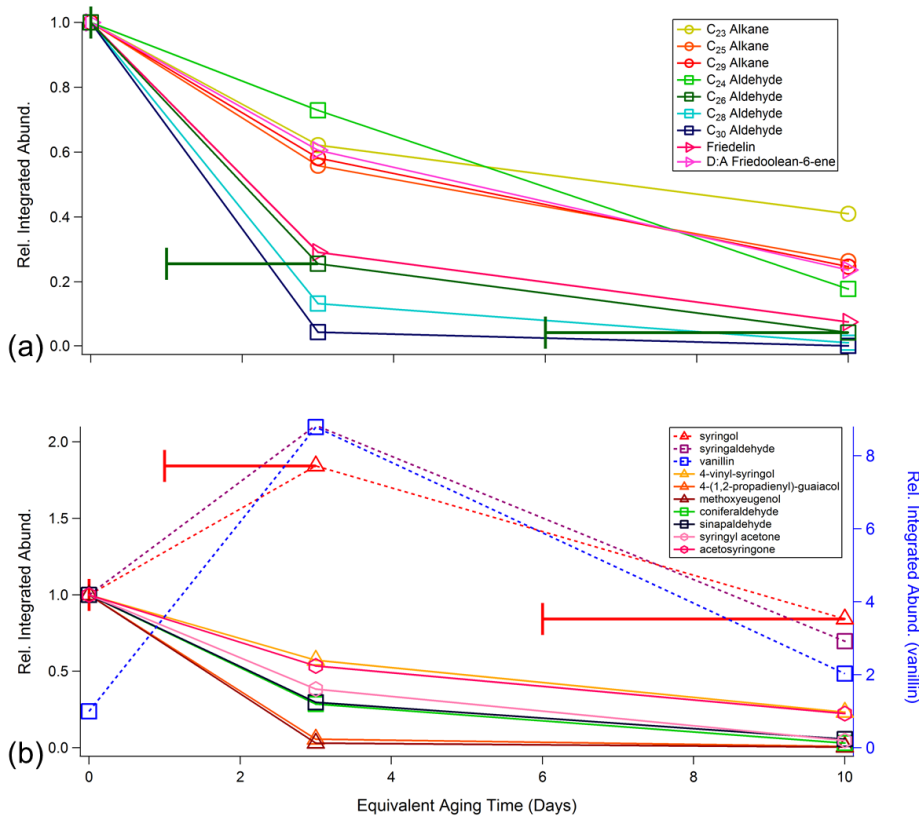


**Figure 2:** Chromatograms for (a) leaf BBOA and (b) heartwood BBOA at different levels of oxidation.

2330

Corresponding names and structures for numbered compounds are given in Tables S4-S5 and Figures S6-S7.

For each plot, all traces are normalized to the point of highest abundance within the average unaged chromatogram.



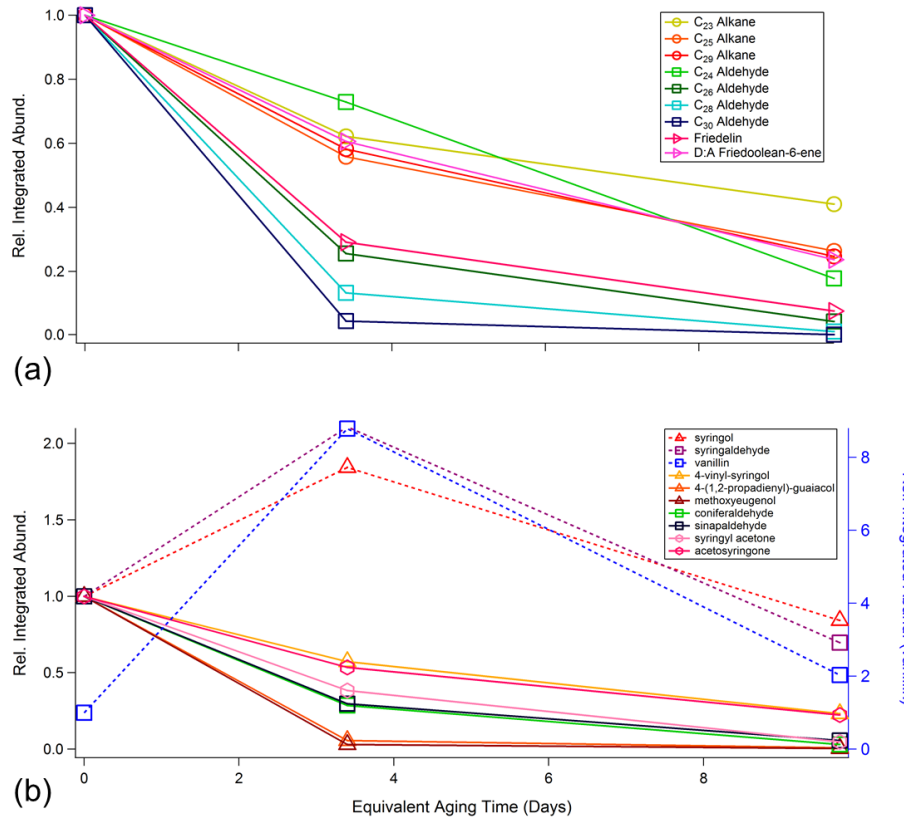
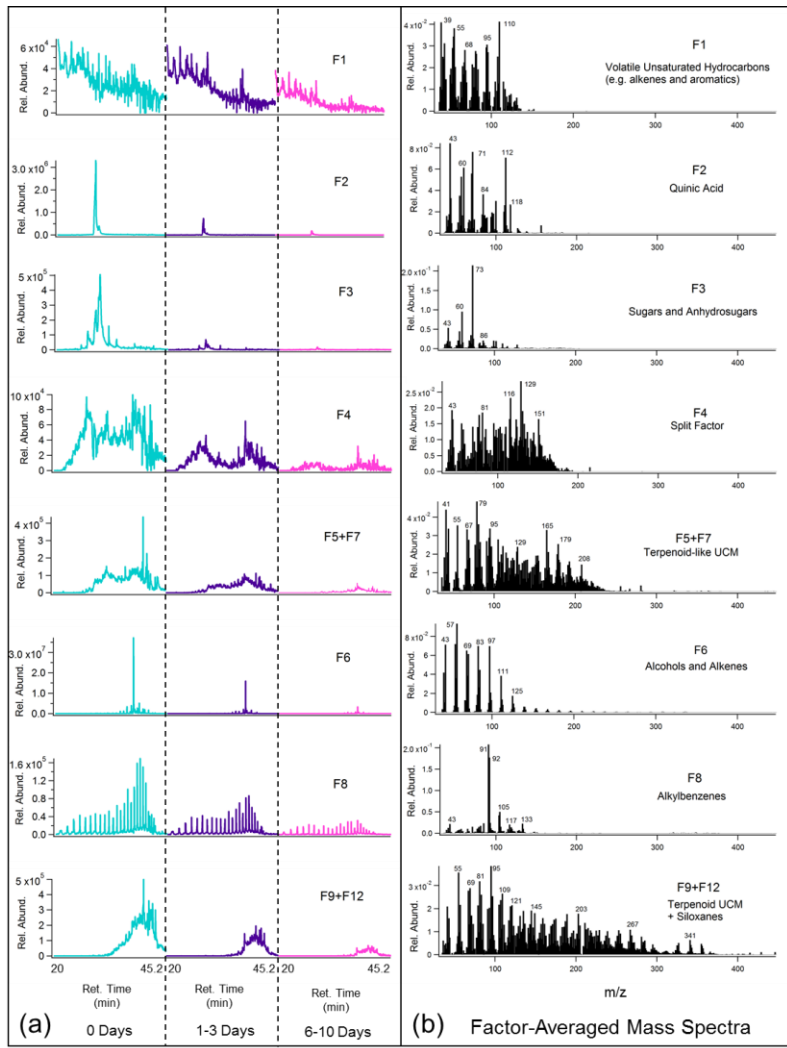


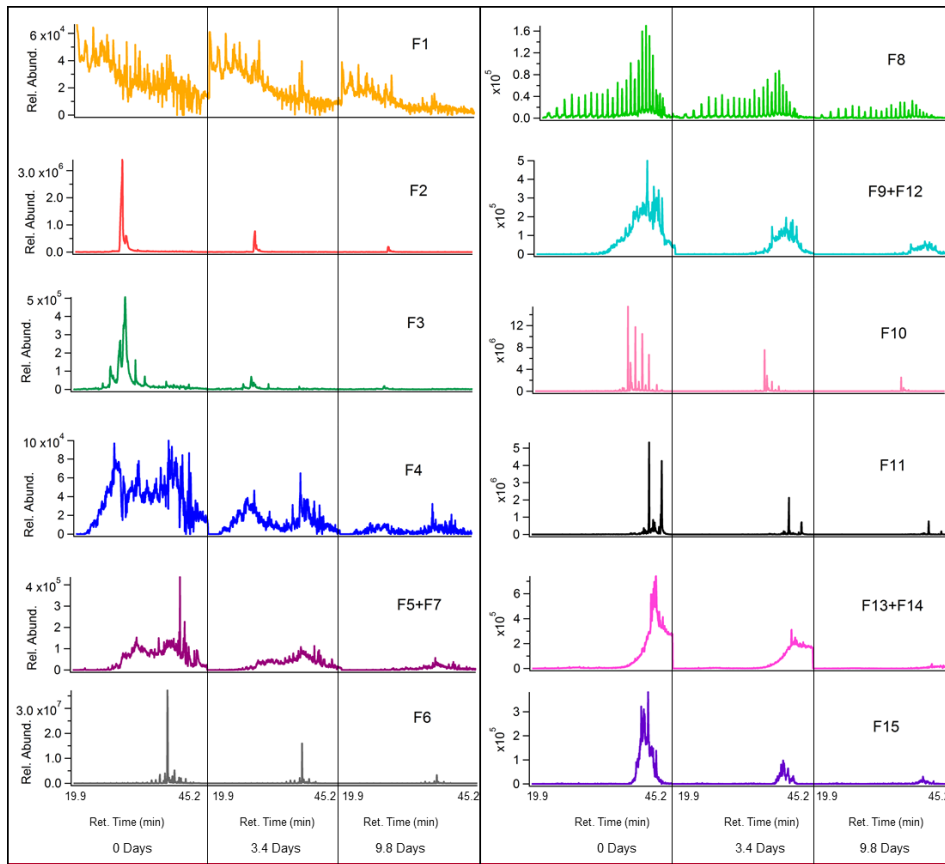
**Figure 3:** Relative changes in integrated abundance as a function of equivalent aging time (per  $\text{SO}_2$  calibrations) for primary compounds identified in (a) oak leaf BBOA chromatograms, and (b) oak heartwood BBOA chromatograms. For each compound, the integrated abundances were first normalized to appropriate volume concentrations, then subsequently normalized to corresponding abundances at no oxidation ("0 days"). Compounds that decrease in abundance are indicated with solid lines, while compounds that deviate from this trend are given with dotted lines. Raw compound abundances are provided in Supplemental Information (Tables S6 and S7). X-axis error bars denote equivalent aging time ranges calculated for this study and are applicable to all TAG data presented here, though they are only included on one compound per panel to preserve figure readability.

2340

2345



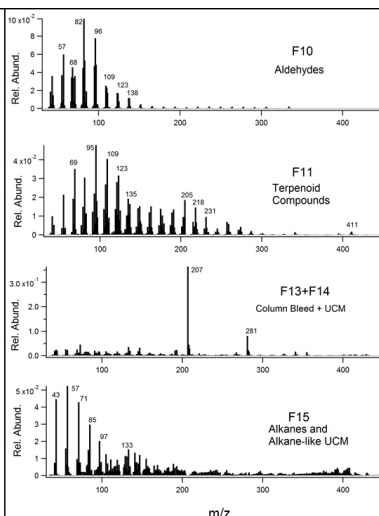
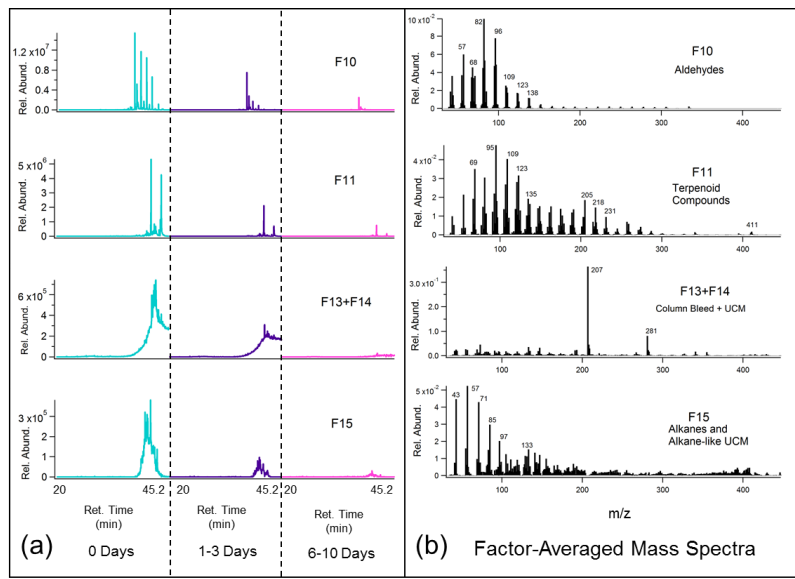


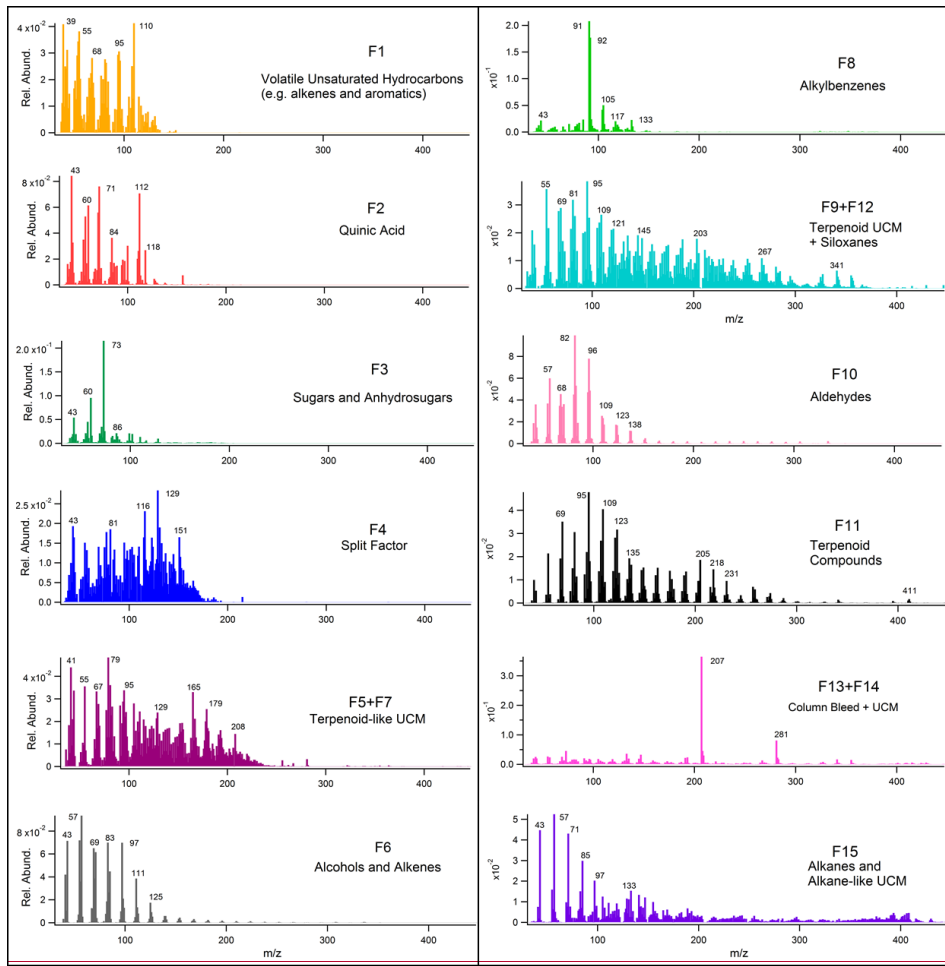


**Figure 4:** Average binned chromatograms and mass spectra for factors 1-9+12+15 (F1-9+12+15) in PMF 15-factor solution on TAG oak leaf BBOA compound window data. Relevant plots obtained in PMF calculations are provided in Supplemental Information (Figures S99a and S101a). These chromatograms were obtained from PMF calculations by averaging binned data corresponding to triplicate chromatograms at each level of oxidation. The triplicate-averaged binned chromatograms at each equivalent aging time are displayed in one trace; different aging times are demarcated with vertical lines across the x-axis.

2355

2360

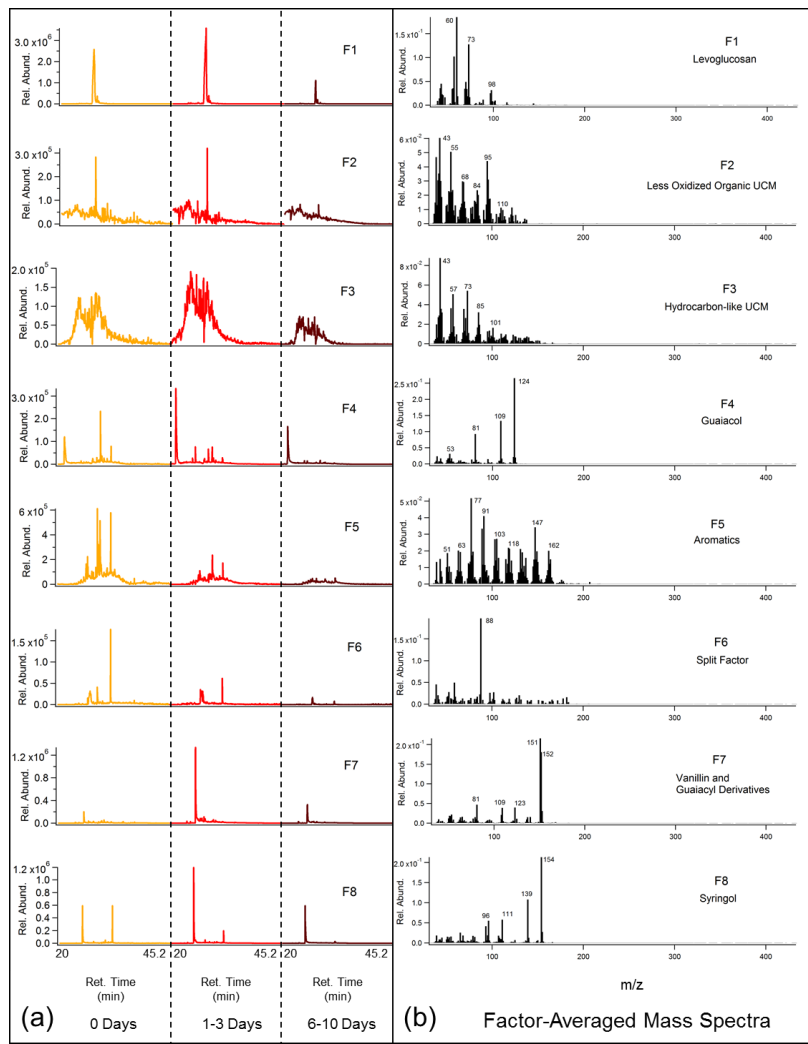


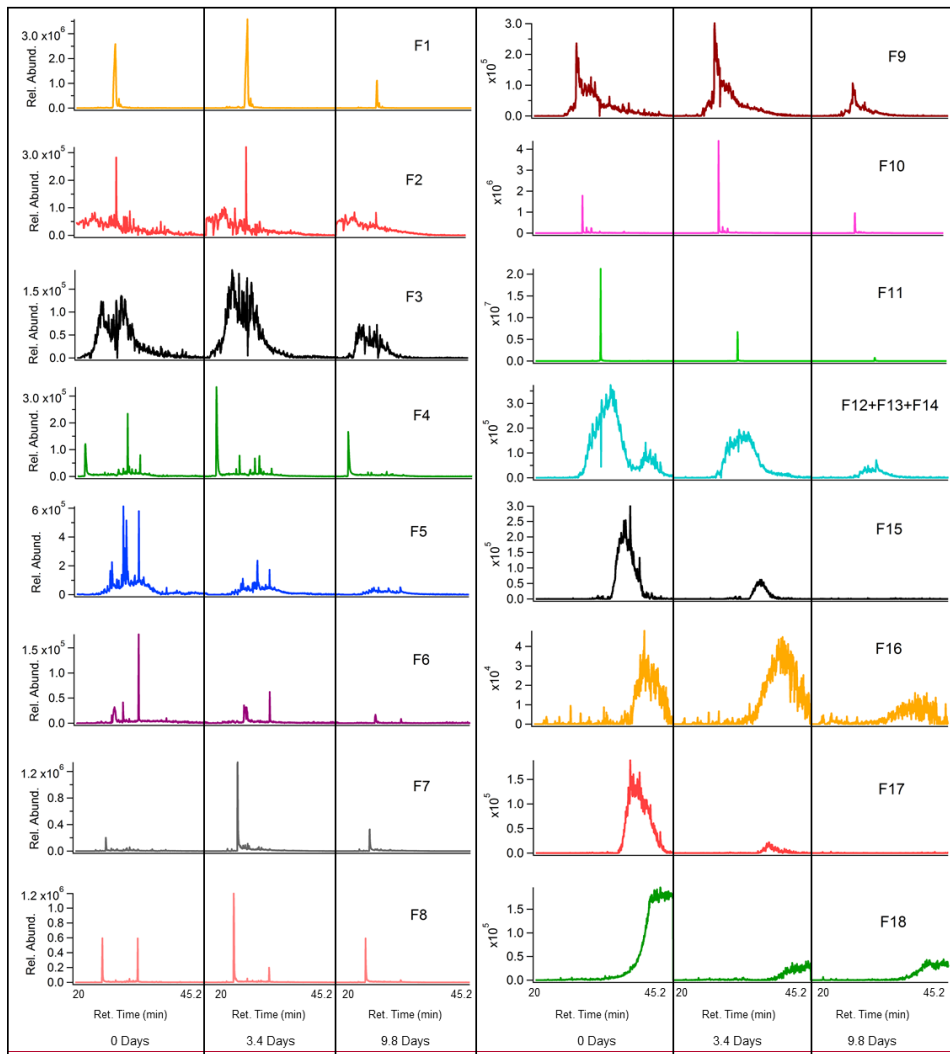


**Figure 54, cont'd:** Mass spectra for factors 10-15 (F10-15) in PMF 15-factor solution on TAG oak leaf BBOA compound window data. Relevant plots obtained in PMF calculations are provided in Supplemental Information (Figures S10 and S11). Relevant plots obtained in PMF calculations are provided in Supplemental Information (Figures 9a and 10a).

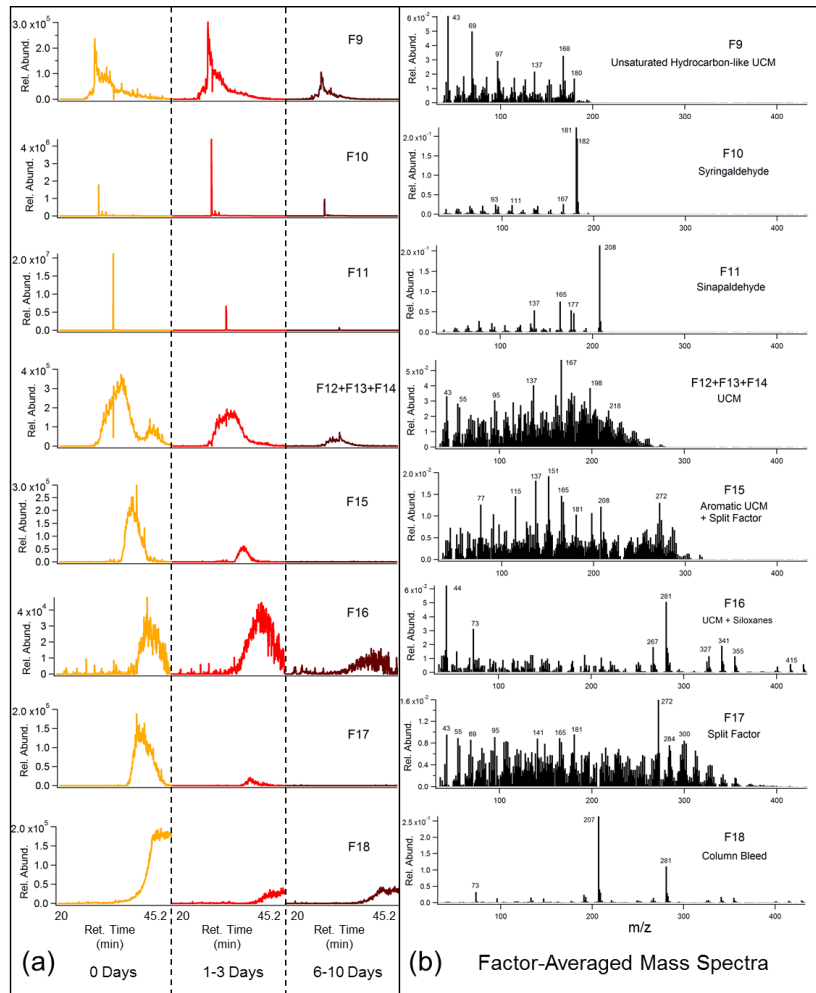
2365







**Figure 65:** Average binned chromatograms and mass spectra for factors 1-18 (F1-F18) in PMF 18-factor solution on TAG oak heartwood BBOA compound window data. Relevant plots obtained in PMF calculations are provided in Supplemental Information (Figures S9-9b and 10b-S10). These chromatograms were obtained from PMF calculations by averaging binned data corresponding to triplicate chromatograms at each level of oxidation. The triplicate-averaged binned chromatograms at each equivalent aging time are displayed in one trace; different aging times are demarcated with vertical lines across the x-axis.



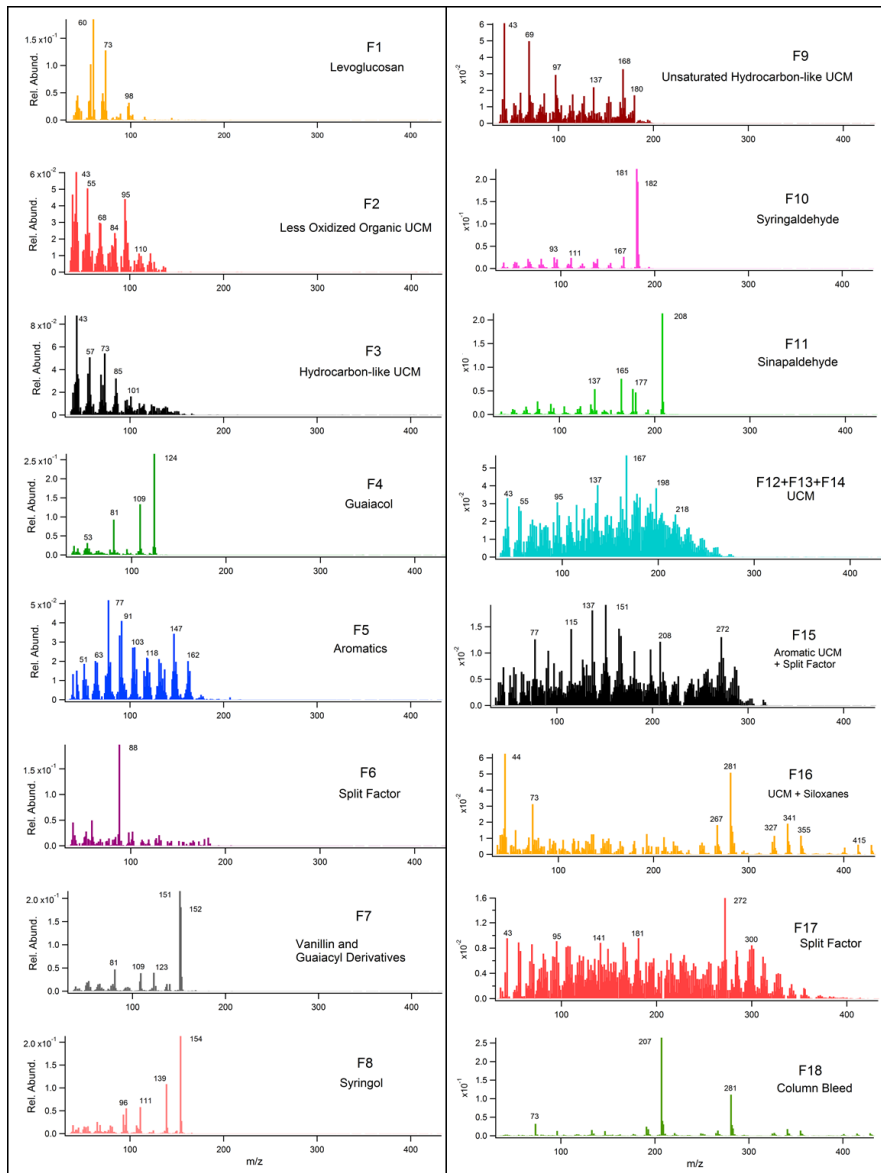


**Figure 75, cont'd:** Average binned chromatograms and mass spectra for factors 9-18 (F9-18) in PMF 18-factor solution on TAG oak heartwood BBOA compound window data. Relevant plots obtained in PMF calculations are provided in Supplemental Information (Figures S9 and S10). Mass spectra for factors 1-18 (F1-18) in PMF 18-factor

solution on TAG oak wood BBOA compound window data. Relevant plots obtained in PMF calculations are provided in Supplemental Information (Figures 9b and 10b).

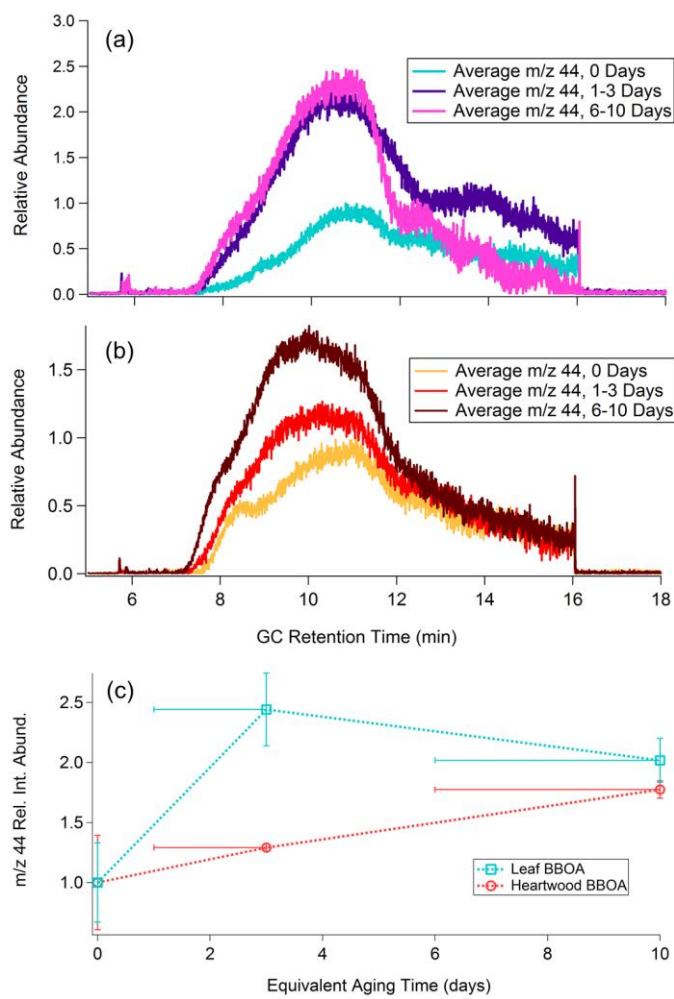
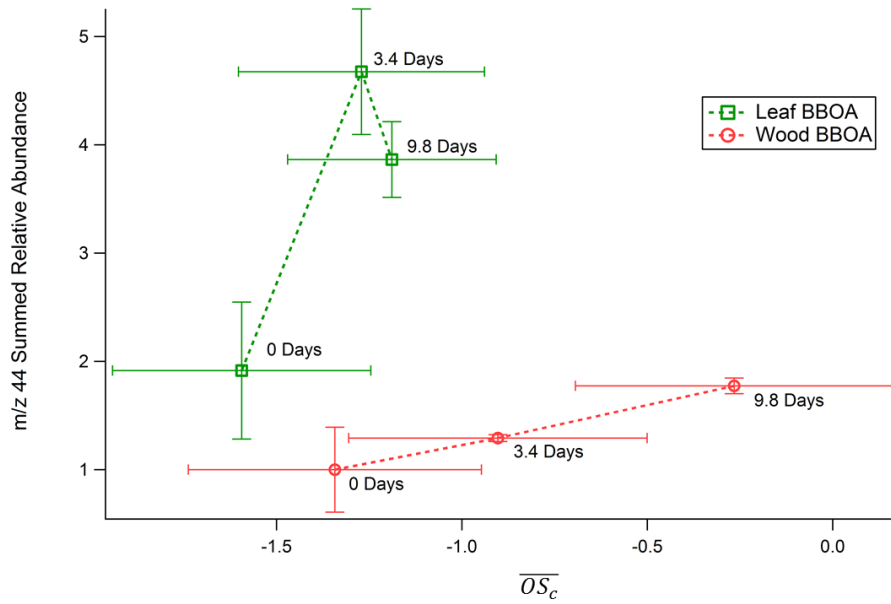
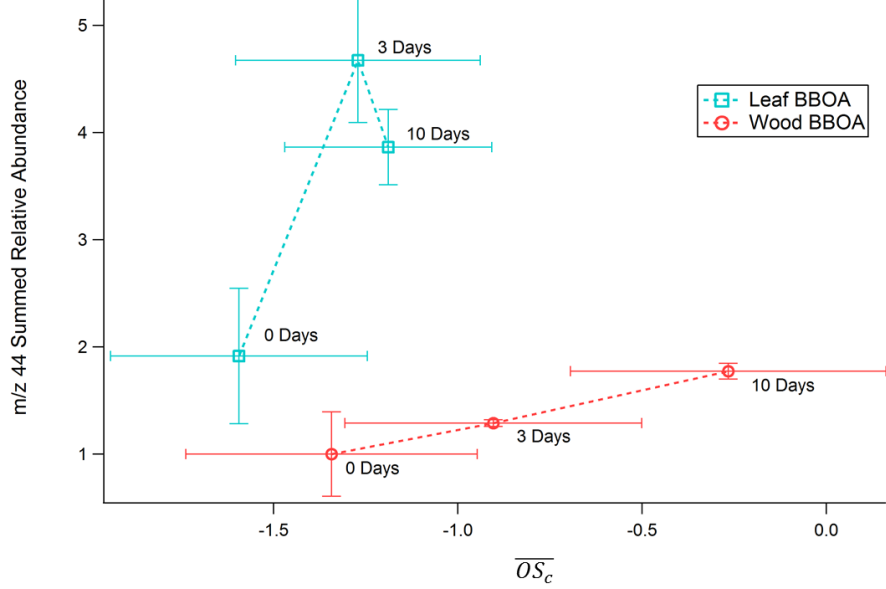


**Figure 86:** (a) Average  $m/z$  44 single ion chromatograms (SICs) across different distinct levels of photochemical aging for leaf BBOA, normalized to the point of highest abundance within the averaged unaged chromatogram (“0 days”). (b) Average  $m/z$  44 single ion chromatograms (SICs) across different levels of photochemical aging for heartwood BBOA, normalized to the point of highest abundance within the averaged unaged chromatogram. (c) summed relative  $m/z$  44 decomposition signal as a function of photochemical aging for both fuels ( $\pm$  one standard

deviation). These values were obtained by averaging triplicate  $m/z$  44 decomposition signals at each level of photochemical aging. For each fuel type, all summed abundances are normalized to the unaged  $m/z$  44 signal (“0 days”). [The x-axis error bars denote the equivalent aging time range and are applicable for all measurements obtained in this study.](#)

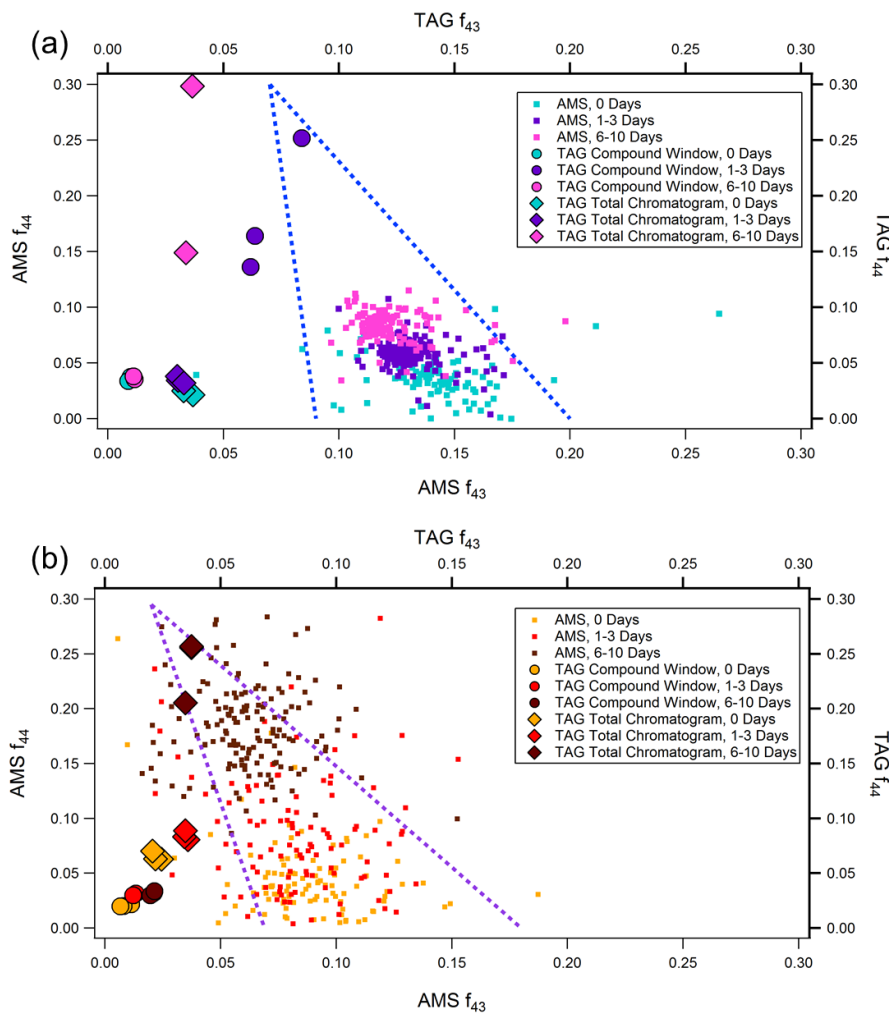
2395



2400 **Figure 97:** TAG decomposition  $m/z$  44 integrated relative abundances for PAM-aged ~~wood and leaf~~<sup>leaf and</sup>  
~~heartwood~~ BBOA as functions of AMS  $\overline{OS}_c$ . Here, all TAG data have been normalized to the unaged ( $\sim 0$  days) wood  
BBOA integrated  $m/z$  44 abundance.

2405

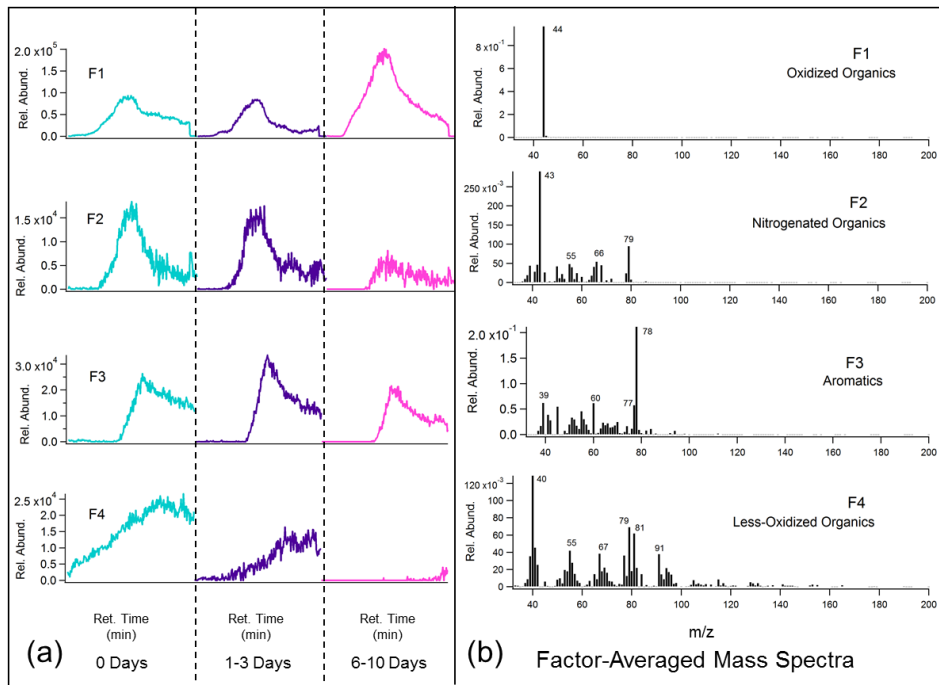
2410

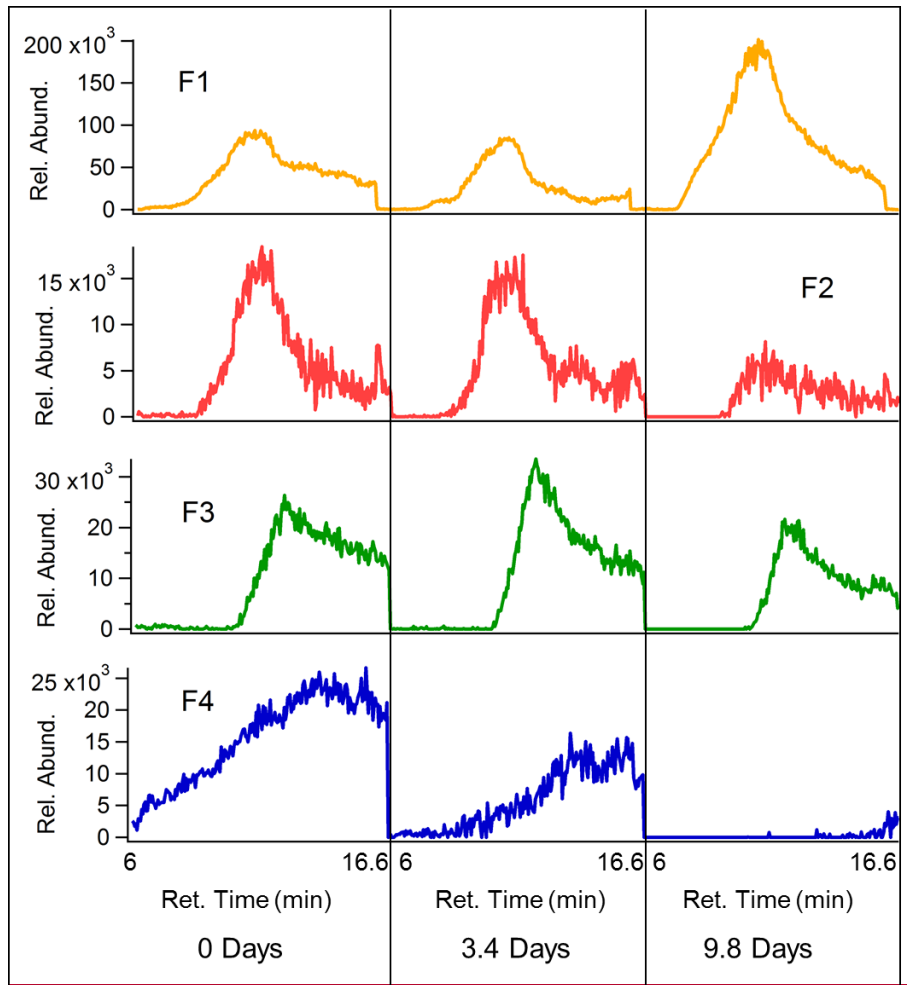


**Figure 108:** AMS and TAG  $f_{44}$  vs  $f_{43}$  at different levels of photochemical aging for (a) oak leaf and (b) oak wood BBOA. TAG  $f_{44}$  and  $f_{43}$  values were obtained using Eq. (1). To minimize noise, AMS data is plotted only for points where sufficient total organic concentrations were achieved, around the peak of the concentration profile. The triangles formed by the blue dotted lines provide guidelines for the evolution of OA chemical composition across  $f_{44}$  vs  $f_{43}$  space; the apex of the triangle indicates the direction of photochemical oxidation (Ng et al., 2010).<sup>2415</sup>

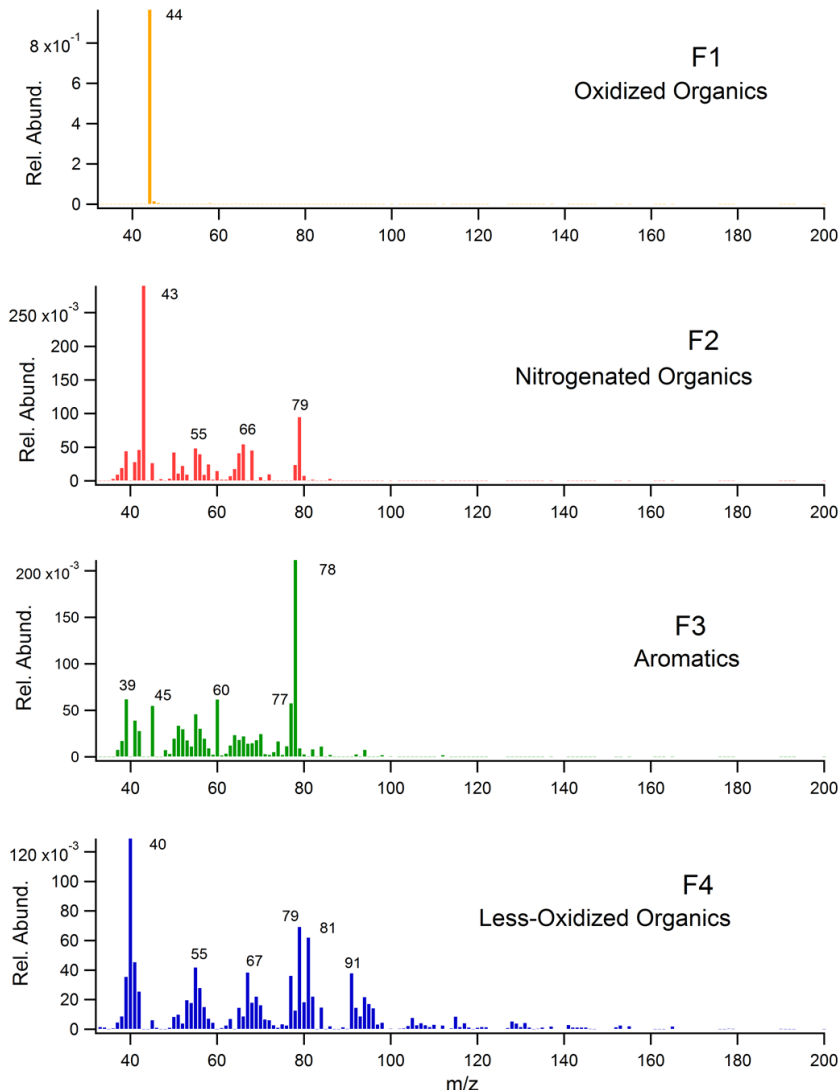
Field Code Changed

2420

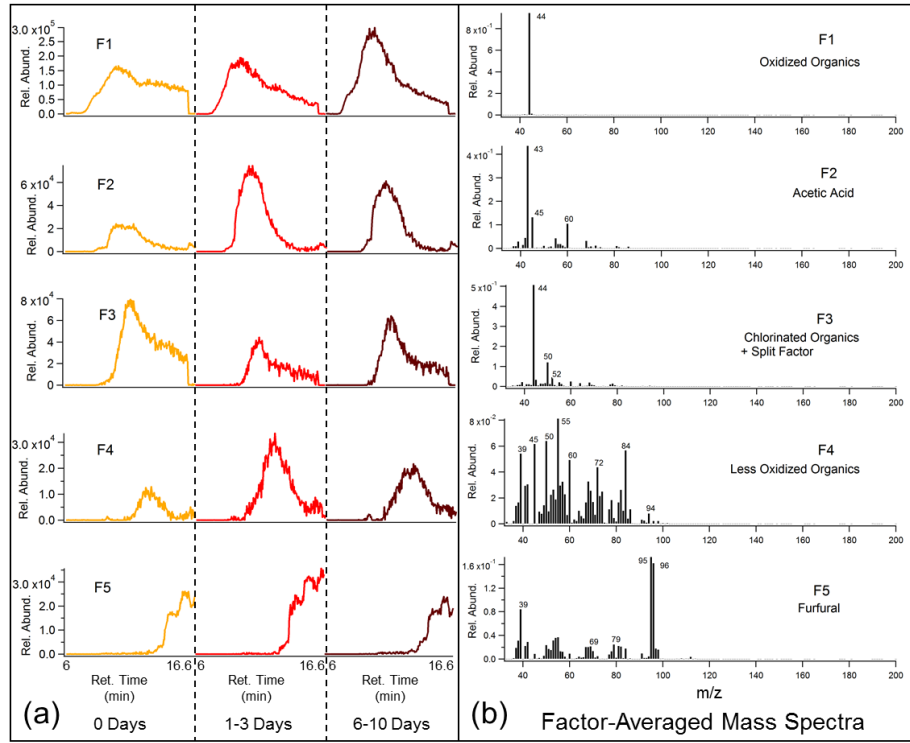


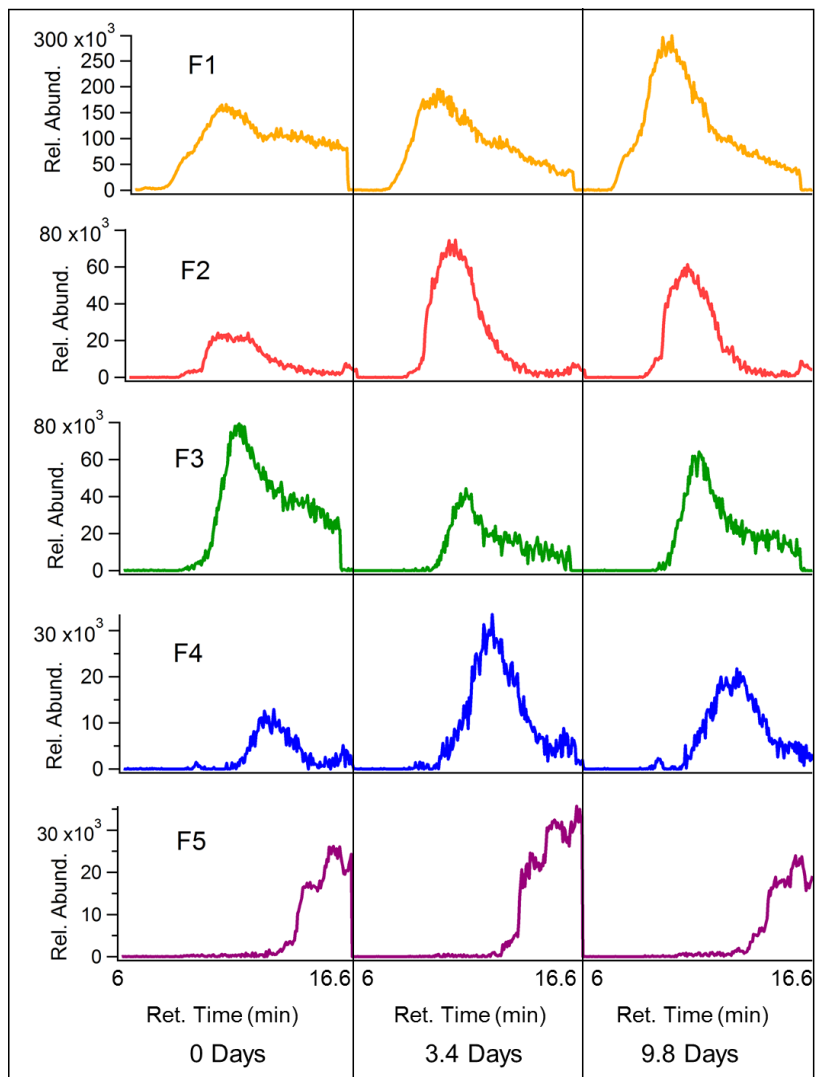


**Figure 119:** Average binned chromatograms [and mass spectra](#) for factors 1-4 (F1-4) in PMF 4-factor solution on TAG oak leaf BBOA decomposition window data. Relevant plots obtained in PMF calculations are provided in [Supplemental Information \(Figures 9e-S9 and 10e-S10\)](#). These chromatograms were obtained from PMF calculations by averaging binned data corresponding to triplicate chromatograms at each level of oxidation. The triplicate-averaged binned chromatograms at each equivalent aging time are displayed in one trace; different aging times are demarcated with vertical lines across the x-axis.

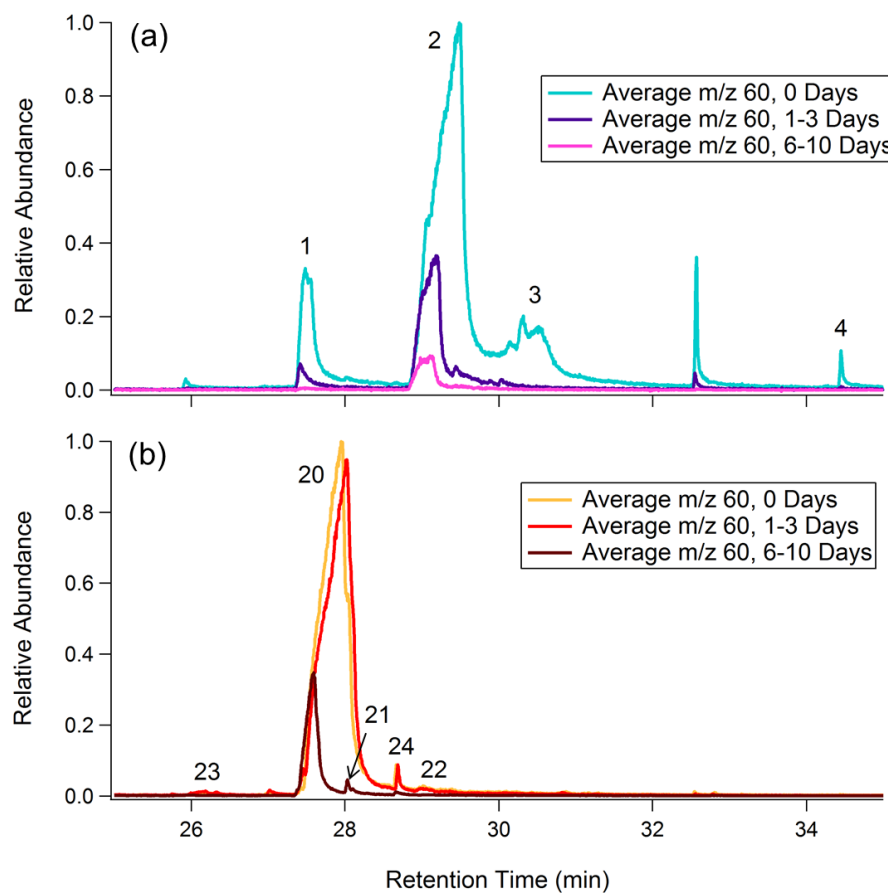


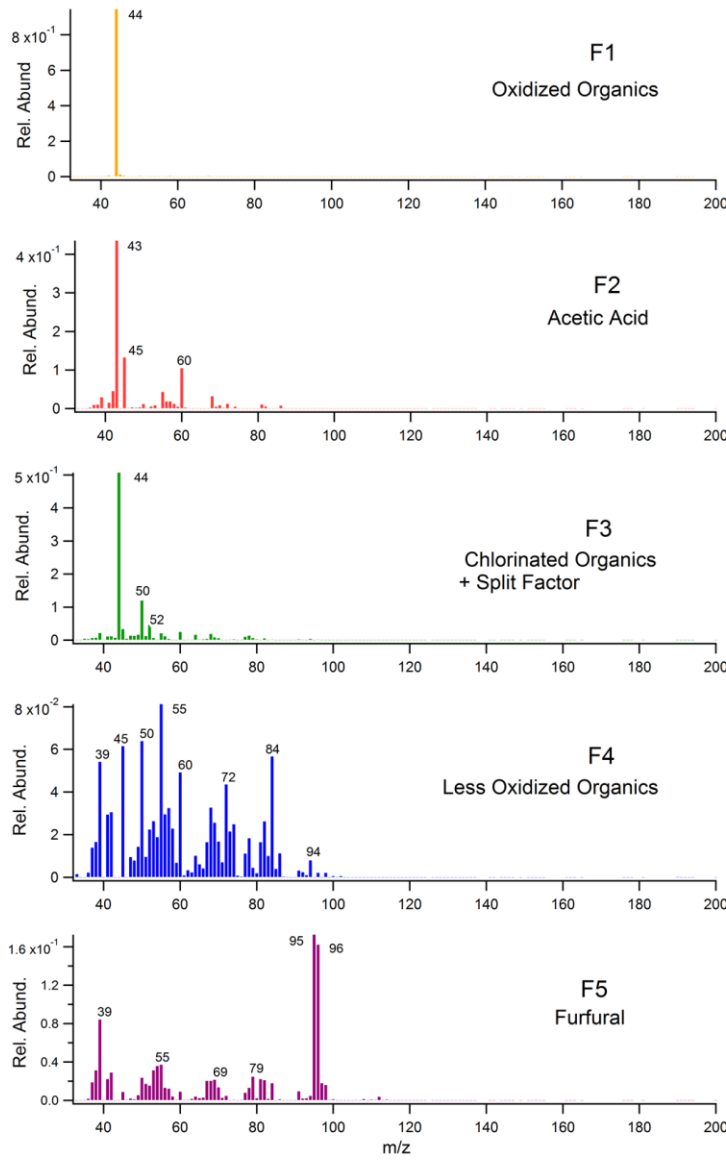
**Figure 12:** Mass spectra for factors 1-4 (F1-4) in PMF 4 factor solution on TAG oak leaf BBOA decomposition window data. Relevant plots obtained in PMF calculations are provided in Supplemental Information (Figures 9e and 10e).





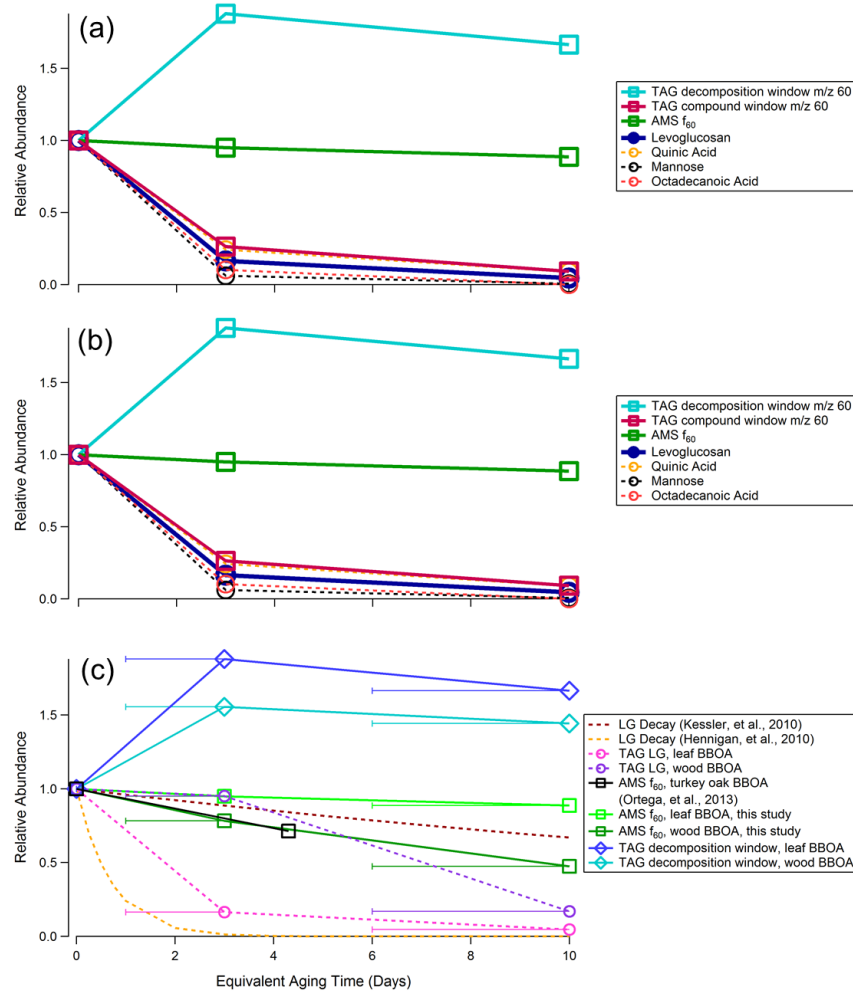
**Figure 1310.** Average binned chromatograms [and mass spectra](#) for factors 1-5 (F1-5) in PMF 5-factor solution on TAG oak wood BBOA decomposition window data. Relevant plots obtained in PMF calculations are provided in Supplemental Information (Figures [S99d](#) and [40dS10](#)). These chromatograms were obtained from PMF calculations by averaging binned data corresponding to triplicate chromatograms at each level of oxidation. The triplicate-averaged binned chromatograms at each equivalent aging time are displayed in one trace; different aging times are demarcated with vertical lines along the x-axis.





2445 **Figure 14:** Mass spectra for factors 1-5 (F1-5) in PMF 5 factor solution on TAG oak leaf BBOA decomposition window data. Relevant plots obtained in PMF calculations are provided in Supplemental Information (Figures 9d and 10d).

2450 **Figure 1f:** Average  $m/z$  60 single ion chromatograms (SICs) across the compound window for (a) leaf BBOA; (b) wood BBOA. For each plot, all traces are normalized to the point of highest abundance within the average unaged chromatogram. Individual compounds are labeled according to identifications provided in Supplemental Information (Figures S5-S6 and S6S7; Tables S3-S4 and S4S5).



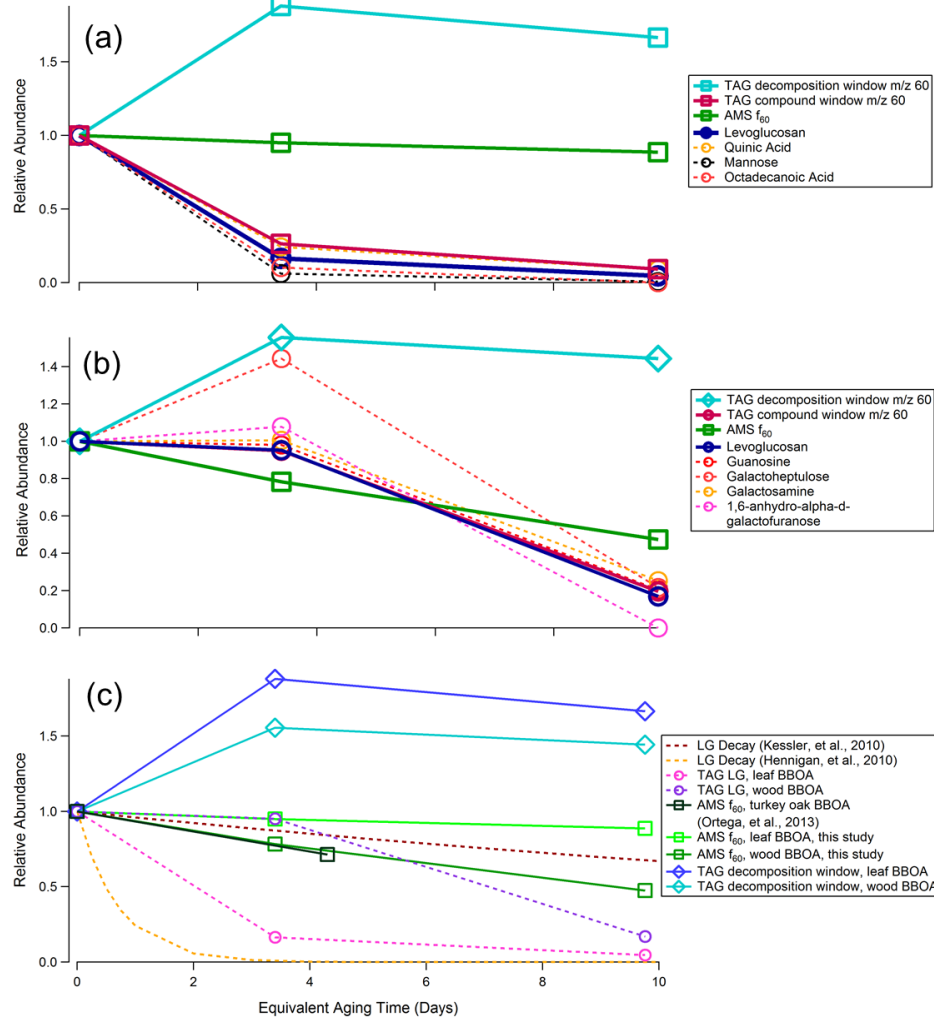


**Figure 4612.** Relative changes in abundance for different  $m/z$  60 fragmenting species in (a) leaf and (b) wood BBOA; (c) TAG and AMS  $m/z$  60 species as a function of  $\text{OH}_{\text{exp}}$ . Levoglucosan (LG) decay rates were calculated using two different literature  $k_{LG}$  values (Hennigan et al., 2010; Kessler et al., 2010) with an assumed typical outdoor  $\text{OH}-\text{OH}$  concentration of  $1.5 \times 10^{-6}$  molec  $\text{cm}^{-3}$  (Mao et al., 2009). Additionally, normalized AMS  $f_{60}$  values for turkey oak (*Quercus laevis*) BBOA obtained during the FLAME-3 campaign were adapted from Figure 10b in Ortega, et al. et al. (Ortega et al., 2013) and are included for comparison. The x-axis error bars denote the equivalent aging time range

2460

Field Code Changed

Field Code Changed

Field Code Changed

and are applicable for all measurements obtained in this study, though they are only included in panel (c) to preserve figure readability.

**Table 1.** Qualitative levels of PAM-reactor oxidation with corresponding OH-OH exposure ( $\text{OH}_{\text{exp}}$ ) estimations and equivalent aging times. The  $\text{OH}_{\text{exp}}$  estimations were made using methods described in Supplemental Information (Methods: PAM Calibrations and Equivalent Aging Estimations).

Qualitative Level of Oxidation	$\text{OH}_{\text{exp}}$ (molec $\text{cm}^{-3}$ s)	Equivalent Aging Time (days)
low-mid	<u><math>1.7 \times 10^{11}</math></u> - <u><math>4.44 \times 10^{11}</math></u>	<u>1-3</u> - <u>4</u>
high	<u><math>7.7 \times 10^{11}</math></u> - <u><math>1.326 \times 10^{12}</math></u>	<u>6-9</u> - <u>8</u> - <u>10</u>